UC Berkeley
UC Berkeley Electronic Theses and Dissertations

Title
Live Imaging of Segmentation Clock Dynamics in Zebrafish

Permalink
https://escholarship.org/uc/item/0813z4j6

Author
Shih, Nathan Pui-Yin

Publication Date
2013

Supplemental Material
https://escholarship.org/uc/item/0813z4j6#supplemental

Peer reviewed|Thesis/dissertation

eScholarship.org
Powered by the California Digital Library
University of California

Live Imaging of Segmentation Clock Dynamics in Zebrafish

By

Nathan Pui-Yin Shih

A dissertation submitted in partial satisfaction of the

requirements for the degree of

Doctor of Philosophy

in

Molecular and Cell Biology

in the

Graduate Division

of the

University of California, Berkeley

Committee in charge:

Professor Sharon L. Amacher, Chair
Professor Craig T. Miller
Professor David A. Weisblat
Professor Patricia Zambryski

Fall 2013

Live Imaging of Segmentation Clock Dynamics in Zebrafish

©2013

by Nathan Pui-Yin Shih

Abstract

Live Imaging of Segmentation Clock Dynamics in Zebrafish

by

Nathan Pui-Yin Shih

Doctor of Philosophy in Molecular and Cell Biology

University of California, Berkeley

Professor Sharon Amacher, Chair

Segmentation is a developmental program in animals that generates semi-repetitive structures along the body axis. In vertebrates, somites are formed sequentially from the mesoderm of the extending tailbud, eventually giving rise to structures such as axial muscles and vertebrae. Somites form with great regularity, every thirty minutes in zebrafish. The periodicity of somite formation is controlled by a set of oscillating genes known as the segmentation clock. To better understand the dynamics of the clock and its role in patterning somites, I have explored its behavior through an *in vivo* clock reporter, *her1:her1-venus*. I show that individual cells in the presomitic mesoderm express oscillating clock expression, consistent with predictions made by mathematical modeling and analysis in fixed embryos. I am able to rapidly track a large number of PSM cells using novel semi-automated cell tracking and fluorescence quantification programs. Through these methods, I find that the clock oscillations are coordinated through the Notch pathway, and a loss of Notch function causes slower and desynchonized clock oscillations. I also explore the interaction of mitosis and the segmentation clock, and find the two processes are connected. Finally, I investigate the slowing of the segmentation clock in real-time, and find that oscillations in the anterior PSM are about twice the periodicity of somitogenesis. This has interesting implications for the role of the segmentation clock in patterning somites, including the potential to polarize somites. By studying the segmentation clock in real-time, I am able to better investigate and understand the mechanisms driving somitogenesis.

Dedicated to…

Mom and Dad, for their endless love and support

Alethia, because she is a huge stinkybutt, but my favorite one.

and to Van,
How wonderful life is while you're in the world.

Table of Contents

Chapter 1: An Introduction to Somitogenesis and the Segmentation Clock

Somitogenesis in Zebrafish and Other Vertebrates 1
A Clock and Wavefront Model of Somitogenesis 2
Meinhardt's Pendulum-Escapement Model of Somitogenesis 4
Drosophlia Segmentation and the Discovery of Associated Genes 5
Segmentation in Short Germ Arthropods 7
Discovery of Segmentation Clock Genes in Amniotes 8
The Role of Segmentation Clock Genes in Zebrafish 10
Synchronization of Zebrafish Clock Gene Expression through the Notch Pathway 12
Components of the Notch, FGF, and Wnt Pathway Cycle in the Amniote Segmentation clock 15
Regulation of Clock Expression, Transcripts, and Proteins 17
Molecular Components of the Wavefront 19
Imaging the Segmentation Clock *in vivo* 21
Biological Clocks in Other Systems 22

Chapter 2: Single-Cell-Resolution Imaging of the Impact of Notch Signaling and Mitosis on Segmentation Clock Dynamics

Introduction 24
Results 26
  Live Imaging of Segmentation Clock Activity with Single-Cell Resolution 26
  Last Oscillation Occurs in S-1 and Lasts about Twice the Period of Somite Formation 27
  PSM Cells Oscillate in Notch Pathway Mutants and Do So Asynchronously 28
  Most Dividing Cells Undergo Temporary Disruptions in Oscillation Synchrony 28
  After Mitosis, Sibling Cells Oscillate in Tight Synchrony with Each Other in Wild-Type and Notch Mutant Embryos 29
  Noise Induced by Cell Division is Likely Reduced Because Mitosis Preferentially Occurs During the "Off" Phase of the Oscillation Wave 29
Discussion 30

Chapter 3: Slowing of the Segmentation Clock Establishes a Two-Segment Periodicity in Zebrafish

Introduction 57
Results 58
Discussion 61

Chapter 4: Asymmetric Segmentation Clock Signaling as a Mechanism to Pattern Somite Polarity

Introduction 78

Results and Discussion 78

Chapter 5: Future Directions and Closing Remarks

Depletion of *pnrc2* activity may reduce clock reporter expression levels 85
Attempts to develop a clock reporter that does not affect the segmentation clock 86
The 300bp regulatory region upstream of *mespb* is insufficient to mimic the endogenous expression domain 87
Generating a *her1* and *her7* double mutant will to explore more comprehensive clock knockdown 88
It may be possible to dissect the 8.6kb upstream of *her1* for core regulatory regions 89
Closing Remarks 89

References 106

Appendix A: Documentation of MATLAB Programs for Image Segmentation, Cell Tracking, and Data Analysis 116

Appendix B: Materials and Methods 129

List of Figures

Figure 2.1: The Zebrafish Transgenic *her1:her1-venus* Line Recapitulates Dynamic her1 Expression 33
Figure 2.2: General strategies taken to generate a dynamic reporter of *her1* oscillations. 35
Figure 2.3: Impact of *her1:her1-Venus* transgene homozygosity on cyclic gene expression. 37
Figure 2.4: Detection and Analysis of Clock Oscillations at Single-Cell Resolution 39
Figure 2.5: Graphical user interface of our MATLAB-based 3D segmentation and tracking program. 41
Figure 2.6: Notch Signaling Is Required for Synchronous Oscillation in Neighboring PSM Cells 43
Figure 2.7: The *her1:her1-Venus* transgene is expressed in a salt-and-pepper pattern in Notch pathway mutants. 45
Figure 2.8: Mitosis Produces Highly Synchronized Sibling Cells that Gradually Resynchronize with Neighbors 47
Figure 2.9: Sibling cells that drift apart from each other after division eventually re-synchronize with their local neighbors. 49
Figure 2.10: After Mitosis, Sibling Cells Oscillate in Tight Synchrony in a Notch-Independent Manner 51
Figure 2.11: Most sibling cells remain synchronous for at least two oscillations of the clock. 53
Figure 2.12: Mitosis Preferentially Occurs during the Off Phase of the Her1 Oscillation Wave 55
Figure 3.1: Clock expression slows and amplifies as it enters the anterior PSM. 64
Figure 3.2: Synchrony of anterior PSM cells depends on distance between cells 66
Figure 3.3: Cells in the posterior PSM oscillate in-phase with each other. 68
Figure 3.4: Correlation of clock wave and somite boundary formation. 70
Figure 3.5: In anterior PSM tissue, clock expression has a two-somite periodicity 72
Figure 3.6: Clock gene oscillations in hes6 MO-injected embryos show the same two-segment periodicity in the anterior PSM as in wildtype. 74
Figure 3.7: A modified model of segmentation clock expression. 76
Figure 4.1: Experimental and theoretical examples of the segmentation clock generating a sawtooth pattern 81
Figure 4.2: The slowing of the segmentation clock affects amplitude and symmetry of clock expression 83
Figure 5.1: *pnrc2* morpholino, H2B-cerulean mRNA, and lyn-mCherry mRNA co-injected into a *her1-venus* heterozygous embryo. 92
Figure 5.2: Variability of maximum fluorescence in cells tracked in four embryos. 94
Figure 5.3: Rib counts of various *delta* and *her* mutants in 21 dpf larvae 96
Figure 5.4: Confocal images of the *mespb:venus-PEST* reporter line. 98
Figure 5.5: High-resolution melt analysis of *her7* ZFN-injected embryos compared to wildtype. 100
Figure 5.6: Distribution of bioinformatically-predicted binding sites of the 8.7kb upstream of *her1*. 102

Figure 5.7: Examples of imaging the *her1-venus* reporter line using different confocal microscopes. 104
Figure A.1: Screenshots of GUI interface 106

Acknowledgements

I first and foremost want to express gratitude to my parents, for providing me with the excellent genetic material, deeply nurturing environment, and priceless resources that made my journey to and through graduate school possible. I would also like to thank my sister, who has provided me with equal parts friendly sibling rivalry and affection. Without my family, I would not be anywhere near where I am today, and to them I am eternally grateful.

I would like to thank my science teachers throughout the years, whose teachings have left a lasting impression on me as a scientist: Mrs. Witt, Mr. Bowen, and Professor Padian. Thanks as well to the professors of my favorite undergraduate class, Dr. Levine, Dr. Gerhart, and Dr. Harland, for introducing me to the wonders of animal development. I was greatly blessed with excellent scientific mentors in my undergraduate years, Jenny and Marvalee, for building the foundation for my future scientific endeavors.

I could not have asked for a better mentor than Sharon. She is the perfect combination of kind, nurturing, intelligent, and invested that any graduate student would be blessed to have. She is largely responsible for any of my scientific success during my graduate years, helping me grow through individualized scientific attention and warm, genuine encouragement. I am especially appreciative of the special care she took in looking after me during my last year, after she had moved away. I always felt supported, even from afar.

The positive philosophies of her and her husband, Jay, are clearly reflected in everyone that works for them. The Amacher-Hollick lab was a fun and friendly place during their time at Cal, with holiday parties that were the envy of all the other labs. They built labs with fantastic people, and I am so happy to have developed such warm and happy relationships with all of them.

Special thanks also to Craig, for taking me in after Jay and Sharon moved to Ohio. Craig treated me as one of his own, consulting me for zebrafish opinions and patiently explaining to me the technical details of his lab’s research. He has built an excellent research environment, always filled with deep scientific conversation and endless humor. I also greatly appreciate his lab members, who welcomed me into their ranks without a second thought.

I would like to acknowledge my French collaborators, Emilie and Paul, for their invaluable science and mentorship. Emilie trained me from the very beginning, and set rigorous standards for how science should be done. Paul welcomed me to Montreal, and together we exchanged very exciting ideas and speculations about somitogenesis. My graduate experiences are all the richer for having worked with both of them.

Thank you to the fish and imaging facility staff, for their behind-the-scenes work to ensure my science always ran smoothly. Deb, Jen, Mel, Kait, and Jessie all made sure the fish were always fed and happy. Thanks to Holley and Sam, for always attending to my concerns and keeping “Rachel” in perfect, working order.

I salute to my fish, for their dedication to scientific progress.

A shout out to my friends from high school, college, OASES, CUHK, and grad school, for making the stresses of my doctorate more bearable and making sure my productivity was never as high as it could be.

And finally, my love and thanks to Van, for being the best partner I could ask for throughout my years here at Cal. Thank you for being my biggest cheerleader and the staunchest fan of my science. I couldn’t have done it without you.

Chapter 1

An Introduction to Somitogenesis and the Segmentation Clock

In organisms, the pacing of cyclic processes is controlled by biological clocks. These clocks drive a broad range of activities in a rhythmic manner, regulated by internal molecular feedback and external environmental influences. By investigating the nature and mechanisms of biological clocks, we can better understand their role in essential developmental and life cycle processes. Perhaps the most well-known of these is the circadian clock. Derived from the Latin roots of *circa* (“around”) and *diem* (“day”), circadian rhythms describe processes that endogenously cycle approximately every 24 hours and adjust based on external cues such as light and heat. Many organisms exhibit repetitive behavior based on the rotation of the Earth, whether it be a plant aligning its leaves to adjust for the sun or a human child falling asleep shortly after trying to stay up past her bedtime. Other biological processes have a period faster or slower than a day, known as ultradian or infradian rhythms, respectively. Infradian rhythms are often paced by astronomical phenomenon, such as the moon’s influence on the tide or changing seasons as the Earth orbits the sun. Examples include increased activity in fruit bats during a full moon and the migration of birds south for the winter (Riek *et al.* 2010; Gwinner 1989). Examples of ultradian rhythms include eye blinking and heart rates, as well as the loop of *C. elegans* defecation (Wollnik 1989; Lloyd and Stupfel 1991; Branicky and Hekimi 2006). Biological clocks are clearly responsible for properly pacing a plethora of behaviors that are based on the timing of environmental events.

But biological clocks also play a major role in more intrinsic processes, such as properly patterning a developing organism. Through molecular oscillator networks, structures can be carefully timed and formed in a periodic manner. An excellent example of this is animal embryo segmentation, where a field of seemingly undifferentiated tissue is divided into semi-repetitive structures. In vertebrates, segmentation sequentially forms repetitive epithelial blocks of tissue called somites, which eventually give rise to structures such as axial muscles and vertebrae (Dequeant and Pourquié 2008; Pourquié 2011; Holley 2007) . This formation of somites – known as somitogenesis – is a tightly periodic process within each species, occurring every 120 minutes in mice, every 90 minutes in chick embryos, and every 30 minutes within zebrafish (Pourquié 2011). My dissertation investigates the molecular mechanisms underlying this cyclic process and their role in accurately generating a somite.

Somitogenesis in Zebrafish and Other Vertebrates

The optical transparency and external fertilization of zebrafish embryos make it an excellent model organism to study developmental processes such as somitogenesis. The real-time development of a zebrafish embryo can be observed without having to dissect it out of the parent or culture it in a petri dish. After fertilization, zebrafish embryos undergo a series of rapid divisions to create a 128-cell blastula (Kimmel 1995). This ball of cells continues to divide, creating a cap of cells resting on top of the yolk (Kimmel 1995). At this point cells undergo epiboly, where they begin to thin and extend down the yolk. Once the cells spread to 50% of the yolk, gastrulation begins (Kimmel 1995). Cells accumulate around the leading edge of the spreading cells to form a germ ring and involute under the extending epiblast (Kimmel 1995). These involuting cells make up the hypoblast, which eventually gives rise to the mesoderm and endoderm (Kimmel 1995, Rohde *et al.* 2007). At the same time, the cells begin to converge towards the dorsal side of the embryo. These cells will also extend along the anterior-posterior axis to begin creating the shape of the embryo.

After gastrulation, the segmentation period begins (10-24 hours post-fertilization). Cells around the margin of the gastrula are the precursors to the paraxial mesoderm, the tissue that eventually makes up each somite. These margin cells converge towards the dorsal side of the embryo and future notochord, contributing to the elongation of the embryo axis along the anterior-posterior axis (Kimmel 1995). Signals from the notochord will be important in patterning the paraxial mesoderm (Stickney *et al.* 2000). The tailbud forms in the posterior end of the developing embryo, which will continue to grow and divide throughout the segmentation process. Somites form sequentially from anterior to posterior, with somites forming at a rate of two per hour at 28°C (Kimmel 1995; Schroter *et al.* 2008). Somites are sequentially pinched off from the presomitic mesoderm, transitioning from a loose mesenchymal structure to a tight epithelial arrangement. The first forming structure to mark the somite is actually the posterior boundary of the 1st somite, which is followed by the approximately simultaneous formation of the 2nd somite and the anterior boundary of the 1st somite (Kimmel 1995). From this point, somites continue to form sequentially as the tail bud extends through cell divisions, forming 30-34 somites in total (Kimmel 1995). Once somites are formed, they can be distinguished as either myotome (muscle precursors) or sclerotome (bone precursors). In zebrafish, most of the somite is composed of myotome, with only the ventral layer of cells made up of sclerotome (Morin-Kensicki *et al.* 2002). As the somites mature, they take on a chevron shape and sclerotome cells migrate medially to align with the notochord (Stickney *et al.* 2000). The myotome can be subdivided into two broad classes of cell types, with slow muscle cells lining the lateral-most portion of the somite and fast muscle cells occupying the majority of the somite, between the slow muscle cells and sclerotome. These subcategories in the somite eventually give rise to important structures such as axial muscles and vertebrae.

Somite formation is similar in other vertebrates, though differences in initial developmental programs before somitogenesis influence the segmentation process. In avian and mouse models, the primitive streak forms along the midline acts as the site for gastrulation. Future somitic cells involute towards the midline and end up in the rostral portion of the primitive streak (Pourquié 2001). Cell transplant experiments have demonstrated that only a small number of cells in the gastrula are fated for the early somites, while the fates of cells in more posterior somites are determined at a later time. Transplant of anterior primitive streak cells causes the paraxial mesoderm to form lateral plate mesoderm, clearly indicating that the fate of caudal mesoderm is not determined early on (Garcia-Martinez and Schoenwolf 1992). Lineage tracing experiments have shown that cells in the caudal PSM can give rise to somites as well as intermediate or lateral mesoderm (Stern and Vasiliauskas 1998). Taken together, it is clear that the dynamic process of somitogenesis is tightly regulated at a local level, with PSM cells determining their fate relatively late in their development.

A Clock and Wavefront Model of Somitogenesis

As somites form from the developing presomitic mesoderm, the question arises of how this dynamic process is regulated. Early observations of somitogenesis in *Xenopus* noted that the number of somites formed was standard within a species, within a 4% range (Maynard Smith 1960). These somites were coordinated with the embryo's body plan, with a specific somite count corresponding to other body landmarks such as limbs and pelvic girdle. The greatest variation appeared in the caudal region, near the tail. This coordination with the whole-embryo body plan holds true even when the embryo is reduced in size, resulting in fewer cells being incorporated into the same number of smaller-sized somites (Spemann 1903). In 1976, Cooke and Zeeman explored what was controlling the constancy of somite number: was the embryo signaling a specific number of somites, or signaling a specific somite size relative to the body size? Both strategies would generate the same number of somites, but through wholly different mechanisms. Previous models had proposed that the size and shape of each somite could be prepatterned by some set of simple cellular variables, and that the sequential formation of somites was based on this existing spatial prepattern across the PSM (Maynard Smith 1960; Bard and Lauder 1974). Interestingly, the limits of molecular biology at the time prevented a clear understanding of what that cellular variable would be, but suggested a series of morphogen gradients as a possibility. The spatial distribution of the eventual somites would be prepatterned by local signal, causing groups of cells to respond to the unique prepattern of each somite number while ignoring neighboring, alternative possibilities. This prepatterning hypothesis, however, creates a situation where – in the case of *Xenopus* – thirty unique values of the prepatterning signal have to account for each of the thirty separate somites. The complexity required to generate this pattern cast doubt on this model's viability. The case against prepatterning a set number of somites is further challenged when considering the slight variation of somite number within species and the grossly varying number of somites among different species. A prepatterning model of somitogenesis should not create any variation in somite number because each individual somite would be signaled by a unique variable value. This would also require the generation of new variable values for animals with more somites, with as much as 400 somites for snakes (Gomez *et al.* 2008). While prepatterning may be a viable model for certain body structures, the repetitive and regular nature of somites required a more complex model to be sufficiently explained.

Cooke and Zeeman proposed a clock and wavefront model of somitogenesis to better explain the phenomenon of sequential somite formation. They observed that somites were differentiated from the seemingly naïve PSM in a sudden and rapid manner. This abrupt change could be described using a special field of mathematics known as catastrophe theory. Developed by Rene Thom (1972) and championed by Zeeman, catastrophe theory describes phenomena that experience a sudden shift in behavior from only small changes to influencing variables. A common example is a ship at sea staying upright or capsizing: a boat will stay afloat while different levels of wave tilt it, but a small increase in wave strength may tip the boat, causing it to quickly transition to a new, stable state of being capsized. In a way, this was analogous to somitogenesis, where cells would begin as undifferentiated PSM cells, experience cellular signals until breaching a threshold, and then suddenly flip into a new stable state of a somite.

Two distinct cellular signals were needed for this bifurcated system to work. The first is an anterior-posterior positional gradient, which they dubbed the "wavefront". The use of gradients along an axis is a common theme in developmental biology, including the role of *sonic hedgehog* (*shh)* in patterning the vertebrate neural tube and decapentaplegic (Dpp) in patterning the polarity of a fly wing (Turing 1952; Ruiz *et al.* 2003; Wartlick *et al*. 2011). Since the tailbud of a developing vertebrate embryo is constantly elongating, a cell within the undifferentiated PSM must be able to detect its position within the PSM relative to the tailbud and the forming somites. Cooke and Zeeman proposed that this positional information signal will define the specific region where somites will form. This wavefront would match the speed of embryo elongation and scale proportionally to any changes in embryo size. But a sweeping wavefront would only be able to define cells in a gradual manner, which is not enough to generate discreet somites. To address this, they proposed a second component of the model: the clock. As the wavefront travels down the elongating embryo, an oscillator within all PSM cells is segmenting the tissue at regular intervals. The oscillator was theorized to smoothly transition between a restrictive and permissive phase. When in the restrictive phase, cells encountering the wavefront would not undergo somite formation. But when the clock was permissive, cells in the proper position of the wavefront would be signaled towards a catastrophic change from presomitic mesoderm to somite[1]. Through these two mechanisms, somites of equal size would be patterned within the developing PSM, with the pace of the clock and location of the wavefront determining the size, periodicity, and number of somites. This model also explained slight flexibility in somite number and adjustments for embryo size. Depending on the expression of wavefront gradients, slight differences in somite size could cause a couple more or less somites to form. A smaller or larger embryo would adjust the gradients of positional information so that the wavefront would be in the same relative position, scaling the somites to match the embryo.

Through experimental observations and mathematical theories, Cooke and Zeeman were able to direct the search for molecular mechanisms controlling somitogenesis. The behavior of somite formation matched the characteristics of catastrophe theory, suggesting a dynamic method of segmenting the vertebrate body plan. While they lacked the tools to dissect the actual molecular mechanisms behind this process, they aptly described the features in the search for clock and wavefront candidates: genes that would oscillate with a periodicity that matched somitogenesis and genes that generated anterior-posterior gradient within the elongating PSM.

Meinhardt's Pendulum-Escapement Model of Somitogenesis

Though receiving less attention in recent years than the clock and wavefront model, Hans Meinhardt proposed an alternative explanation of how embryos in general segmented[2] (1982, 1986). He proposes a pendulum-escapement model, using grandfather clocks as an analogy. He contends that there are at least two states a cell can experience, either as a posterior or anterior compartment. Undifferentiated cells oscillate between these two states, the speed of these oscillations based on a long-range morphogen. He expected a sweeping of wave of gradual state changes to begin at and be driven by a high concentration of the morphogen in the tail-bud. This is compared to the oscillations of a pendulum in a grandfather clock: the speed of the pendulum swing is controlled by the weight and length of the pendulum (in this case, the morphogen gradient) and each oscillation is marked by the discrete progression of the minute hand (the establishment of an anterior or posterior compartment). Each change in state acts as a "gating" mechanism, similar to locks in a shipping channel. At any given time, cells can only be in one state, with one state allowing preparation but not transitioning, and the other state allowing transitioning but not preparation. In the shipping channel analogy, the ship can either be rising up the channel or passing out of the channel. When the top gate is closed, and water filling the lock can be considered preparation for continuation. Once the lock is filled, the top gate can be opened, allowing for the ship to transition on through the canal. In the same vein, the sequential establishment of both the anterior and posterior compartments is required to form each somite boundary (Meinhardt 1982).

---

[1] Cooke and Zeeman (1976) note that while there were known examples of long biological oscillators such as circadian rhythms and very short oscillators such as neuronal synapses, an intermediate-length oscillator had not yet been described. This makes their capacity to postulate the existence of a segmentation clock based solely on the morphological periodicity that much more impressive.

[2] This theory has received less attention because original work was done based on fly models, which we now know is quite different than the vertebrate method of segmentation. It is also based on a diffusible molecule to drive the oscillations, which differs from the cell-autonomous oscillations observed in PSM cells (personal communications between Paul Francois and Olivier Pourquié)

Meinhardt also addresses unique challenges that somite boundary formation would create for his model. Proper somitogenesis requires periodic somite formation, subdivision of somites into anterior and posterior compartments, an intrinsic clock for somite formation, and signaling among PSM cells to determine the somite structure. His model is motivated by the challenge local PSM cells face when trying to determine a somite boundary. Boundaries clearly form between the posterior and anterior portion of each somite, but this is not enough to signal proper boundary formation since under this local signaling a boundary should also form at the center of each somite. Embryos are also not defining each segment based on the identity of the previous one, as fly mutants can have segment identity cross segment boundaries. To address this, he adds a third cellular state, the segment border, which would help direct where exactly the boundary would form and give polarity to the cellular states incorporated into each somite (Meinhardt 1982).

Meinhardt also made some predictions about how components controlling cellular states would behave to produce uniform somites. He expected the substances controlling anterior or posterior states to be autocatalytic, locally exclusive, and promote each other's expression at long range (Meinhardt 1986). This would allow for the switching between these two states to be rapid, specific, and continuous. The local and long-range activity should cause oscillations close to the high levels of morphogen gradient, while cells far from the morphogen source would crystallize, stabilizing the alternating pattern of anterior-posterior compartments. A mechanism for the "gating" he proposed earlier is also suggested, that perhaps substance "X" could be produced but not activated in one state and then activated but not produced in the next state. Only the alternation of the cell between these two states would allow for proper differentiation of PSM cells (Meinhardt 1986).

This pendulum-escapement model of somitogenesis has many similarities to the clock and wavefront model (Cooke and Zeeman 1976), including cellular oscillations and a positional gradient. Both are able to explain how embryos can be scaled to adjust somite size based on whole-embryo size. Meinhardt (1986) contended that his version links the behavior of the oscillations, wavefront, and periodic pattern into one mechanism rather than two. As the scientific community considered these two models, molecular evidence began to test the accuracy of these assertions.

***Drosophlia* Segmentation and the Discovery of Associated Genes**

The discovery of genes linked to the clock and wavefront model of somitogenesis were not realized in a vacuum. Instead, a breadth of work done in arthropod segmentation laid the foundations for discovering the vertebrate counterparts. To best understand the motivations behind the search for vertebrate segmentation genes, a brief history of arthropod segmentation first needs to be addressed.

Much of the groundbreaking work in animal segmentation was first done in *Drosophila* (Nusslein-Volhard and Weischaus 1980). Fruit flies undergo a highly-derived developmental plan in which nuclei rapidly divide without becoming partitioned off into separate cells, creating a structure known as the syncytium. The open flow of cytosol allow for rapid diffusion of signaling molecules to define polarity and differentiate segments across the body. The anterior end of the embryo is patterned by maternally deposited *bicoid* and *hunchback*, while posterior end is patterned by *nanos* and *caudal* (Scott and Carroll 1987; Peel 2004; Damen 2007). These genes express varying concentrations of these morphogens, differentially activate seven bands of gap genes (*knirps*, *Kruppel*, *giant*, and zygotic *hunchback)* across the embryo (Peel 2005). These gap genes subsequently activate narrower, uniform stripes of pair-rule genes – named for the loss of alternating segments in mutant embryos – such as *even-skipped*, *odd-skipped, paired, runt,* and *hairy* (Scott and Carroll 1987; Peel 2004; Peel 2005; Damen 2007). These stripes of pair-rule gene expression are then refined even more through the expression of segment polarity genes such as *engrailed, wingless,* and *hedgehog,* which define the future boundaries of segments within the fly (Damen 2007). The simultaneous formation of these boundaries is a derived characteristic known as long-germ development. All the cells required for the embryo body are generated before any boundaries form, rather than the more basal process of concurrently extending the body axis and sequentially forming each boundary.

Following the discovery of these axis and segment patterning genes, further work elucidated the molecular mechanisms involved (Jaeger 2009*)*. Maternally deposited mRNA and protein define the initial anterior-posterior axis. mRNA of *bicoid*, a transcription factor, is concentrated in the anterior, while Nanos protein is localized in the posterior of the embryo. The presence of Bicoid inhibits the transcription of a posterior-determining transcrption factor gene *caudal* in the anterior of the embryo (Peel *et al.* 2005). At the same time, Nanos protein inhibits translation of the anterior-determining transcription factor gene *hunchback* (Peel *et al.* 2005). Together, these maternal effect genes create gradients of transcription factors that regulate the expression of initial segmentation zygotic transcripts. The maternal effect genes activate seven broad bands of gene expression from the four different gap genes. The mechanisms of how early polarity signals regulate segmentation were elucidated through genetic analyses and enhancer dissections. Caudal protein activates the posterior domains of *giant* and *knirps*, while Bicoid drives the anterior domains of *giant* and *hunchback* expression, as well as *Kruppel* expression (Peel *et al.* 2005). Maternal Hunchback feeds back to promote zygotic *hunchback* expression, as well as repressing the expression of more posterior bands of gap genes (Peel *et al.* 2005).

These gaps genes form an expression profile that can then regulate more refined stripes of pair-rule genes. How these various gap genes can generate seven uniform stripes of each pair-rule gene has been studied through various enhancer analyses (Reinitz and Sharp 1995). The most famous of these pair-rule genes, *even-skipped* (*eve)*, was shown to have distinct enhancer regions that differentially responded to the local concentration of gap genes (Reinitz and Sharp 1995). The 2nd stripe of *eve*, for example, is broadly activated in the anterior third of the embryo by binding of Bicoid and Hunchback in a region approximately 1kb upstream of the *eve* transcription start site (Reinitz and Sharp 1995). This broad domain is refined by repression by Giant in the anterior and Kruppel in the posterior (Small *et al.* 1991). Another pair-rule gene, *hairy*, was also shown to have upstream regulator regions that controlled the expression of each stripe. The posterior borders of stripes 5 and 6 are repressed by Giant and Hunchback respectively, while the anterior borders were both controlled by Kruppel. The two stripes were also shown to be at least partially activated by Knirps (Langeland *et al.* 1994). These seven stripes of pair-rule genes go on to drive an even more refined fourteen stripes of segment polarity genes. The segment polarity gene *engrailed* is repressed by the presence of Eve protein, but activated by another pair-rule gene *fushi tarazu* (*ftz)* (Peel *et al.* 2005)*. ftz* is expressed within the gaps between *eve* expression. Due to the repression by *eve* and other pair-rule genes, *ftz* is only able to drive *engrailed* expression in the most anterior and posterior boundaries of its expression, resulting in two stripes of *engrailed* expression for each stripe of *ftz* (Fujioka *et al.* 1995). These stripes of *engrailed* go on to define the parasegments – the position of the future segment boundaries – of the animal.

This complex gene network helped shape our understanding of what components contribute to animal segmentation. However, due to the highly derived nature of the *Drosophila* segmentation program, findings in the fruit fly may be limited in their applicability to other segmented organisms. To better understand how these genes affected segmentation in a more typical developmental plan, we next must explore their role in more basal organisms.

Segmentation in Short Germ Arthropods

The pair-rule genes define parasegments in anthropods, both long germ and short germ. Rather than laying down all the cells necessary and then segmenting the entire embryo simultaneously, short germ arthropods segment sequentially from an extending posterior presegmental zone. Similarly, pair-rule genes are expressed in a periodic manner from the extending growth zone (Damen 2007). As these stripes of expression progress anteriorly in the growth zone, they pattern segments and cause them to form sequentially. Interestingly, the spacing of this pair-rule expression is not conserved across arthropods. In the beetle *Tribolium,* pair-rule genes are expressed with a double segmental periodicity: the distance between each stripe of pair-rule gene is two segments in length and eventually accounts for two parasegments formed (Sommer and Tautz 1993; Patel *et al.* 1994; Choe *et al.* 2006). Flour beetles express pair-rule genes in a manner similar to flies, and knockout of pair-rule genes cause phenotypes reminiscent of fly knockouts of the same pair-rule genes (Schroder *et al.* 1999, Choe and Brown 2007). A further functional analysis of *Tribolium* pair-rule genes has suggested that a hierarchy of interacting genes mediates segmentation. This network has some similarities to the *Drosophila* pair-rule genes, with homologues of *eve, run*, and *odd* regulating each others' expression domains, eventually promoting expression of downstream targets such as *paired* and *sloppy-paired* (Choe *et al.* 2006). These genes then activate classic the parasegment genes *wingless* and *engrailed*. More careful analyses of *Tribolium* segmentation genes clearly shows stripes of *odd* are progressing anteriorly in a dynamic fashion within the growth zone (Sarraizin *et al.* 2012).

Other insects express pair-rule genes, some with double segment periodicity (grasshopper, Liu and Kaufman 2005; cockroach, Pueyo *et al.* 2008), some with a pair-rule stripe of a single segment length (milkweed bug, Davis and Turner 2001), and some with an intermediate-sized stripe of expression (cricket, Mito *et al.* 2007). In spiders, pair-rule genes are expressed with a segmental periodicity, with a stripe of expression marking each forming segment (Damen *et al.* 2005). In the centipede, an arthropod known for its many segments, the double segmental periodicity of pair-rule genes is present in the posterior growth zone (Chipman *et al.* 2004). Interestingly, the brine shrimp appears to have dynamic expression of *eve* in the posterior growth zone and a narrow stripe of expression in the anterior growth zone, marking the future position of the next forming segment (Copf *et al.* 2003). As it will become clear in a further section, this expression pattern of brine shrimp has some similarity to the pattern seen in clock genes in segmenting vertebrates.

One significant difference between some short germ and long germ arthropods is the role of the Notch pathway. While gap genes directly activate pair-rule genes in *Drosophila*, the role of gap genes is less clear in short germ arthropods. Gap genes such as *Kruppel* do play a role in regulating *eve* expression in the beetle, but the regulation seems to be indirect and affects segments more posterior in the embryo (Cerny *et al.* 2005). The role of gap genes does not seem to be conserved outside of insects, as gap genes do not seem to be required in segmenting the centipede (Chipman and Stollewerk 2005). Instead, the Notch pathway appears to be necessary to segment a variety of arthropods, including centipedes, millipedes, and spiders (Kadner and Stollewerk 2004; Jansen *et al.* 2005; Damen *et al.* 2005). Disruption of the Notch pathway in spiders causes the pair-rule gene *hairy* to lose its coordinated stripes of expression and become randomly expressed in a "salt-and-pepper" pattern (Stollewerk *et al.* 2003). Thus, the components that regulate pair-rule genes differ across the arthropod clade. One evolutionary explanation for these differences was offered by Damen (2007): the Notch pathway was the ancestral regulator of pair-rule genes, and through time a derived insect lineage gap genes became co-regulators of their expression. With this redundancy in place, the Notch pathway lost its regulatory capacity over pair-rule genes (presumably being co-opted for other developmental processes).

The molecular mechanisms driving segmentation in arthropods are actually similar to those driving somitogenesis in vertebrates. Though the molecular mechanisms of somitogenesis will be discussed in much greater detail later on, the Notch pathway and homologs of the pair-rule gene family *hairy* play an important role in proper vertebrate segmentation. The similarities of components used in some short germ arthropods and vertebrates beg the comparison: do these two groups share an evolutionarily ancestral segmentation mechanism? While the Notch pathway is important in both groups, its role in arthropods appears to be more upstream than in vertebrates (Damen 2007). If the two processes were from the same ancestral program, there would have been several instances in which segmentation was lost, such as in urochordates, nematodes, echinoderms, and spoon worms (Damen 2007). It could also be possible that these similarities are simply a co-option of the same pathway from the limited options available to metazoan development. It seems unlikely, however, given the similarities in both the components involved and their expression patterns. By examining the development of both arthropods and vertebrates, a better understanding can be gained about how segmentation arose in animal development.

Discovery of Segmentation Clock Genes in Amniotes

The first gene implicated to play a clock-like role (as suggested by Cooke and Zeeman) for somitogenesis was an ortholog to a fly pair-rule gene, the avian *c-hairy1* (Palmeirim *et al.* 1997). A key feature of this gene was that it appeared to be expressed cyclically with a periodicity that matched that of chick somitogenesis, approximately 90 minutes. Embryos fixed at different times within that 90 minute-interval showed distinctly different patterns of *c-hairy1* expression within the PSM. Three classes of *c-hairy1* expression were noted: (I) a broad expression domain in the caudal 70% of the PSM, (II) a narrower domain of about three somite-lengths in the rostral half of the embryo, and (III) a smaller-than-a-somite stripe of expression near the somite-PSM boundary. Intermediates between each of these classes were also observed. While these expression profiles were observed in fixed embryos, taken together they suggested that a wave of *c-hairy1* was sweeping through the PSM from the caudal to rostral end with a periodicity that matched somite formation. To verify this, embryos were bisected and each half was fixed at different time points. Halves fixed 30 minutes apart have differing expression patterns, suggesting that clock expression changes as time passes. When fixed 90 minutes apart, the expression profiles matched, suggesting that this expression of *c-hairy1* was cycling in time with somitogenesis. Cell-tracing experiments demonstrated that the wave of expression could not be explained by cell movement. Several other experiments were done to explore the nature of this clock cycling: removing the caudal portion or surrounding tissue did not affect the clock expression in culture, and treatment with cycloheximide to inhibit protein translation did not prevent the wave of clock expression from being transcribed. These findings indicated that *c-hairy1* was rhythmically expressed in the PSM at the same rate as somitogenesis. It appeared to be a cell-autonomous process, not requiring external cellular signals or even protein translation for proper expression. This initial discovery of a segmentation clock gene provided a robust mechanism for timing somite formation. It also had striking similarities to the basal short-germ segmentation process in arthropods, hinting at an evolutionary connection between the two processes.

Soon after this initial discovery, a wealth of work was done to discover and characterize other cycling genes in chicks and mice. *Lunatic Fringe* (*lfng*), which encodes a Notch pathway glycosyltransferase necessary for somite formation in mice (Johnston *et al.* 1997; Cohen *et al.* 1997) and proper wing development in flies (Hukriede *et al.* 1997), was shown to cycle with the periodicity of somite formation in chicks (McGrew *et al.* 1998) and mice (Aulehla and Johnson 1999). Careful fixation of embryos revealed a similar expression pattern as observed for *c-hairy1*, with waves of expression in the PSM, narrowing as they progressed rostrally. Avian *Lunatic Fringe* (*lFng*) was tested in many of the same ways (McGrew *et al.* 1998) as it was tested in avian *c-hairy1* (Palmerin *et al.* 1997). Expression patterns of *lFng* and *c-hairy1* were shown to have overlapping, dynamic expression patterns within the PSM. *lFng* still cycled after the removal of neighboring cells or the caudal region, but suspended cycling activity in the presence of the translation-inhibiting drug, cycloheximide. A more thorough study of the chick *lFng* demonstrated the precise concentration of *lFng* signal two-somite lengths from the newest forming somite (Aulehla *et al.* 1999), which is now known in the field as S-1[3]. Three phases of expression previously noted (Palmerim *et al.* 1997) were also seen, with *lFng* signal progressing accordingly when the two halves of the embryo were fixed at staggered time intervals. Expression patterns were less stringently tested in the initial examination of mice *Lunatic fringe* (*Lfng)*, but the slower segmentation time of the organism allowed for higher resolution of each phase of these progressing clock expression waves (Forsberg *et al.* 1998).

Other cyclic *hairy*-related genes were also discovered in chicks and mice. *c-hairy2* was found to be expressed in the chick PSM alongside *c-hairy1*, albeit with a shifted expression pattern (Jouve *et al.* 2000). Expression of the two *c-hairy* genes is synchronous and overlapping in the posterior PSM, but is shifted into alternating bands in the most anterior PSM, reminiscent of *eve* and *ftz* in *Drosophila.* Bisecting embryos and assaying each side for expression of different genes showed that *c-hairy1* is expressed in the posterior half of newly formed and presumptive somites in the rostral PSM, while *c-hairy2* is expressed in the anterior half of these new and presumptive somites. Jouve *et al.* (2000) also described the cycling of a mouse *hairy*-like gene, *Hairy and enhancer-of-split 1* (*Hes1*) in the developing PSM. This gene had been implicated in neuronal development (Ishibashi *et al.* 1995) but not somitogenesis. Cultured PSM tissue showed oscillations similar to *c-hairy1*, with a wave of gene expression propagating through the PSM and refining in the caudal portion of the presumptive somite S0. *Hes1* knockout mice, however, still expressed oscillating *Lfng* transcripts, indicating that *Hes1* cycling

---

[3] Naming conventions in the field have dubbed the newest formed somite named S1 and the second-newest formed named S2 (Pourquié and Tam, 2001). The next presumptive somite was named S0, while the two subsequent future somites were named S-1 and S-2. In Aulehla 1997, SI bordered S-I, with no existence of S0.

does not drive *Lfng* cycling. Given both these components are downstream to the Notch pathway, knockout of the Notch ligand *Delta1* (*Dll1*) would test the necessity of the Notch cascade in driving cyclic clock expression. Previous work had demonstrated that loss of *Dll1* function downregulated *Lfng* and caused segmentation defects. *Dll1* mutants exhibited a loss of both *Hes1* and *Lfng* cycling, indicating both of these processes require proper Notch signaling to progress. This created a conundrum of in determining how these oscillating clock genes contributed to somite formation. *c-hairy1* and *c-hairy2* both could oscillate without protein synthesis while *L-fng* could not, but knockout of the mouse *Hes1* did not disrupt *Lfng* cycling nor somitogenesis. Jouve *et al.* (2000) offered a possible explanation that a second *hairy*-like gene existed that played a larger role in regulating somitogenesis. Their prediction proved correct.

Two back-to-back papers from the Kageyama group (Bessho *et al.* 2001a, Bessho *et al.* 2001b) described the discovery and characterization of *Hes7*, a transcription factor that exhibited homology to *Hes1*. Analysis of the promoter region indicated that *Hes7* was Notch responsive, another similarity shared with *Hes1* and *Lfng*. *In situ* expression data indicated that *Hes7* expression was limited to the PSM and exhibited the dynamic, sweeping pattern observed in previous of clock genes (Bessho *et al.* 2001a). This pattern was carefully scrutinized using previous strategies of bisecting the embryo and fixing each half at separate times (Bessho *et al.* 2001b). *Lfng* and *Hes7* expression were shown to cycle every 120 minutes, a rate that matches the periodicity of somite formation in mice. A *Hes7*-knockout mouse line was generated to examine the loss-of-function effects. Importantly, knockout mice exhibited severe morphological abnormalities in spinal development due to defects in somitogenesis. Notch expression was also affected, with various Notch components experiencing weaker and more diffuse expression. Having a much more significant impact on somitogenesis, *Hes7* appeared to a central component to the vertebrate segmentation process.

Together, these cycling genes helped build a consensus of the mechanisms underlying the segmentation clock and somitogenesis. The periodic, sweeping expression of each of these genes pointed to an intrinsic mechanism of keeping time within the developing embryo. But while these patterns were suggestive, the specifics of how each component contributed to properly forming somites were still unknown.

The Role of Segmentation Clock Genes in Zebrafish

The roles of *hairy*-related genes were being explored in zebrafish concurrent with the work done in amniote somitogenesis. A zebrafish homolog to *hairy* was described to play a role in somitogenesis (Muller *et al.* 1996), though it was not suggested to have the periodicity of a segmentation clock. *hairy/Enhancer-of-Split 1*(*her1*) was detected in the developing PSM, with alternating bands of expression reminiscent of its pair-rule counterpart in *Drosophila*. They noted three to four domains of expression, broad in the posterior and narrowing in the anterior. More stripes were observed here than in the avian counterpart due to more rapid somitogenesis in zebrafish compared to chick. Each domain corresponded to an alternating future somite, with a gap of expression between the domains of approximately one somite size. Lineage tracing experiments were done to clarify where cells in different regions of the tailbud and PSM were being incorporated into somites. Injections into the tailbud determined that somite primordia were not determined at such an early stage; cells from a single tracer-labeled clone were found in as many as five somites. This is consistent with the idea that the extending tailbud is a dynamic region with a high level of cell division and little or no prepatterning. Conversely, injections into the PSM just posterior of the newest formed somite revealed that these cells were incorporated into a single somite. This was consistent with observations in avian embryos that cells within the PSM were not experiencing high amounts of division or movement. They then used lineage tracing to examine whether cells within the stripes of *her1* expression corresponded to somites. In their key experiment, they used the 3rd somite as a landmark for injection, injecting cells just posterior to the newest formed somite. When fixed immediately, these cells were within what they designated Domain I, the most anterior and narrow stripe of expression. Experimental embryos were then injected in the same region but allowed to progress to form several more somites. Lineage tracing revealed that cells injected as part of the anterior-most *her1* expression domain invariably were incorporated into the 5th somite. These data led them to conclude that *her1* was behaving in a similar fashion to pair-rule genes, marking the position of alternating somites through alternating expression. Their analyses did not take into account the clock and wavefront model, nor did they note any dynamic progression of clock signal across the PSM. This dynamic progression was probably difficult to observe with such a rapid pace of somitogenesis. In hindsight, the attempt to invoke a directly similar segmentation mechanism as arthropods overreached the observations. But this work helped dissect the role of *her1* in somitogenesis and made careful observations in how the stripes of expression were spatially positioned.

Whether or not zebrafish segmented differently than amniotes was unclear, especially given the evolutionary time that separates the two groups. Some papers published after the discovery of *c-hairy1* expression in chicks still referred to zebrafish *her1* expression as pair-rule (van Eeden *et al.* 1998; Takke *et al.* 1999), though those laboratories may have been biased in their position in the debate[4]. The issue of whether *her1* was expressed in alternating segments like a pair-rule gene or a sweeping wave as seen in mice and chicks was finally resolved by comparing its expression to a somite marker (Holley *et al.* 2000). *MyoD* is a reliable marker that is expressed in the most posterior boundary of each formed somite and in the next one or two presumptive somites. *her1* expression was assayed alongside *MyoD* using a double *in situ* to observe how the two correlated. They found that the expression domains of these two genes were never spaced more than one somite-length apart; each stripe of *her1* expression corresponded to the formation of one somite boundary as marked by *MyoD*. The distance between the two anterior stripes *her1* expression varied between one- and two-somites in length. They also carefully staged embryos at early and late 12-somite stage to show that the expression pattern differed: while both had two distinct stripes in the anterior PSM, the later embryos' stripes were shifted more anteriorly. This was evidence of a propagating wave of cyclic gene expression, similar to those seen in chick and mice. These finding confirmed that the expression pattern of *her1* are not expressed as pre-patterned somite primordia, but a sweeping wave of clock expression with the periodicity of somitogenesis.

Similar to the mouse and avian counterpart, more than one *hairy*-related gene was shown to cycle within the zebrafish PSM. A second *hairy/Enhancer-of-split related* gene, *her7*, with sequence similarities with *her1*, was identified (Leve *et al.* 2001). It too, had a cyclic expression pattern that matched the *her1* expression domain, except that it was missing the anterior-most *her1* stripe (Oates and Ho 2002). The roles of both these *her* genes were tested using morpholinos to knock down gene function (Oates and Ho 2002; Henry *et al.* 2002, Gajewski *et al.* 2003). Separately, the loss of either of these genes only caused minor morphological defects. *her1* MO-injected embryos had slight defects in the anterior-most somites, while *her7* MO-injected embryos failed to form robust boundaries after somite 11 (Henry *et al.* 2002). Knockout of *her1* or *her7* also caused disruptions in expression of *her1*, *her7,* and Notch ligands *deltaC* and *deltaD* (Oates and Ho 2002; Henry *et al.* 2002; Gajewski *et al.* 2003). More recent work using mutant lines has found that *her1* mutants have defects in the anterior-most somites, while *her7* mutants have defects between somites 8 to 17 (Choorapoikavil *et al.* 2012). These two *her* genes appeared to play semi-redundant roles in regulating Notch components and cyclic gene expression. To determine what joint role these two genes had, *her1* and *her7* morpholinos were co-injected into embryos (Oates and Ho 2002; Henry *et al.* 2002). This caused much more severe defects, causing somites to be almost twice in size, with alternating strong and weak boundaries throughout the entire body axis (Henry *et al.* 2002). These findings were recapitulated in the *b567* mutant, which had a large genomic deletion that included both *her1* and *her7* (Henry *et al.* 2002). These two cycling *her* genes appeared to work in tandem to semi-redundantly regulate the proper timing of somitogenesis.

---

[4] The Takke paper came from the Campos-Ortega lab, the same one as the original *her1* description (Muller, 1996). The van Eeden paper came from the lab of Nusslein-Volhard, winner of the Nobel prize for her discovery of pair-rule genes in *Drosophila*

A Notch-ligand, *deltaC,* was also shown to oscillate in the zebrafish PSM (Jiang *et al.* 2000). Embryos fixed at the 10-somite stage were shown to have distinct stripes of expression, with slight variations depending how early or late the previous somite had formed. These patterns once again recapitulated the cycling patterns of *her1* and *her7* in zebrafish and their counterparts in chick and mice. While embryos in chick and mice could be bisected, cultured, and fixed to demonstrate the dynamic change in expression as time passed, the zebrafish embryo was too small for such a manipulation. Instead, embryos were mounted into the middle of a special device that had two distinct temperatures on either side. This clever setup caused the embryo to develop at different rates and mimicked fixing each half at a different timepoint. They clearly demonstrated that the clock expression stripes were shifted over time, with the stripes of expression at a later phase on the warmer side. They could expose embryos to this temperature gradient for an extended period to synchronize *deltaC* patterns, but the warmer side developed one somite more than the cooler side (Jiang *et al.* 2000). Temperature sensitivity of somitogenesis was carefully documented almost a decade later (Schroter *et al.* 2008), showing that segmentation speed linearly correlated with temperature.

Cyclic genes that corresponded to somite formation were firmly established in the zebrafish model. There were differences in this system compared amniotes, including the lack of any *lunatic fringe* cycling within the PSM (Prince *et al.* 2001; Qiu *et al.* 2004). Across three diverse vertebrate species, somitogenesis is clearly controlled by waves of periodic Notch-pathway genes. With such a dynamic expression pattern, the molecular mechanisms and signaling pathways driving this process were investigated.

Synchronization of Zebrafish Clock Gene Expression through the Notch Pathway

Work in *Drosophila* has shown that *Enhancer of split* genes, which are related to *hairy*, are a known downstream component of the Notch pathway (Fisher and Caudy 1998). As many *hairy*-related genes were seen to oscillate in the PSM, researchers investigated how the Notch pathway properly regulated cyclic gene expression. Shortly after the discovery of the *her1*expression pattern, the mRNA of various Notch components were injected into zebrafish embryos to test their effect on somitogenesis. Two *her* genes, two Delta ligands, and a Notch receptor were all found to disrupt normal somite boundary formation and cyclic *her1* expression

(Takke *et al.* 1999). A forward genetic screen for mutations disrupting somitogenesis isolated several lines that disrupted somite formation after forming only a few somites: *beamter* (*bea*), *deadly seven* (*des*), *after eight* (*aei*), and *fused somites* (*fss*) (van Eeden *et al.* 1996). These mutations had a similar phenotype to Notch pathway mutations in mice (Conlon and Rossant 1995). *fss* is actually a T-box gene, *tbx6*, a cell-autonomous factor necessary to drive the anterior-most stripe of *her1* expression (Holley *et al.* 2000; Nikaido *et al.* 2002; Brend and Holley 2009). *bea*, *des*, and *aei* identify Notch pathway components *deltaC* (Julich *et al.* 2005), *notch1a* (Holley *et al.* 2002), and *deltaD* (Holley *et al.* 2000), respectively. The loss of any of these components resulted in disruption of *her1* expression into a "salt and pepper" expression pattern. Expression of cyclic genes still seemed to exist at varying levels throughout the PSM, but without the coordinated waves of synchronous expression observed in wildtype embryos (Jiang *et al.* 2000; Holley *et al.* 2002; high resolution *in situs* in Julich *et al.* 2005). This pattern suggested that cells were still cycling cell-autonomously, but unable to synchronize with their neighbors for any coordinated clock expression (Jiang *et al.* 2000). A similar "salt and pepper" *her7* expression pattern was observed in these mutant lines (Oates and Ho 2002).

Julian Lewis (2003) proposed a simple negative-regulatory loop to explain these findings. Since *her1*/*her7* cease oscillating when knocked out, they are thought to play a role in regulating their own expression. Previous work on the structure of *hairy* genes in *Drosophila* shows a conserved WRPW domain that acts as a transcriptional repressor (Fisher *et al.* 1996). The "salt and pepper" expression pattern of these cyclic genes in Notch mutants suggested that these genes were still being expressed at various levels (Jiang *et al.* 2000). This differential expression was important, as this would be the pattern expected if cells were actually still oscillating, just not in synchrony with its neighbors. If an intracellular oscillation mechanism of *her* genes exists and requires *her* genes to properly function, then it was possible that these genes were feeding back on themselves to auto-inhibit their own expression. Work done in mice demonstrated a delay between *Hes7* transcription and translation as well as binding of *Hes7* to its own regulatory region (Bessho *et al.* 2003). Together, these data suggested that the intrinsic delay and auto-inhibition of *her* genes were sufficient to generate cycling activity. Lewis (2003) tested this mathematically and found that, with the proper transcriptional and translational delays and turnover rates, this system was robust enough to sustain oscillations given just intracellular activity. This model of clock oscillations was surprisingly robust, overcoming perturbations such as dampening of protein expression and stochasticity of transcription rates. Lewis was also able to incorporate observations of the Notch pathway's role in synchronizing cell expression. When he modeled the oscillations of two neighboring cells without any communication, the cells drifted in and out of synchrony with each other. *deltaC* is expressed in a similar domain as *her1*, and could plausibly be acting at the same time. Since the intracellular domain of the Notch pathway can activate *her* expression, the expression of *deltaC* could nudge neighboring cells into synchrony by timing the activation of *her* expression. The specific delay in Notch signaling was also necessary to properly synchronize cells. Simulations delaying Notch signaling to match the periodicity of *her* cycling had in-phase clock cycling, while a longer delay in Notch caused cells to cycle out of phase. Based on his findings, he proposed a simple, testable model of how clock expression was able to generate the clock patterns observed within the developing zebrafish PSM.

The Lewis group then tested their theoretical proposition by quantifying the delays in transcription, translation, and protein decay necessary to drive clock gene cycling (Giudicelli *et* *al.* 2007). They derived a mathematical expression to correlate the spacing of clock expression stripes in the PSM to the temporal spacing of the waves of clock expression:

$$\frac{T_0}{T(x)} = 1 - \frac{u(x)S_0}{S(x)}$$

where T is the period of oscillation, T_0 indicates the period of cells within the tailbud, while $T(x)$ represents cells x distance away from the tailbud, with the PSM-somite boundary at length L. $u(x)$ represents the velocity of cell movements relative to the tailbud, S_0 represents the length of one somite, and $S(x)$ represents the spatial wavelength from peak to peak of clock expression. They assume that cells in the anterior PSM move one somite length for each turn of the clock ($u(x) = 1$), that periodicity of the clock in the tailbud is the same as somitogenesis ($T_0 = 1$), and that $S_0 = S(x)$ near the PSM-somite boundary. By measuring the distance separating each peak of clock expression in fixed embryos, they could extrapolate the periodicity of cells within the PSM. Based on their calculations, they showed that the periodicity of the clock slowed as it progressed anteriorly through the PSM, diverging to infinity at the PSM-somite boundary. They were also able to use this equation to calculate the delay caused by transcription using fluorescent *in situ* hybridization, which could differentiate between nuclear and cytoplasmic transcripts: approximately 4 minutes for the *her* genes and 8 minutes for *deltaC*. They assayed *deltaC* transcripts and DeltaC protein to calculate the translational delay, which was actually 30 minutes, or a full turn of the clock. Finally, they used a heatshock promoter to drive ectopic *her7* expression to measure the rates of *her* gene decay, the repressive activity of *her* genes on cyclic clock expression, and ability of the embryo to recover from heatshock and clock overexpression. These data experimentally verified components of their simple auto-regulatory loop model of the segmentation clock.

Several other studies also validate the theoretical model put forth by Lewis, describe the behavior of clock activity, and clarify the role of Notch during segmentation. One approach was to use transplant experiments and high-resolution *in situ* hybridization to observe clock expression behavior in *her1* wildtype and deficient cells (Horikawa *et al.* 2006). The high-resolution *in situ* experiments could image the cellular localization of transcripts, and whether it was in the nucleus (transcription) or cytoplasm (translation). A clear hierarchy of expression was observed in each stripe of *her1* clock expression: there was first a region with no expression, while more anterior regions had points of nuclear expression, and the most anterior of the stripe had cytoplasmic transcript (Horikawa *et al.* 2006; Mara *et al.* 2007; Ozbudak *et al.* 2007). This verified that the wave travels from posterior to anterior and the hypothesis that delays in transcript processing accounted for the stripes of clock expression. Furthermore, a transplant experiment of *her1/her7*-MO injected cells into a wildtype embryo showed that *her*-deficient donor cells caused the host cells to accelerate their *her1* cycling (Horikawa *et al.* 2006). The lack of *her* genes to repress *deltaC* and Notch signaling caused Notch to always be on, causing *her* genes to be expressed more quickly. When *deltaC* was knocked out alongside the *her* genes, this accelerated clock expression was lost (Horikawa *et al.* 2006). When embryos were treated with DAPT, a gamma-secretase inhibitor that blocks Notch pathway activity, the oscillations of cells were seen to drift out of synchrony in *her1* expression. DAPT caused desynchronization of clock oscillations after several somites formed, though the exact length of time was dependent on the dosage of drug used (Horikawa *et al.* 2006; Riedel-Kruse *et al.* 2007; Mara *et al.* 2007; Ozbudak *et al.* 2008). When DAPT was washed out, clock gene expression in PSM cells re-synchronized after some delay (Reidel-Kruse *et al.* 2007; Mara *et al.* 2007). Wildtype PSM cells transplanted from one PSM to another were initially out of phase, but became synchronized after three cycles of the clock (Horikawa *et al.* 2006). These studies also showed that the initiation of clock expression in early somitogenesis did not require Notch activity (Riedel-Kruse *et al.* 2007), cells were resistant to noise such as mitosis (Horikawa *et al.* 2006), *deltaC* synchronized expression while *deltaD* promoted tailbud clock expression (Mara *et al.* 2007), and that PSM cells lacking Notch signaling had a 30% decrease in clock expression (Ozbudak *et al.* 2008). Together, these findings were strong evidence that the Notch pathway was able to synchronize and partially activate clock expression in the face of stochasticity of individual cell oscillations.

Another model was put forth to unify this data, proposing that the synchronized oscillations of individual PSM cells could be best described using delayed coupling theory (Morelli *et al.* 2009). This model had four key features: (1) an extending tailbud that matched the velocity of somite formation, (2) local synchronization of oscillating cells, (3) a time delay in the coupling of oscillation signals, and (4) a frequency profile that accounted for the slowing of the clock as cells approached the anterior PSM/somite boundary (Morelli *et al.* 2009). To test if these elements properly explained segmentation clock behavior in vertebrates, the time delays of Notch-based coupling were altered experimentally (Herrgen *et al.* 2010). Embryos treated with DAPT or mutant for Notch-pathway components were found to have a longer periodicity of somitogenesis and subsequently larger somites. The spacing of clock expression in fixed embryos also had a corresponding slowing when the coupling process was hindered, with longer distances between each stripe of *deltaC* (Herrgen *et al.* 2010). Embryos mutant for a non-oscillating *hairy*-related gene, *hes6*, exhibited a slower clock, with increased somite size (Schroter and Oates 2010). Despite making larger somites, the total axis length of the embryos did not change. These findings helped separate the processes of axis elongation and somitogenesis, as well as explain how delays in cell-to-cell synchronizations could generate a slowing of clock periodicity as cells shifted anteriorly in the PSM.

Our understanding of the mechanisms of the segmentation clock was greatly enhanced by the discovery of Notch components and the elucidation of their synchronizing role. Despite the intrinsic noise caused by many separate cellular oscillators within the PSM, the Notch pathway is able to synchronize neighboring cells. Some recent models suggest that the stochasticity of the system (Knierer *et al.* 2013) and random cell movements (Uriu *et al.* 2010) may actually strengthen the ability of PSM cells to resynchronize. This system is finely tuned by the delays caused by transcription, translation, and signaling of Notch components such as *deltaC* and *her1/her7*. These components can collectively organize a dynamic process, generating waves of cyclic gene expression that drive the periodicity of somite formation.

Components of the Notch, FGF, and Wnt Pathway Cycle in the Amniote Segmentation Clock

There are some marked differences in the control of cyclic gene expression in amniotes compared to zebrafish. The number of cycling genes is drastically different. While only several Notch pathway genes have been observed to be cycling in zebrafish, many examples of oscillating genes have been detected in amniotes (Krol *et al* 2011). Several genes from the Notch, FGF, and Wnt pathways exhibit oscillatory behaviors within the PSM of chicks and mice (reviewed in Dequeant and Pourquié 2008; Oates 2012). In the Notch pathway, other *hairy*-related genes such as *Hes5* (Dunwoodie *et al.* 2002) and *Hey1* (Leimeister *et al.* 1999) were oscillate, though knockouts of these genes did not produce segmentation defects. Knockout of

Hes7 (which does cause segmentation defects) activity caused upregulation of *Lfng* and *Hes7*, indicating that *Hes7* played a role in periodically repressing itself and other cyclic genes (Bessho 2003). This auto-regulatory activity is similar to the behavior in zebrafish clock genes. Knockout of *Lfng* also prevents proper cycling activity (Morimoto *et al.* 2005), though overexpression of *Lfng* does prevent *Lfng* and *Hes7* from cycling (Serth *et al.* 2003). Another upstream Notch component, *Nrarp*, oscillates in its expression, periodically regulating the Notch intracellular domain (Wright *et al.* 2009; Kim *et al.* 2011). *Nrarp* also stabilizes *Lef1*, a Wnt pathway transcription factor (Ishitani *et al.* 2005). This cross-pathway interaction suggests connections between Notch and other pathways regulating the segmentation process.

The Wnt and FGF pathway also have cyclic components that seem to act upstream of the cycling Notch elements. Periodic expression has been observed for genes such as *Axin2* (Aulehla *et al.* 2003), *SP5* (Weidinger *et al.* 2005), *Myc* (Dequeant *et al.* 2006), *Dact* (Suriben *et al.* 2006), and *Dkk1* (Dequeant *et al.* 2006). These all play important roles as readouts and regulators of the Wnt pathway. Knockout of these genes cause segmentation defects, with the exception of *Axin2* (Dequeant and Pourquié 2008). Wnt activation stabilizes β-catenin, a transcription factor that functions upstream of both Notch and Wnt (Aulehla *et al.* 2003). The cycling of Wnt regulators cause cycling of β-catenin stability, and this feeds back to regulate oscillations in Wnt as well as Notch. Loss of β-catenin activity disrupts cyclic Wnt and Notch activity (Dunty *et al.* 2008), though a constitutively active β-catenin mutant still allows cycling of the clock in the PSM (Aulehla *et al.* 2008). *Lfng* still oscillated in these mutants with an expanded anterior domain, suggesting that the presence of β-catenin promotes oscillations of clock genes (Aulehla *et al.* 2008). The Wnt pathway seems necessary to drive cyclic expression in the PSM, but is not sufficient to drive oscillations. Components of the FGF pathway cycle as well, including negative feedback inhibitors *Dusp6* and *Spry2* (Dequeant *et al.* 2006). Targets downstream of FGF also cycle: *Snai1* (Dale *et al.* 2006), *Dusp4* (Niwa *et al.* 2007), and the cyclic phosphorylation of *ERK* (Niwa 2007). FGF signaling appears to be upstream of Notch signaling, as Notch pathway mutants and DAPT treatment fail to disrupt cycling in FGF components (Niwa *et al.* 2007). Knockout of FGF signaling using the drug SU5402 abolishes FGF component cycling and stops Notch pathway component cycling as well (Wahl *et al.* 2007). In fact, deletion of the FGF receptor *Fgfr1* causes disruptions in oscillations in the Wnt, FGF, and Notch pathway (Wahl *et al.* 2007). Surprisingly, oscillations of *Lfng* can still occur in *Fgfr1* mutants with the presence of constitutively active β-catenin (Aulehla *et al.* 2008). It is clear that the FGF and Wnt pathways are upstream of Notch, but there is no clear single factor that controls periodic expression across all these pathways.

Two high-throughput studies have searched for different oscillating genes in the PSM. In one, mouse embryos were fixed during somitogenesis, with half the embryo assayed for clock expression, and the other half was used for a microarray study (Dequeant *et al.* 2006). The latter PSM half was divided into 17 categories, based on the expression of *Lfng*. Each piece of PSM could be labeled as corresponding to a certain phase of the clock before being processed using a microarray. They could then assay how expression patterns of various genes in the PSM correlated with the periodic expression of an established clock gene. This method showed cycling in known oscillators such as *Hes1* and *Axin2*, as well as many novel hits within the Notch, FGF, and Wnt pathways. Interestingly, they were able to show that cyclic Notch pathway genes were expressed in phase with cyclic FGF pathway genes, and that these were expressed in anti-phase with Wnt pathway genes (Dequeant *et al.* 2006). A broader version of this experiment encompassed mice, chicks, and zebrafish (Krol *et al.* 2011). Chick embryos were dissected in a similar manner as mice, assaying one half for *lFng* expression and running the microarray analysis on pieces of the second half. Zebrafish embryos were too small to be bisected; for these, a small section of PSM was removed for the microarray assay while the rest of the embryo was processed for *her7* expression. Mouse candidate genes from this study (Krol *et al.* 2011) were compared to the previous study (Dequeant *et al.* 2006) to find common candidates. The common candidates were enriched for genes that cycled in-phase in the Notch and FGF pathways, and in anti-phase with genes in the Wnt pathway. A similar dataset was extracted from the chick data, demonstrating for the first time that Wnt components cycled in chicks, and did so out of phase with cyclic FGF and Notch genes. The zebrafish data diverged from the amniote data, with most oscillating genes only found in the Notch pathway. Known oscillators were clearly detected: *her1*, *her7*, *deltaC*, and *her15*, as well as a couple new *her* oscillators: *her2* and *her4*. Most interestingly, they found oscillations in *tbx16*, which encodes a T-box factor responsive to both FGF and Wnt, and *rhov*, which encodes a small GTPase targeted by Wnt. These genomic searches for cyclic genes within the PSM revealed an evolutionary conservation for the pathways driving somitogenesis, but plasticity in terms of which genes were actually cycling.

The amniote segmentation clock appears to be more complicated than the simpler auto-regulatory loop observed in zebrafish (Dequeant and Pourquié 2008). While Notch components cycle in amniotes and zebrafish, the control of these cyclic expression patterns in amniotes seem to be controlled by other upstream cycles of Wnt and FGF factors. The identification of a central oscillator that controls all these genes has yet to be identified. It remains possible that the concurrent cycling of these many factors may be an emergent property of a complex network rather than the work of a single, unknown gene.

Regulation of Clock Expression, Transcripts, and Proteins

Understanding the regulatory elements that control cyclic gene expression is key to understanding segmentation clock behavior. The segmentation clock appears to be tightly controlled through several mechanisms: regulation of expression, post-transcriptional processing, and rapid turnover of transcript and protein. All these types of control have been studied in both zebrafish and mice.

The first attempt to dissect the zebrafish *her1* enhancer helped broadly determine key regions necessary for clock expression. *her1* and *her7* are transcribed in a head-to-head orientation, separated by approximately 11kb of DNA on chromosome 5 (Henry *et al.* 2002; Gajewski *et al.* 2003). Gajewski *et al*. were able to dissect the *her1* enhancer by generating transgenic GFP lines driven by different blocks of this regulatory region. The 8.6kb directly upstream of *her1* was sufficient to recapitulate *her1* expression in both the anterior and posterior PSM, though there was ectopic expression in the notochord (Gajewski *et al.* 2003). This ectopic expression was attributed to a notochord repressor region not included in the 8.6kb region. Further culling of this enhancer demonstrated that the first 5kb in the 5’ edge drives posterior expression of *her1*, while the next 500bp drives anterior stripe expression. They saw oscillating reporter transcripts through *in* situ hybridization that matched *her* expression, but the use of GFP as a reporter resulted in broad expression of the fluorophore. This was interpreted as reflecting the greater stability and perdurance of GFP protein compared to Her1. Another study explored the 3.3kb upstream of *her1* more carefully, searching for binding sites that regulated proper expression (Brend and Holley 2009). *Cis*-regulatory elements were identified that controlled oscillating expression, including binding sites for Her proteins, Tbx24, and Suppressor of Hairless (a component downstream of Notch). These proteins were shown to bind *in vitro*, and abolishment of these sites caused disruption of the anterior PSM expression of *her1*. Brend *et al.* noted that the expression pattern they observed did not fully overlap with *her1* expression, suggesting that this region was insufficient to recapitulate anterior *her1* expression. The proper expression of *her1* may rely more on regulation in the posterior PSM, rather than the anterior. They also found evidence that this anterior control region repressed *her1* function in the formed somites (Brend and Holley 2009).

Promoter analysis has also been done in mice, analyzing the upstream regions of *Hes1* (Sasai *et al.* 1992), *Hes7* (Bessho *et al.* 2001) and *Lfng* (Morales *et al.* 2002). N-box and E-box binding sites were identified to be targets of the *Hes* genes, causing transcriptional repression (Sasai *et al.* 1992; Bessho *et al.* 2001). Oscillations in *Lfng* also rely directly on Notch binding RBP-J sites in its upstream promoter (Morales *et al.* 2002). To test the role of the Notch pathway, a constitutively active form of Notch was co-expressed with a reporter driven by fragments of the *Hes* promoters. This caused an upregulation of *Hes7* expression, with similar activity observed in *Hes1* (Bessho *et al.* 2001). A 400-bp region upstream of *Hes7* has recently been shown to be essential, containing *Tbx6* and *Lef1* (a Wnt pathway transcription factor) binding sites (Gonzalez *et al.* 2013). Treatment with a *Gsk3* inhibitor blocks the Wnt pathway, and extends the oscillatory period of *Hes7* (Gonzalez *et al.* 2013). Genetic analyses and binding assays have emphasized the importance of Notch, Wnt, FGF, and T-box regulation in properly driving clock expression.

Besides periodic regulation of these clock genes, the lifespan of the transcripts and proteins also play an important role in inducing oscillatory expression. Work done in amniotes has helped build our understanding of these short-lived molecules. The untranslated regions (UTR's) of cyclic transcripts are essential to the short, periodic lifespans of clock genes: while reporter lines with the *Lfng* 3' UTR degraded quickly, reporters with the viral SV40 UTR were much more stable (Chen *et al.* 2005). In chicks, they also tested the role of post-transcriptional regulation by flanking a GFP reporter with the endogenous *Lfng* 5' and 3' UTRs and compared the rates of degradation with those of the *Fgf8* UTRs, a much more stable transcript (Hilgers *et al.* 2005). They saw that *Lfng* UTRs were sufficient to destabilize the reporter. Some work has suggested that the regulation of cyclic transcripts may in part be due to targeting by microRNAs such as *mir-125a-5p* (Riley *et al.* 2013), supporting the theory that the rapid turnover of clock expression is partially due to the degradation of the transcript. In zebrafish, both *her1/her7* transcripts and proteins have a rapid turnover rate. A heatshock line driving *her1* (along with its endogenous 3'UTR) showed degradation of the HA-tagged protein within five minutes and the transcript within half an hour (Giudicelli *et al.* 2007). The rapid turnover of these *hairy*-related proteins may be due to the presence of abundant lysine-residues, known targets of ubiquitination and subsequent degradation. While normal *Hes7* proteins have a half-life of approximately 22 minutes, deletions of the lysine residues in the protein causes the lifespan to increase up to 50% (Hirata *et al.* 2004). Modeling of the segmentation clock has shown that repressor activity must have a half-life of no longer than 6 minutes in order to oscillate within PSM cells (Ay *et al.* 2013).

A few studies have looked at the mechanisms controlling the rates of clock expression and degradation. Delays in transcription and translation have been predicted in the auto-inhibitory loop model of clock expression (Lewis 2003). To see which of these factors contributed most to the delays necessary to cause an inhibitory feedback loop, the Lewis group measured the rate of polymerase transcription in PSM cells (Hanisch *et al.* 2013). They created a transgenic line that had an artificial 21kb intron inserted into *her7*. They performed high-resolution *in situs* that assayed for two portions of the intron ~10kb apart. They could then measure the distance between the appearance of the two signals and estimate the time it took for the polymerase to cover the 10kb distance. Surprisingly, the polymerase moved much quicker than measured in cell culture, transcribing 4.8kb per minute. This rapid transcription rate meant that the delays required for auto-inhibitory clock oscillations were not due to transcription, but from another source. Delays calculated from mice and chicks have shown that this transcription speed varies based on the periodicity of the clock within the species, but that the main contribution to the delays in cycling of genes such as *Hes7* and *Lfng* come from post-transcriptional processing and export (Hoyle *et al.* 2013). Work in mice has shown that the introns in *Hes7* are essential in driving clock oscillations and properly forming somites (Takashima *et al.* 2011; Harima *et al.* 2012). A transgenic line of *Hes7* was generated that deleted the three introns from the gene (Takashima 2011). Using a clock reporter, they found that this deletion caused the clock to cycle 19 minutes faster. Embryos with this missing-intron version of *Hes7* knocked into the wildtype *Hes7* loci had severe developmental defects, failing to segment properly and correlating with a loss of proper *Hes7* cycling in the PSM. This intron-less version of *Hes7* was unable to rescue *Hes7*-null mice, while a version of *Hes7* that includes the introns was rescue the nulls (Takashima *et al.* 2011). In a follow-up work, they found that combinatorial deletion of different introns would generate some mice that were viable, but with a higher number of vertebrae (Harima *et al.* 2012). The change in introns changed the kinetics of clock cycling, causing it to cycle faster and creating a greater number of somites that were smaller in size. Together, these works have helped define where the delays in the clock occur: transcription rates seem to be relatively quick, and most of the delays come from post-transcriptional intron splicing and export.

After the transcript is processed and exported, the lifespan of the transcript is an important element of controlling clock expression. If these transcripts are not degrading at a rapid rate, their persistence could interfere with the proper cycling of the clock. A mutant was identified in zebrafish that was defective in clock transcript degradation (Dill and Amacher 2005). Through ENU-mutagenesis, the *tortuga* mutant was identified as being responsible for degrading cyclic *her1* transcripts. When *her1* expression was assayed in *tortuga* mutants using an intronic probe, clock expression was normal. But assays using exonic probes showed a persistence of *her1* transcript for much longer than in wildtype embryos. Somites form normally, but defects are observed later as muscle fibers fail to properly elongate (Dill and Amacher 2005) although careful analyses have since shown that fewer somites form in *tortuga* mutants (Amacher lab, unpublished data). Unpublished work has shown that the *tortuga* mutant is actually a large deletion of the genome, which accounts for the varying phenotypes of mutant embryos that extend beyond segmentation. Careful analyses of genes in this deleted region have suggested that *pnrc2* is responsible for the failure to degrade *her1* transcripts (Amacher lab, unpublished data). *pnrc2* is a known player in catabolism of nuclear-transcribed mRNAs and nonsense-mediated decay (Cho *et al.* 2009; Cho *et al.* 2012).

The oscillatory nature of the segmentation clock relies on precise delays in generating clock transcripts and proteins, as well as a well-regulated, short lifespan of these molecules. Disruptions in this timing disrupt the cyclic behavior of segmentation clock genes, subsequently causing issues in somitogenesis. The proper expression in the clock is regulated at many levels, and they must all work in concert for the clock to correctly cycle.

Molecular Components of the Wavefront

As these waves of clock expression sweep through the developing PSM, how are they being translated into discrete segments? The second half of Cooke and Zeeman's model of somitogenesis is a wavefront, a positional signal that helps determine when PSM cells transition into somites (reviewed in Aulehla and Pourquié 2010). This determination front was first identified through an inversion experiment, where small pieces of PSM were removed, inverted, and grafted back into a chick embryo (Dubrulle *et al.* 2001). They found that grafts in the posterior PSM (before S-2) were naïve, and could adjust so that the proper somite polarity developed in these cells despite the inversion. More anterior PSM cells were committed to their fate, forming inverted somites after they were inverted via microsurgery. This determination front at S-2 was consistent with the activation of adhesion molecules, which drive the transition of mesenchymal PSM cells to epithelial somitic cells (Linask *et al.* 1998; Horikawa *et al.* 1999). A posterior-to-anterior gradient of *FGF8* was observed in the tailbud, with higher levels in the posterior PSM compared to the anterior (Dubrulle *et al.* 2001). This gradient of FGF was also observed in mice and zebrafish (Dubrulle and Pourquié 2004; Sawada *et al.* 2001). This gradient is caused by a production of *FGF8* transcripts in the tailbud and gradual degradation of these transcripts as PSM cells were displaced anteriorly (Dubrulle and Pourquié 2004). Intronic probes for *FGF8* only label transcript in the tailbud, while exonic probes detect a gradient of transcripts from the tailbud into the anterior PSM (Dubrulle and Pourquié 2004). The FGF8 protein persists even longer than the transcript, creating a gradient of FGF8 across the entire PSM. When FGF8 expression is increased through electroporation or FGF-soaked beads, PSM cells are seen to preserve their caudal fate or form smaller somites (Dubrulle *et al.* 2001). Pharmacological treatment of embryos using the FGF inhibitor SU5402 results in larger somites, indicating that the FGF gradient originates from the posterior (Dubrulle *et al.* 2001; Sawada *et al.* 2001). There is at least some redundancy in FGF activity in the tailbud; in zebrafish, knockout of *fgf8* or *fgf24* individually has no effect, but the knockout of both causes the failure of posterior mesoderm formation (Draper *et al.* 2003).

A Wnt gradient was also detected to emanate from the tail bud in mice (Aulehla *et al.* 2003; Dunty *et al.* 2008; Aulehla *et al.* 2008). This Wnt gradient generates a β-catenin gradient, and both were shown to be necessary to induce the FGF gradient (Aulehla *et al.* 2008). When a constitutively active version of β-catenin is expressed throughout the PSM, there is an expansion of the posterior PSM, with genes such as *Fgf8, Axin2,* and *Msgn1* having expanded domains of expression (Aulehla *et al.* 2008). Interestingly, the oscillations of cyclic Wnt pathway components seem independent of these gradients, and the expansion of the Wnt gradient is not enough to abolish Notch pathway oscillations (Aulehla *et al.* 2008; Dequeant and Pourquié 2008).

In concert with these two posterior gradients, a retinoic acid (RA) gradient originates from the anterior PSM and formed somites. RA synthesis occurs in the anterior region of the PSM and not in the posterior PSM, creating a gradient of RA detectable by an RA-responsive reporter (Niederreither *et al.* 2002; Vermot *et al.* 2005). A loss of RA synthesis causes bilateral asymmetries in somite formation, though somitogenesis nevertheless can progress (Niederreither *et al.* 2002; Vermot *et al.* 2005). Drug treatments of transplanted PSMs with RA agonists reduce the domain of the FGF gradient, while treatments with FGF-soaked beads cause a reduction of the RA domain and a reduction of somite size (Diez del Corral *et al.* 2003).

Together, these opposing gradients of RA versus Wnt and FGF set up a critical region in the PSM known as the determination front. The relatively low levels of these gradients create a bistability window, where cells can commit to transition from undifferentiated PSM to somites

(Aulehla and Pourquié 2010). Because these molecules are only produced at the anterior/posterior edges of the PSM, their constant degradation causes the determination front to progress posteriorly as the embryo extends in length. This preserves the relative position of the determination front even though cells in the PSM are constantly being displaced anteriorly by the extending tailbud. This determination front can be marked using the gene *Mesoderm Posterior* (*Mesp*). In mice, *Mesp2* is necessary for somite polarity formation: mice mutant for *Mesp2* generate somites with only caudal fates, exhibit fused vertebrae, and do not survive (Saga *et al.* 1997). A stripe of *Mesp2* expression appears at the determination front, around S-2 or S-1 (Saga *et al.*1997; Takahashi *et al.* 2000). *Mesp* expression requires RA signaling (Moreno and Kintner 2004) and is suppressed by high levels of FGF (Delfini *et al.* 2005). The stripe of *Mesp2* is also shifted anteriorly when a higher level of Wnt is expressed (Aulehla *et al.* 2008). These data strongly indicate that *Mesp* plays an important role in defining the determination front and signaling the transition of PSM cells into somites.

This readout of the determination front is useful in understanding how the clock and wavefront interact. Early analyses of two *mesp* genes in zebrafish, *mespa* and *mespb*, demonstrated a clear connection between the wavefront readout and the segmentation clock genes (Sawada *et al.* 2000). *mespa* and *mespb* are expressed in two distinct bands in the anterior PSM, spaced about one somite-length apart at S-1 and S-2. Embryos mutant for Notch component *dlc* and *tbx6* show diffuse *mesp* expression, suggesting that these two pathways regulate *mesp*. Overexpression of *mespb* also causes segmental defects, with asymmetries in somite formation and a reduced anterior domain of *her1* expression. When *her1* and *mespb* are examined in double *in situs*, they appear to have correlated expression patterns: each band of anterior *her1* expression is directly posterior to the thin stripe of *mespb* expression, but do not overlap. As each stripe of *her1* sweeps anteriorly through the PSM, the stripes of *mespb* appear to move with it (Sawada *et al.* 2000). In mice, *Mesp2* has been implicated in helping determine somite formation. The loss of *Mesp2* in mice causes caudalization of the embryo, while overexpression of *Mesp2* causes somites to acquire a rostral fate (Dahmann *et al.* 2011). *Mesp2* reacts to clock and wavefront components, including the Notch intracellular domain (NICD) and Tbx6 (Aulehla *et al.* 2008; Oginuma *et al.* 2008). *Mesp2* expression in S-1 cells occurs in a simultaneous manner, though loss of Notch oscillations cause *Mesp2* to be expressed in a "salt and pepper" pattern (Oginuma *et al.* 2010). An *in vivo* reporter of *Mesp2* was generated by Niwa *et al.* (2011), where they used it to test the response of the determination front to FGF and Notch signals. They found that while Notch oscillations swept progressively from the posterior to anterior PSM, oscillations of FGF in the posterior PSM were simultaneous. *Mesp2* reacts to manipulations of both the FGF and Notch pathway: *Hes7* knockouts causing constitutive expression of *Mesp2* while knockout of FGF receptors through drug treatments causes precocious *Mesp2* expression (Niwa *et al.* 2011).

Complex gradients and mechanisms control the signaling of positional information in the PSM. How exactly these gradients interact with the oscillating segmentation clock is an outstanding question, and investigations in their interactions will reveal the mechanisms regulating this robust developmental process.

Imaging the Segmentation Clock *in vivo*

Much of the work in fixed embryos has been limited by the lack of temporal resolution. To address this problem, several attempts have been made to capture behavior of the segmentation clock in real time. The first *in vivo* reporter was described in mice, based on the mouse *Hes1* clock gene (Masamizu *et al.* 2006). Two clock reporter lines were generated, both using the 2.5kb upstream of *Hes1* to drive two versions of a destabilized reporter, luciferase fused with either one or two ubiquitin moieties. Both reporters showed oscillatory behavior, but the one with two ubiquitin moieties oscillated with a period more similar to the endogenous *Hes1* protein, and was used for the rest of their studies. Cell lines transfected with this reporter showed oscillating gene expression for up to 36 hours in about half the cells (Masamizu *et al.* 2006). A stable transgenic line was generated in mice, and cultured PSMs recapitulated clock behavior in real time: sweeping waves of clock expression began in the posterior PSM and moved anteriorly with a periodicity that matched that of somite formation. When the PSM was disassociated, individual cells continued to oscillate; these oscillations were not nearly as robust compared to an intact embryo, however, and after a few oscillations had a tendency to cycle more randomly or stop completely (Masamizu *et al.* 2006). A version of this reporter was generated for another study using *Hes7*. In order to test the role of introns in delaying clock oscillations, a version of the reporter was generated that included the 2kb of introns found in the endogenous *Hes7*. This iteration of the reporter oscillated with a longer periodicity than the intron-less version of the reporter. Another study also imaged the real-time behavior of another cycling gene in mice, *Lfng* (Aulehla *et al.* 2008). They constructed their reporter by using the fast-folding fluorophore Venus, fused with a destabilizing PEST sequence, and driven with the 2kb upstream of *Lfng*. They saw results similar to that of the *Hes1* reporter: a wave of cyclic gene expression swept up the PSM with a periodicity that matched that of somite formation. Even in the background of a constitutively-active β-catenin, this reporter continued to cycle, albeit with a weaker amplitude of expression (Aulehla *et al.* 2008).

A review of these *in vivo* reporters stressed the limitations of exploring such a dynamic process in the mouse model (Soroldoni and Oates 2011). One major problem was that these mouse PSMs had to be cultured *ex vivo* for up to ten hours, a stressful process for the tissue and the scientist. They also noted that the low level of expression required high exposure times and pixel binning, resulting in poor spatial and temporal resolution. They also suggested that the magnification and numerical aperture of the microscopes could be improved (Soroldoni and Oates 2011). Clearly, an *in vivo* reporter with higher resolution would be beneficial in studying the more nuanced processes of segmentation.

Biological Clocks in Systems with Longer Periods

The segmentation clock is not alone as an oscillating gene network driving a developmental process. Another well-known example is how cyclic gene expression drives root branching in *Arabidopsis*. Lateral roots are known to sequentially branch off from the main root in a periodic fashion. To study this phenomenon, researchers designed a luciferase reporter to follow the expression of DR5, a regulatory sequence that is responsive to auxin, a plant growth hormone. (Moreno-Risueno *et al.* 2010). They found that DR5 was activated at the prebranch site of future lateral root formation, with a new branch marked by DR5 every ~6 hours. Eventually, lateral roots formed and the primary root bent at these sites of expression. Similar to microarray experiments done in vertebrates, Moreno-Risueno *et al*. searched for and found two oscillating gene networks, one oscillating in phase with DR5 and one oscillating in anti-phase. They validated this through luciferase reporters as well (Moreno-Risueno *et al.* 2010). Plant growth is also regulated by the circadian rhythm, with high levels of protein accumulation at night and high levels of transcription by a circadian clock-regulated process promoting growth faster growth in plants (Dodd *et al.* 2005, Nozue *et al.* 2007). This differential regulation by the circadian clock may actually provide an evolutionary advantage in the cases of hybrid and allopolyploid plants (Ni *et al.* 2009).

Circadian mechanisms are well-documented in a wide range of biological processes, including longevity and immunity. A circadian clock mutant in mice, called *after hours*, causes the circadian cycle to intrinsically extend to 27 hours rather than the normal 24 hours (Godinho *et al.* 2007). Variations of circadian clocks that are greater or less than 24 hours have shown a 20% decrease in lifespan compared to more accurate clocks (Libert *et al.* 2012). Proper clock function has also been implicated in plant immunity. The *circadian clock-associated 1* gene is necessary to anticipate the spread of pathogens at dawn (Wang *et al.* 2011). Similarly in *Drosophila*, individuals infected by pathogens at night survive better than flies infected during the day (Lee *et al.* 2008). There has also been evidence that the cycles of metabolism and circadian clock align, though some new observations note that these two clocks may be independently derived (Rey and Reddy 2013).

A longer biological clock, a seasonal timer, has also been explored. Certain seasonal preparations take an extended amount of time, such as storing food, growing extra fur, and completing spermatogenesis. Several methods have been employed by various organisms to measure the seasons, including an interval timer that measures day length and a circannual clock that can intrinsically measure the season without daily influence from the environment (Paul *et al.* 2008). These various biological clocks are evidence of the importance of temporal control in biology.

Chapter 2

Single-Cell-Resolution Imaging of the Impact of Notch Signaling and Mitosis on Segmentation Clock Dynamics

Summary

Vertebrate body segmentation is controlled by the segmentation clock, a molecular oscillator involving transcriptional oscillations of cyclic genes in presomitic mesoderm cells. The rapid and highly dynamic nature of this oscillating system has proved challenging for study at the single-cell level. We achieved visualization of clock activity with a cellular level of resolution in living embryos, allowing direct comparison of oscillations in neighbor cells. We provide direct evidence that presomitic mesoderm cells oscillate asynchronously in zebrafish Notch pathway mutants. By tracking oscillations in mitotic cells, we reveal that a robust cell-autonomous, Notch independent mechanism resumes oscillations after mitosis. Finally, we find that cells preferentially divide at a certain oscillation phase, likely reducing the noise generated by cell division in cell synchrony and suggesting an intriguing relationship between the mitotic cycle and clock oscillation.

Introduction

In vertebrates, the metameric vertebrae and axial muscles are derived from repeated mesodermal segments, called somites, which form from the presomitic mesoderm (PSM) during embryogenesis. As a result of gastrulation and tail elongation, the PSM progressively extends by entry of new cells in its caudal part. At the same time, somites are sequentially pinched off from its anterior part and deposited along the anterior-posterior axis. A striking feature of PSM segmentation is its spatial and temporal periodicity. Somitogenesis is controlled by a molecular oscillator, called the segmentation clock, that cycles within the PSM with the same period as somite formation (Oates *et al.*, 2012; Pourquié, 2011). According to the ‘‘clock and wavefront’’ model and its modern variations, somite periodicity and total somite number are determined by the clock interacting with a positional signal called the wavefront. The position of the wavefront is set by global gradients across the anterior-posterior axis of the embryo and moves posteriorly as the tailbud extends. Future somite boundaries become specified in the PSM when a group of neighboring cells in the permissive phase of the clock encounters the wavefront (Cooke and Zeeman, 1976; Oates *et al.*, 2012; Pourquié, 2011).

Much progress has been made in understanding the molecular nature of the segmentation clock. The activity of a molecular oscillator in the PSM was revealed by the striking discovery of the first ‘‘cyclic’’ gene, *cHairy1*, a member of the hairy and Enhancer-of-split related family (Palmeirim *et al*., 1997). Since then, it has been established that other vertebrate *Hes/her* genes also cycle, along with additional genes of the Notch, FGF, and Wnt signaling pathways (Oates *et al.*, 2012; Pourquié, 2011). Typically, the expression of cyclic genes in fixed embryos presents as stripes in the anterior PSM and homogenous staining, of variable intensity from one embryo to another, in the posterior PSM. Careful analysis of multiple fixed embryos and, more recently, real-time live imaging, have revealed that waves of cyclic gene expression originate in the posterior PSM at the same pace as somite formation and move anteriorly across the PSM (Aulehla *et al.*, 2008; Masamizu *et al.*, 2006; Oates *et al.*, 2012; Takashima *et al.*, 2011). The expression pattern of cyclic genes within individual PSM cells over time has been inferred from these observations, assuming that very little cell movement takes place once cells internalize into the PSM. First, cells entering the posterior PSM oscillate with the same period as somite formation, and do so in synchrony with their neighbors. The oscillations then slow down as the cells reach the anterior PSM, and stop upon somite formation. The slowing of oscillations creates small delays between cells and results in stripes of cyclic gene expression in the anterior PSM. Thus, the clock is composed of a multitude of elementary oscillators, the PSM cells, which are finely coordinated with each other.

Oscillation dynamics and coordination appear to be controlled by a complex genetic and biochemical network, although the exact nature of this network remains unknown and likely varies from one organism to another (Oates *et al.*, 2012; Pourquié, 2011). A conserved feature in vertebrates is the involvement of cycling *Hes/her* transcriptional repressors (Krol *et al.*, 2011). It has been suggested that a negative feedback loop created by Hes/Her proteins downregulating their own transcription generates alternating oscillations of proteins and transcripts, constituting a core cell-autonomous mechanism that is essential for clock oscillations (Bessho *et al.*, 2003; Hirata *et al.*, 2002; Giudicelli *et al.*, 2007; Lewis, 2003; Takashima *et al.*, 2011). Notch signaling is also largely implicated in the clock regulation, because *Hes/her* genes are Notch targets and somites are disrupted when Notch signaling is impaired (Oates *et al.*, 2012; Pourquié, 2011). Because Notch receptors are activated in one cell by ligands of the Delta/Jagged/Serrate family on adjacent cells, Notch was proposed to be essential for coupling PSM cell oscillations, although its precise role as an initiator or synchronizer of the clock is still debated (Holley, 2007; Lewis *et al.*, 2009; Oates *et al.*, 2012; Pourquié, 2011). In zebrafish, embryos with impaired Notch signaling display defects of somite boundary formation and ‘‘salt and pepper’’ expression of cyclic genes, although the first anterior-most somites do form normally (Holley, 2007). These defects have been interpreted as evidence that PSM cells cycle but progressively fall out of synchrony in the absence of Notch signaling, suggesting a role for Notch signaling in synchronizing oscillations in PSM cells (Horikawa *et al.*, 2006; Jiang *et al.*, 2000; Mara *et al.*, 2007; Ozbudak and Lewis, 2008; Riedel-Kruse *et al.*, 2007).

Many insights into segmentation clock regulation have been obtained via transcript detection in fixed embryos (Giudicelli *et al.*, 2007; Horikawa *et al.*, 2006; Mara *et al.*, 2007; Soroldoni and Oates, 2011). Because the oscillation period is short, ranging from ~30 min in zebrafish to 2 hr in mouse, the real-time reporters required to investigate clock dynamics have proved to be an extreme technical challenge (Soroldoni and Oates, 2011). The current mouse reporter strategies allow visualization in real time with tissue-level resolution (Aulehla *et al.*, 2008; Masamizu *et al.*, 2006; Takashima *et al.*, 2011). Imaging the clock in vivo at a single-cell level of resolution is crucial for understanding how the clock activity is precisely related to cell oscillations, and how oscillations are coordinated between PSM cells.

Here, we present a real-time reporter of zebrafish segmentation clock dynamics and a semi-automated three-dimensional (3D) cell tracking and analysis program that allowed us to image clock dynamics with single-cell resolution in the developing PSM. We describe how PSM cells oscillate over time in wild-type (WT) embryos. We show that Notch pathway mutant cells oscillate but are largely out of phase with neighboring cells, providing direct evidence for the role of Notch signaling in clock synchronization. Strikingly, we show that after mitosis, sibling cells oscillate in tight synchrony in wild-type and Notch pathway mutant embryos, highlighting the cell-autonomous and Notch-independent nature of segmentation-clock oscillation resumption after mitosis. Finally, we show that mitosis, a source of biological noise in this system (Horikawa *et al.*, 2006; Zhang *et al.*, 2008), occurs most frequently during the ‘‘off phase’’ of the Her1 oscillation wave, suggesting that regulation of mitosis and clock expression are mechanistically linked.

Results

Live Imaging of Segmentation Clock Activity with Single-Cell Resolution

To investigate the dynamic mechanism of the clock, we developed tools for measuring oscillations in individual PSM cells in living zebrafish embryos. To develop a dynamic reporter that would be compatible with the short periodicity of zebrafish segmentation, we fused the fast-folding yellow fluorescent protein Venus (Nagai *et al.*, 2002) to the C terminus of the Her1 protein, anticipating that destabilization sequences within the Her1 protein would similarly destabilize the fusion protein (Hirata *et al.*, 2002, 2004; Figure 2.1A; Figure 2.2). We used a previously characterized 8.6 kb upstream her1 regulatory region (Gajewski *et al.*, 2003) to drive cyclic expression of Her1-Venus fusion protein, and 1.1 kb of downstream sequence (including the her1 3'UTR and her1 polyadenylation site to mimic endogenous her1 transcript dynamics as closely as possible; Chen *et al.*, 2005; Ozbudak and Lewis, 2008) to generate a stable *Tg(her1:her1-venus)*^{bk15} line (Figure 2.2A). In situ hybridization and immunochemistry in heterozygous transgenic embryos revealed that the reporter transcript and protein are cyclically expressed (Figures 2.1B–2.1D) and oscillate out of phase with each other (Figure 2.1E), consistent with the negative feedback loop proposed for Her cyclic regulation (Giudicelli *et al.*, 2007; Lewis, 2003). As expected for a transcription factor, the Her1-Venus reporter protein localizes to the nucleus. Live time-lapse confocal imaging (Figure 2.1F; Movie S1) reveals that waves of cyclic expression emanate posteriorly and travel anteriorly, and cease when they reach the forming somite boundary.

Expression of other tested reporters was either too stable or non-detectable (Figure 2.2). Fusion of Venus to the N terminus of Her1 protein produced a reporter protein that persisted in the newly formed somites even though the reporter was no longer transcribed, suggesting that the Her1 N terminus is essential for instability (Figures 2.21B, 2.2E, and 2.2E'). A Venus-PEST protein identical to the reporter used by Aulehla *et al.* (2008) for real-time imaging of mouse segmentation clock was also too stable for imaging zebrafish clock oscillations (Figures 2.2C, 2.2F, and 2.2F'). On the other hand, although appending ubiquitin moieties to the N terminus of Venus, in a strategy similar to the one used by Masamizu *et al.* (2006) for imaging the mouse clock, produced a reporter protein with a striped pattern comparable to that of her1 expression in fixed embryos (Figures 2.2D, 2.2G, and 2.2G'), we were unable to detect reporter signal by confocal microscopy (data not shown). Compared with other constructs, the Her1-Venus reporter thus constituted an ideal combination of stability and signal intensity.

Because Hes/Her proteins are thought to negatively regulate their own expression (Brend and Holley, 2009; Giudicelli *et al.*, 2007; Hirata *et al.*, 2002; Lewis, 2003), we tested whether expression of the Her1-Venus fusion protein influenced the endogenous clock. Expression of *her7* cycles similarly in wildtype and heterozygous *Tg(her1:her1-venus)* embryos, although her7 stripes are slightly more diffuse in the latter (Figures 2.1G, 2.1G', 2.1J, and 2.1J'). Expression of *deltaC* (*dlc*), another cyclic gene, and *mespa*, a clock readout, are indistinguishable between WT and heterozygous *Tg(her1:her1-venus)* embryos (Figures 2.1H, 2.1H', 2.1I, 2.1K, 2.1K', and 2.1L), except that the angle between PSM stripes and notochord is broader in transgenic embryos. The slight differences in gene expression do not impact somite periodicity, which is the same in wild-type and heterozygous *Tg(her1:her1-venus)* embryos (Figure 2.1M).

Homozygosity of the reporter transgene does appear to have some impact on the clock. Somite periodicity is slowed (Figure 2.1M) and total segment number is decreased (Figures 2.1N and 2.1O), consistent with a direct relationship between segmentation speed and somite number. In addition, *her7* gene expression is noticeably dampened in the anterior (but not posterior) PSM (Figures 2.3A, 2.3A', 2.3D, and 2.3D'). Despite these differences, *dlc* and *mespa* expression are almost normal in homozygous *Tg(her1:her1-venus)* embryos (Figures 2.3B, 2.3B', 2.3C, 2.3E, S2E', and 2.3F'). To minimize any impact on endogenous clock function, we performed all subsequent analyses on heterozygous *Tg(her1:her1-venus)* embryos.

To analyze reporter expression in individual cells, we injected transgenic embryos with membrane mCherry and histone H2A-Cerulean encoding mRNAs to serve as membrane and nuclear landmarks, respectively (Figures 2.4A and 2.4B), and imaged embryos for 4–6 hr beginning at the 8- to 12-somite stage by confocal microscopy (Movie S2, top left corner). Z-stacks of ~30 images were acquired every 4 min. To efficiently process and analyze the large volumes of imaging data, we developed a MATLAB program to automatically track individual presomitic cells. Individual cell contours were predicted across three dimensions based on shape and fluorescence patterns (Keller *et al.*, 2008) and linked across time points (Sbalzarini and Koumoutsakos, 2005; Figure 2.4C). The reporter fluorescence of each cell was then quantified based on intensity within the predicted nuclear contour (Figure 2.4D). Because of the high nucleus-to-cytoplasm ratio of PSM cells, some errors in the prediction of cell contours occurred, especially along the z-axis, for which spatial resolution is lower. We thus created a graphical user interface to manually validate and, if needed, correct each cell. It also allowed us to label tracked cells with specific properties, such as mitotic cells, for use in subsequent analyses (Figure 2.5). Cells were only validated if it was possible to track them throughout the entire movie. We calculated the phase at each time point of each ''validated cell'' oscillation using a smoothing heuristic (Figures 2.4E and 2.4F) and used it in subsequent analyses.

Last Oscillation Occurs in S-1 and Lasts about Twice the Period of Somite Formation

We tracked and validated the fluorescence intensity of 50–100 PSM cells per time-lapse movie for three embryos that were wild-type apart from the presence of the reporter transgene. The somitogenesis period was lengthened by lowering the temperature to 22°C-23°C (Schroter *et al.*, 2008), which allowed us to obtain enough time for z-stack image acquisition between consecutive time points and to potentially increase the reporter lifetime. Because each embryo was imaged separately and the temperature might vary slightly among imaging experiments, we did not compare cells between movies or calculate exact periods; instead, we made observations and comparisons within a given embryo.

Most of the robust oscillations we detected occurred in the S-3 to S0 region of the PSM (encompassing four anterior-most presumptive somites; Figure 2.6A). Although they were weaker in intensity, robust oscillations were also detected in a number of cells located as far as S-6. Our analyses reveal that cells oscillate in the posterior PSM with a period equivalent to that of somite formation (Figure 2.6A'), as expected from analysis of cyclic gene expression patterns in fixed embryos (Giudicelli *et al.*, 2007; Sawada *et al.*, 2000). The clock period lengthens during the second to last oscillation, at the level of S-2, coinciding with expression of the first markers of anterior-posterior somite patterning (Sawada *et al.*, 2000). During the last oscillation, the signal peaks in S-1 and decreases in S0, with a pseudo-period at the peak that is almost twice the period of somite formation (Figure 2.6A''). The higher fluorescence intensity in anterior relative to posterior PSM cells may result from stronger expression, reduced degradation rate, and/or mechanisms that increase the length of the clock pseudo-period in the anterior PSM and give the reporter more time for maturation and accumulation.

PSM Cells Oscillate in Notch Pathway Mutants and Do So Asynchronously

In situ hybridization analyses have revealed that when Notch signaling is disrupted in zebrafish, cyclic genes are expressed in the PSM in a salt-and-pepper pattern instead of clear stripes (Holley, 2007). This has been interpreted to mean that PSM cells still oscillate, albeit asynchronously, in the absence of Notch signaling (Jiang *et al.*, 2000; Lewis, 2003; Mara and Holley, 2007). To directly address whether Notch signaling is required to maintain synchronous clock expression among neighboring cells, we crossed the segmentation clock reporter into the *beamter* (*bea/deltaC*), *deadly seven* (*des/notch1a*), and *after eight* (*aei/deltaD*) mutant backgrounds. We confirmed that the Venus reporter is expressed in a speckled pattern in fixed embryos, similarly to expression of cyclic genes in Notch pathway mutants (Figure 2.7). Time-lapse analysis and cell tracking revealed that cells do oscillate in the absence of Notch signaling (Figures 2.6B–2.6D; Movie S2).

By pseudo-coloring PSM cells using a color map (Figure 2.6E) indicating phase of oscillation, we obtained snapshots of cell oscillation dynamics relative to position (Figures 2.6F–2.6I) at any given time point. Notch pathway mutant embryos lack the smooth transitions that are indicative of the neighbor-cell synchrony normally observed in wild-type embryos (Figures 2.6E–2.6I; Movie S3). To analyze synchrony on a global scale, we compared the phase of Venus expression for each cell relative to its direct neighbors. To that end, we automatically sorted all possible pairs of validated cells separated by <10 mm (approximately one cell diameter) and calculated the phase difference (‘‘phase shift’’) between cells for each pair of direct neighbors. By computing the phase shift for all validated cell pairs at all time points, we obtained a total of 2,935–19,180 comparisons per embryo, all of which were plotted onto a histogram (Figures 2.6J–2.6M). In wild-type embryos (Figure 2.6J), there is a strong bias toward little or no phase shift (phase shift close to zero), with very few neighbors being in anti-phase (phase shift close to π). A small proportion of desynchronized (anti-phase) cells are expected, for example at segment borders in the anterior PSM. By contrast, Notch pathway mutants were desynchronized (Figures 2.6K-2.6M). Together, these data directly demonstrate that PSM cells cycle asynchronously in the absence of Notch signaling, providing critical support for the role of Notch signaling in the maintenance of neighbor-cell oscillation synchrony.

Most Dividing Cells Undergo Temporary Disruptions in Oscillation Synchrony

Synchrony maintenance in a group of molecular oscillators has been proposed to be essential for counteracting biological noise (Horikawa *et al.*, 2006; Lewis, 2003; Masamizu *et al.*, 2006; Riedel-Kruse *et al.*, 2007). Mitosis has been proposed to be a significant source of noise in oscillating systems (Horikawa *et al.*, 2006; Zhang *et al.*, 2008). Using our segmentation clock reporter, we examined oscillations in sibling cells after mitosis, relative to each other and their neighbors in real time (Figures 2.8A and 2.8B). During division, some cells maintain surprisingly synchronous oscillations with neighbors throughout mitosis (Figures 2.8A and 2.8C; 20% of mitotic events). However, most cells become delayed relative to neighbors following mitosis (Figures 2.8B and 2.8C; 60% of mitotic events), or temporarily display erratic oscillations or no cycling (Figure 2.8C; 20% of mitotic events), which is entirely consistent with the idea of mitosis-induced noise. Measuring synchrony of cells with their neighbors at different times after mitosis shows that the proportion of daughter cells that oscillate in synchrony with their environment increases over time, as anticipated from the existence of a mechanism for synchrony maintenance. The large majority of recently divided cells resynchronize with their respective neighbors within two oscillation cycles (Figures 2.8C and 2.9), consistent with previous estimates (Horikawa *et al.*, 2006).

After Mitosis, Sibling Cells Oscillate in Tight Synchrony with Each Other in Wild-Type and Notch Mutant Embryos

Although synchrony between a dividing cell and its neighbors can be variable, we noticed that siblings are strikingly synchronous over time (Figures 2.8A and 2.8B). By collectively examining mitotic events and comparing the phase of a recently divided cell at every time point after division with the phase of either its sibling or its neighbors (and between non-dividing neighbors as controls), we observed a clear difference between sibling-sibling synchrony and sibling-neighbor synchrony (Figure 2.8D). This global phase-shift analysis confirmed that siblings were significantly more synchronized with each other than with their neighbors (two-tailed t test, $\alpha = 0.05$, $p < 10^5$).

To analyze whether sibling cells might be synchronized by signals received from their shared neighbors, we followed sibling oscillations in Notch pathway mutants, where cell divisions occur in a largely asynchronous background (Figure 2.6). As observed in wild-type embryos (Figure 2.8D), Notch pathway mutant sibling cells were significantly more synchronized with each other than with their neighbors, or than non-dividing cells are with neighbors, in all genotypes tested (two-tailed t test, $\alpha = 0.05$, $p < 10^5$; Figure 2.10 and data not shown). Thus, although blocking mitosis in Notch pathway mutants can delay the onset of global asynchrony (Zhang *et al.*, 2008), mitotic events in Notch pathway mutants that occur once global asynchrony has occurred actually generate a pair of tightly synchronous cells. A comparison of sibling oscillation phases at different times after mitosis revealed that most siblings remained highly synchronous with each other over one full oscillation and at least the beginning of a second oscillation in all genotypes (Figures 2.8A, 2.8B, 2.10A, 2.10C, 2.10E, and 2.11). These findings suggest that clock components that are equally segregated to sibling cells during mitosis are sufficient to govern the timing of at least two subsequent protein oscillations and highlight that a robust Notch-independent, cell-autonomous mechanism drives clock oscillations in the PSM regions we analyzed (S-III to S0).

Noise Induced by Cell Division is Likely Reduced Because Mitosis Preferentially Occurs During the “Off” Phase of the Oscillation Wave

Another striking aspect of oscillations in dividing cells emerged when we examined the oscillation phase of mitotic cells and neighbors upon cytokinesis. As anticipated, mitosis disturbed cyclic expression, and clock reporter levels were at their lowest levels in the large majority of dividing cells at cytokinesis in wildtype and Notch pathway mutant embryos (Figure 2.12A, left; data not shown). Importantly, we discovered in wild-type embryos (in which the oscillation phase of each dividing cell could be compared with the global collective phase of its neighbors) that in the majority of cases, not only were sibling cells in the trough of an oscillation at cytokinesis, but so were many of their neighbors (Figure 2.12A, right). This observation suggests that mitosis tends to occur during the “off” phase of the Her1 oscillation wave at the level of the entire tissue. One hour after mitosis, the phase differences between siblings and their neighbors were generally smaller for cells in which division had occurred at the trough of the oscillation cycle, relative to mitosis at other phases of the cycle (Figure 2.12B). These data suggest an intriguing relationship between clock oscillation and mitosis that may serve to limit mitosis-induced noise.

Discussion

Essential Tools for Analyzing PSM Cell Oscillations

For many years, the dynamics of the segmentation clock has been deduced from expression patterns of cyclic genes in fixed embryos. Because cyclic gene expression patterns vary among different embryos with identical somite numbers, large collections of embryos were required to estimate oscillation dynamics. More recently, high-resolution in situ hybridization has provided further insight into the clock dynamics by allowing discrimination between cells that are actively transcribing cyclic genes (with nuclear nascent transcripts) and cells that are more advanced in the oscillation cycle (with cytoplasmic mature transcripts). However, comparison of oscillation dynamics in neighbor cells, or in cells after clock perturbation, was still limited. Recently developed real-time reporters of the clock revealed the propagation dynamics of the cyclic gene expression wave across the PSM beautifully, but did not allow analysis of the clock at the single-cell level. Reaching such a level of resolution is crucial for understanding the mechanism of the segmentation clock, because PSM cells constitute its elementary oscillators. In this paper, we introduce two tools that are essential for analyzing oscillations in individual PSM cells in vivo.

First, we developed a highly dynamic reporter of the clock, the nuclear localization of which largely facilitated the detection of oscillations at a cellular level of resolution. Among the various reporters we generated, only Her1-Venus displayed instability compatible with the very short period of the zebrafish segmentation clock while maintaining levels of expression in a transgenic line that would be detectable by confocal microscopy. A good reporter should have minimal impact on the oscillations. Because overexpression of *her1* causes somite defects (Takke and Campos-Ortega, 1999), the presence of the entire Her1 sequence in the Her1-Venus reporter could be an issue. However, heterozygous zebrafish embryos from the *Tg(her1:her1-venus)* line showed no effect of the reporter on somite formation and very little impact on cyclic gene expression. Importantly, the Her1-Venus reporter displayed clear expression differences between wild-type and Notch pathway mutant backgrounds, validating its use for analyzing the impact of Notch signaling on the segmentation clock. Although the last three to five oscillations in PSM cells prior to somite formation were efficiently revealed by the Her1-Venus reporter, analysis of cyclic gene expression in the very posterior regions, including the progenitor zone, initiation zone, and posterior-most PSM (Mara *et al.*, 2007), will require further development of clock reporters and imaging techniques.

Second, we generated a semi-automated program that performs 3D segmentation of confocal images into individual cells, tracks cell positions across time, measures the reporter nuclear signal, and computes the oscillation phase at any given time point for any given cell. Using these tools in zebrafish allowed us to compare oscillations in neighbor PSM cells in living embryos. With the rapid progress of in vivo imaging techniques, it will soon be possible to use similar approaches in the mouse.

Oscillations Are Controlled by a Robust Cell-Autonomous Mechanism

Dissociated mouse PSM cells display autonomous oscillations that are asynchronous and irregular, suggesting the presence of an unstable oscillator within PSM cells (Maroto *et al.*, 2005;

Masamizu *et al.*, 2006). We show that after mitosis, sibling cells are strikingly synchronized with each other, usually for initiation of at least two cycles, yet most are delayed relative to their direct neighbors. Although newly generated sibling cells progressively resynchronize with their neighbors in wild-type embryos, the average synchrony remains higher for sibling cells than for random neighbor cells. It was recently shown that cytoplasmic bridges persist between sibling cells for several hours after mitosis in epiblast cells of zebrafish gastrula (Caneparo *et al.*, 2011). These intercellular bridges were not detected in the hypoblast at the gastrula stage (Caneparo *et al.*, 2011), nor have we detected them in PSM cells scatter-labeled with membrane tdTomato (data not shown). Thus, mitosis in the PSM likely generates sibling cells that are physically independent from each other and nevertheless cycle in tight synchrony. This suggests that the biochemical material inherited by sibling cells is sufficient for precise timing of the oscillation start for at least two cycles. Thus, the cell-autonomous mechanism that generates oscillations in zebrafish appears to be more robust than previously anticipated from mouse PSM cell dissociation experiments.

In zebrafish, Her1 and Her7 have been proposed to play an essential cell-autonomous role in generating oscillations. Mathematical modeling revealed that a mechanism of repression of her1 and her7 genes by their own products, involving transcriptional and translational delays, could generate transcript oscillations alternating with protein oscillations (Lewis, 2003). Although our primary goal was to develop a reporter with minimal impact on the endogenous clock, as in heterozygous *Tg(her1:her1-venus)* embryos, we noticed that embryos homozygous for the *her1:her1-venus* transgene displayed a longer segmentation period and fewer somites than wild-type embryos. This observation is consistent with previous work showing that the total number of somites is controlled by a balance between the speed of segmentation and the rate of PSM elongation and wavefront regression (Gomez *et al.*, 2008, Schroter and Oates, 2010). It is not clear whether transgene homozygosity affects the clock because Her1-Venus fusion protein interferes with normal Her1 function or because Her1 activity is too high. At high doses, Her1-Venus may disrupt Hes6 function, a protein that heterodimerizes with Her1 and to control segmentation speed and somite number in zebrafish (Kawamura *et al.*, 2005; Sieger *et al.*, 2006; Schroter and Oates, 2010; Schroter *et al.*, 2012; Trofka *et al.*, 2012). Altogether, these observations support a role for the Her/Hes machinery as a pacemaker of the zebrafish segmentation clock. Whether the robust cell-autonomous mechanism that generates synchronous oscillations in zebrafish sibling cells relies mainly on the *her/hes* negative feedback loop or involves additional complexity remains to be understood.

Role of Notch Signaling

Although a role for Notch signaling in synchronizing oscillations in zebrafish has been proposed for more than a decade (Horikawa *et al.*, 2006; Jiang *et al.*, 2000; Lewis, 2003; Mara *et al.*, 2007; Ozbudak and Lewis, 2008; Riedel-Kruse *et al.*, 2007), the ‘‘salt and pepper’’ expression of cyclic genes in Notch pathway mutants could in theory result from stochastic and/or stable expression in a subset of cells, rather than asynchronous cycling. Here we provide direct evidence that, as anticipated, cells oscillate out of synchrony in the intermediate and anterior PSM of Notch pathway mutants. Because *aei/deltaD* mutants display no cyclic gene expression in the posterior PSM, DeltaD was proposed to be involved in oscillation initiation (Mara *et al.*, 2007). We found that after mitosis, sibling cells in the PSM resumed oscillations with similar delay and synchrony in wild-type and *aei/deltaD, bea/deltaC*, and *des/notch1a* mutant embryos, suggesting that oscillations in the intermediate and anterior PSM are generated independently of Notch signaling. Next-generation reporters will be necessary to analyze the importance of the different Notch pathway components for oscillation initiation in the posterior PSM.

Impact of Mitosis on Cell Synchrony

Using time-lapse microscopy, Horikawa *et al.* (2006) found that 10%–15% of cells undergo mitosis during one cycle of oscillation in the posterior PSM, and that the M phase, during which transcription is largely switched off, lasts at least half the period of a cycle. This suggested that mitosis could be a significant source of noise for oscillation synchrony. The disruption of synchrony between neighbor cells in Notch pathway mutants seems slightly less severe when the cell cycle is disrupted in *emi1* (*early mitotic inhibitor 1*) mutants (Zhang *et al.*, 2008), consistent with mitosis creating noise in the system. Indeed, in *Tg(her1:her1-venus)* embryos, we found that 80% of the cells undergoing division were affected by this event, and most of them were delayed relative to their neighbors. In the remaining 20% of cases for which oscillations were unaffected by mitosis, the off phase of her1 transcript oscillation may have coincided with the general transcriptional depression caused by mitosis. In mice, two groups of cyclic genes (one enriched with genes of the HES family and of the Notch and FGF signaling pathways, and one enriched with genes of the Wnt signaling pathway) oscillate in opposite phase (Dequeant *et al.*, 2006; Krol *et al.*, 2011). Although no such groups of genes cycling in phase opposition were found in zebrafish, the off phase of the her1 transcript may not coincide with the off phase of other important cyclic transcripts (Krol *et al.*, 2011). However, zebrafish her genes broadly oscillate in phase with each other (Krol *et al.*, 2011; Oates and Ho, 2002) and likely represent crucial genes for oscillation genesis. Thus, linking mitosis to the oscillation dynamics of her genes could help reduce the impact of mitosis on the clock. Strikingly, we observed that an unexpected high number of cell divisions occurred during the off phase of the Her1 oscillation wave, and generated siblings that were on average less desynchronized with their environment. This suggests an intriguing hypothesis that mitosis and the clock are linked in such a way that cell division creates less noise than previously thought.

The in vivo reporter we describe, and ‘‘next-generation’’ versions that will undoubtedly be made, will open many new doors of opportunity for understanding somitogenesis. We can now study clock attributes in single cells across space and time, and thus gain a deeper understanding of this dynamic process.

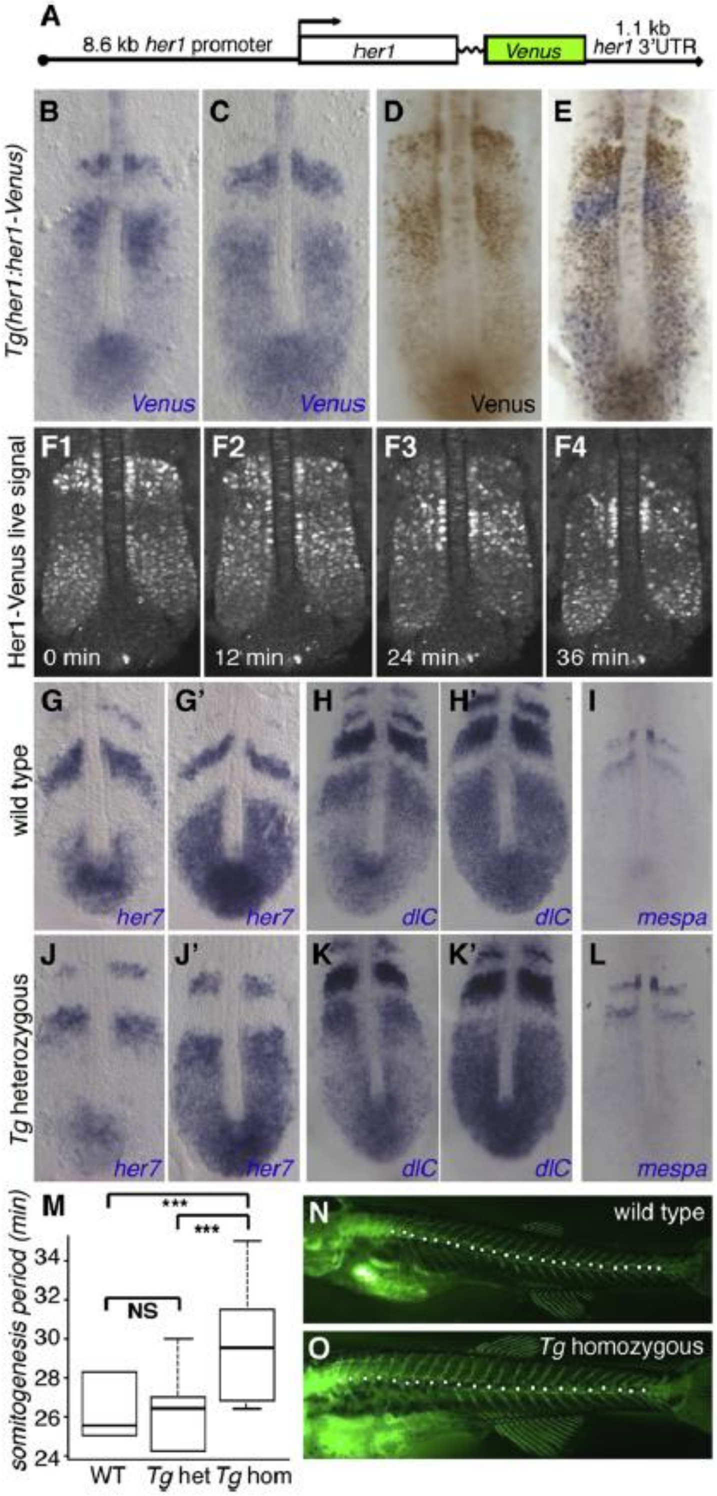
A
8.6 kb her1 promoter
her1
Venus
1.1 kb
her1 3'UTR
Tg(her1:her1-Venus)
B
C
D
E
Venus
Venus
Venus
Her1-Venus live signal
F1
F2
F3
F4
0 min
12 min
24 min
36 min
wild type
G
G'
H
H'
I
her7
her7
dlC
dlC
mespa
Tg heterozygous
J
J'
K
K'
L
her7
her7
dlC
dlC
mespa
M
somitogenesis period (min)
34
32
30
28
26
24
***
***
NS
WT
Tg het
Tg hom
N
wild type
O
Tg homozygous

Figure 2.1: The Zebrafish Transgenic *her1:her1-venus* Line Recapitulates Dynamic her1 Expression

(A) Diagram of the *her1:her1-venus* construct. (B–E) Cyclic reporter transcript and protein expression in heterozygous *Tg(her1:her1-venus)* embryos. Transcript (blue) and protein (brown) are largely expressed out of phase. (F) Still images from Movie S1 (in dorsal view) reveal waves of dynamic reporter expression in the PSM. (G–L) *her7* (G, G', J, and J'), *dlc* (H, H', K, and K'), and *mespa* (I and L) expression in wild-type (G–I) and heterozygous *Tg(her1:her1-venus)* (J–L) embryos. (M) Segmentation speed in wild-type (n = 20), *her1:her1-venus* heterozygous (n = 26) and homozygous (n = 29) embryos. Somites were first counted at the two- to six-somite stage, and then again after 4–5.5 hr of development at 28°C. The box represents segmentation speed values between the first and third quartiles, the bold line represents the median value, and the whiskers represent maximal and minimal values. Homozygous transgenic embryos segmented significantly more slowly than heterozygote and wild-type embryos. A Wilcoxon rank sum test yielded significant differences for wild-type versus homozygote ($p < 10^5$), and heterozygote versus homozygote ($p < 10^5$), but not wild-type versus heterozygote ($p = 0.87$) embryos. (N and O) Segment number and size in wild-type (H) or homozygous *her1:her1-venus* (I) larvae. Calcified skeletal structures were revealed at 21 dpf by calcein staining (Du *et al.*, 2001). The total number of precaudal, transitional, and caudal segments (white dots; Bird and Mabee, 2003) was significantly lower in homozygous transgenic larvae (median = 21 segments, n = 64) than in wild-type larvae (median = 24, n = 33; Wilcoxon rank sum test, $p < 10^5$). Note that the segment size appears larger in homozygous *her1:her1-venus* compared with wild-type larvae.

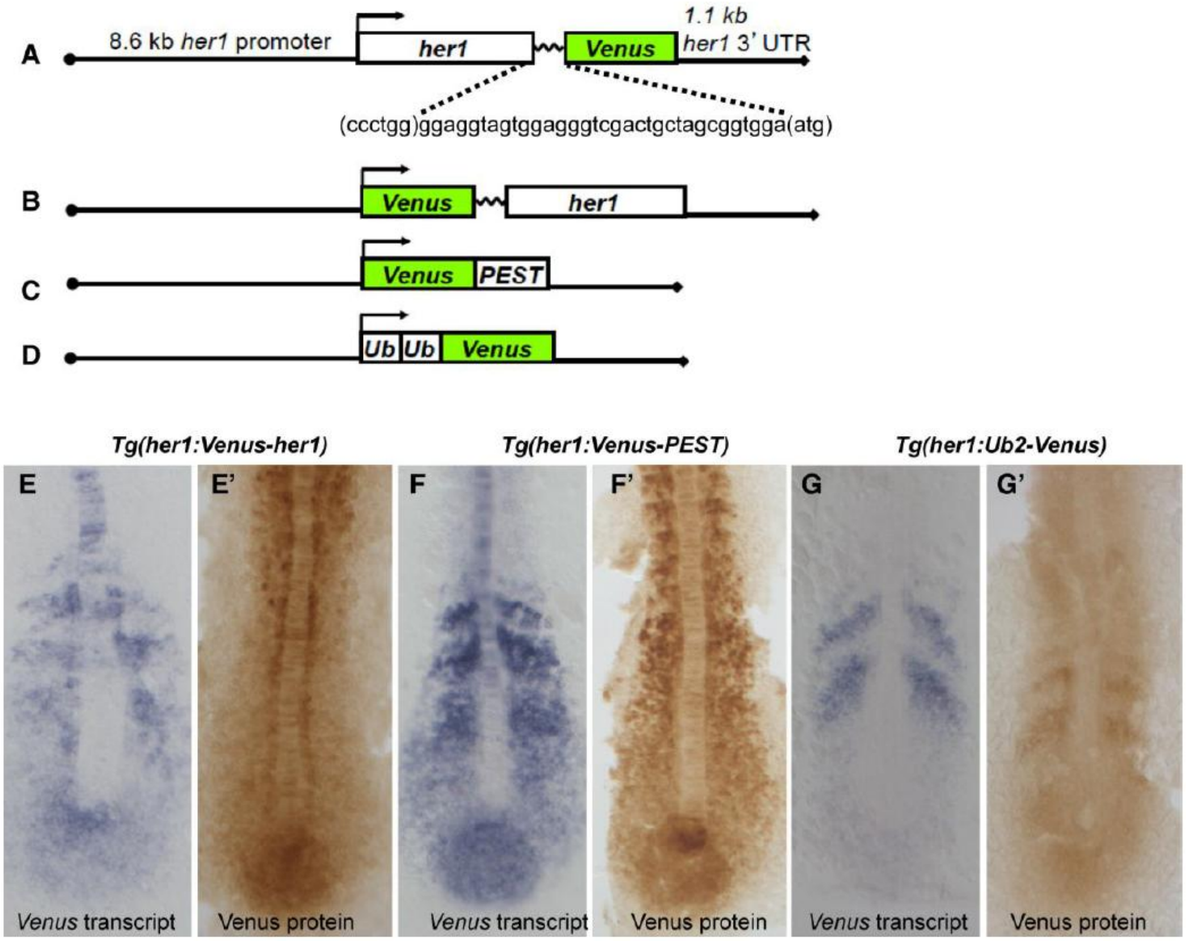
A
8.6 kb *her1* promoter
her1
Venus
1.1 kb
her1 3' UTR
(ccctgg)ggaggtagtggagggtcgactgctagcggtgga(atg)
B
Venus
her1
C
Venus
PEST
D
Ub
Ub
Venus
Tg(her1:Venus-her1)
Tg(her1:Venus-PEST)
Tg(her1:Ub2-Venus)
E
E'
F
F'
G
G'
Venus transcript
Venus protein
Venus transcript
Venus protein
Venus transcript
Venus protein

Figure 2.2: General strategies taken to generate a dynamic reporter of *her1* oscillations. (A-D) Diagrams of the constructs tested. All constructs use the 8.6 kb upstream *her1* regulatory region (Gajewski *et al.* 2003) to drive cyclic expression and contain 1.1 kb of downstream sequence, including the *her1* 3'UTR. (A) The successful *her1:her1-venus* construct described in the main text and Experimental procedures. (B) A *her1:venus-her1* construct in which Venus was fused to the N-terminus of Her1. (C) A *her1:venus-PEST* construct in which a PEST destabilizing sequence (Aulehla *et al.* 2008) was fused to the C-terminus of Venus. (D) A *her1:Ub2-Venus* construct in which two ubiquitin moieties (Masamizu *et al.* 2006) were fused to the Venus N-terminus. (E-G) Reporter transcript (blue) and protein (brown) expression in each transgenic line. The *her1:Venus-her1* reporter (B) was cyclically transcribed (E) but too stable for following Her1 dynamics (E'). The observation that reporter protein, but not transcript, persists in newly formed somites for both transgenes may implicate a role for the Her1 N-terminus in protein degradation. The *her1:Venus-PEST* reporter (C) was similarly too stable (F,F'). In contrast, the *her1:Ub2-Venus* reporter (D) generated cyclic transcript (G) and protein (G'); however, the Ub2-Venus fluorescence was not detectable by confocal microscopy.

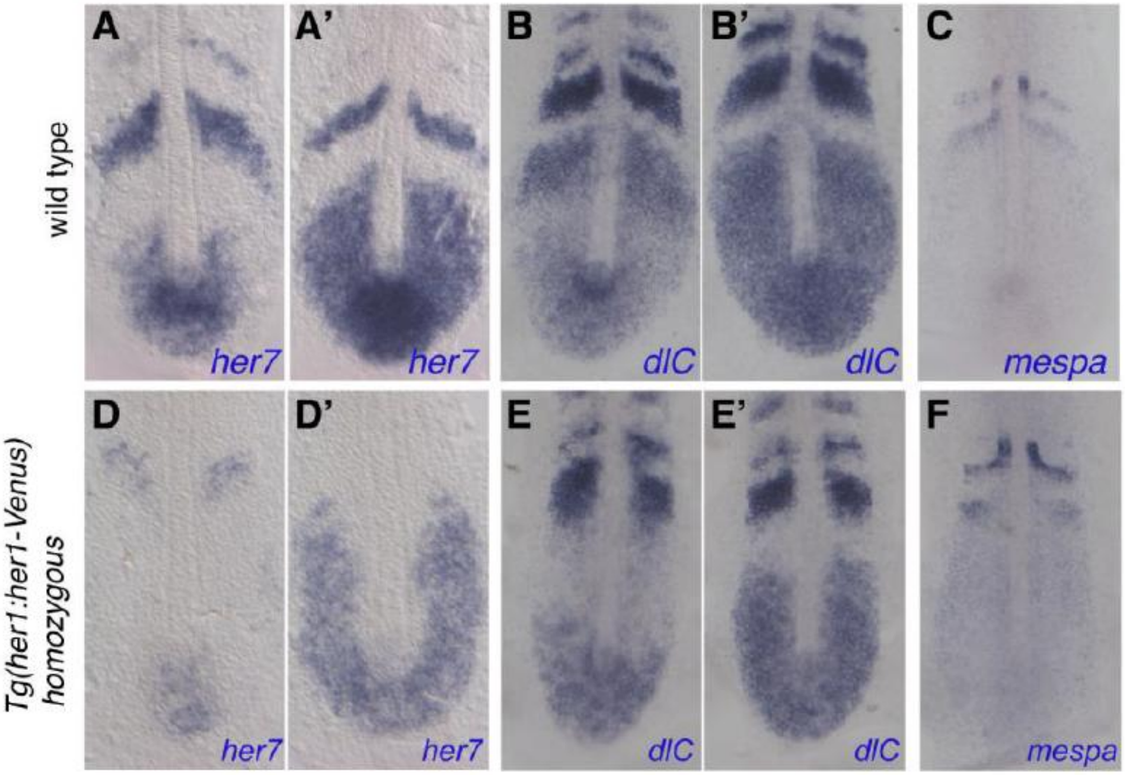
wild type
Tg(her1:her1-Venus) homozygous
A
A'
B
B'
C
her7
her7
dlC
dlC
mespa
D
D'
E
E'
F
her7
her7
dlC
dlC
mespa

Figure 2.3: Impact of *her1:her1-Venus* transgene homozygosity on cyclic gene expression. (A-F) Expression of *her7* and *deltaC* cyclic genes and the *mespa* clock read-out gene in wild-type embryos (A-C) or in embryos homozygous for the *her1:her1-Venus* transgene (D-F). Images in (A-C) are identical to the ones in Figure 1G-I. In homozygous transgenic embryos, *her7* expression remains cyclic in the posterior PSM; however, anterior *her7* stripes are absent (D, D'). In contrast, striped expression of *dlC* (E, E') and *mespa* (F) are relatively unaffected; there is a wider angle between the stripe and notochord compared to wild-type embryos.

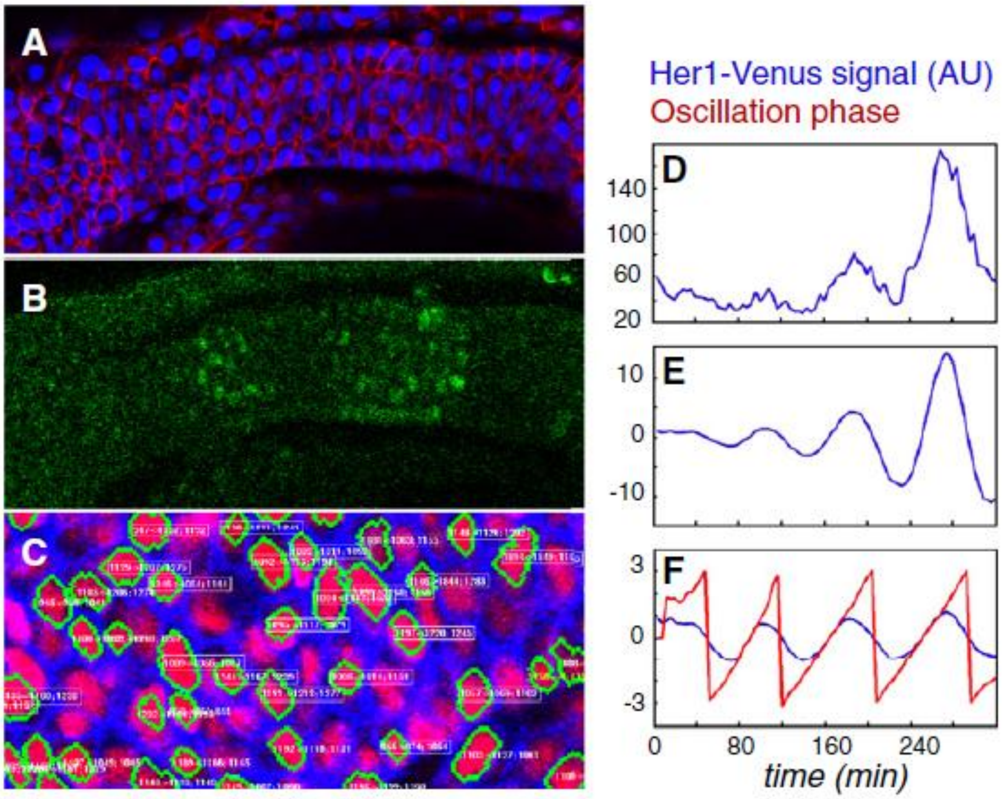
A
B
C
Her1-Venus signal (AU)
Oscillation phase
D
140
100
60
20
E
10
0
-10
F
3
0
-3
0
80
160
240
time (min)

Figure 2.4: Detection and Analysis of Clock Oscillations at Single-Cell Resolution
(A and B) Confocal section of the PSM of a 12-somite-stage heterozygous *her1:her1-venus* embryo (lateral view, anterior left) injected with membrane mCherry and H2B-Cerulean mRNAs at the one-cell stage. Raw signals for membrane-Cherry (red) and H2B-Cerulean (blue) are shown in (A), and for Her1-Venus (green) in (B). (C) Image resulting from automated 3D segmentation of confocal pictures and cell tracking using our MATLAB-based program. Green cell contours are automatically generated and can be manually deleted or added. White and yellow numbers indicate tracking information, which is also automatically generated and can be manually corrected and validated. (D) Raw fluorescence data from a single PSM cell showing four oscillations over time. (E and F) Illustration of the heuristic algorithm used to compute the oscillation phase. First the signal is smoothed, then the average value over a predefined time window comparable to the period is removed (E), and finally the amplitude of the signal is rescaled over the same time window to obtain a pseudo sine wave (F, blue line). Phase (F, red line) is computed as detailed in the Methods section.

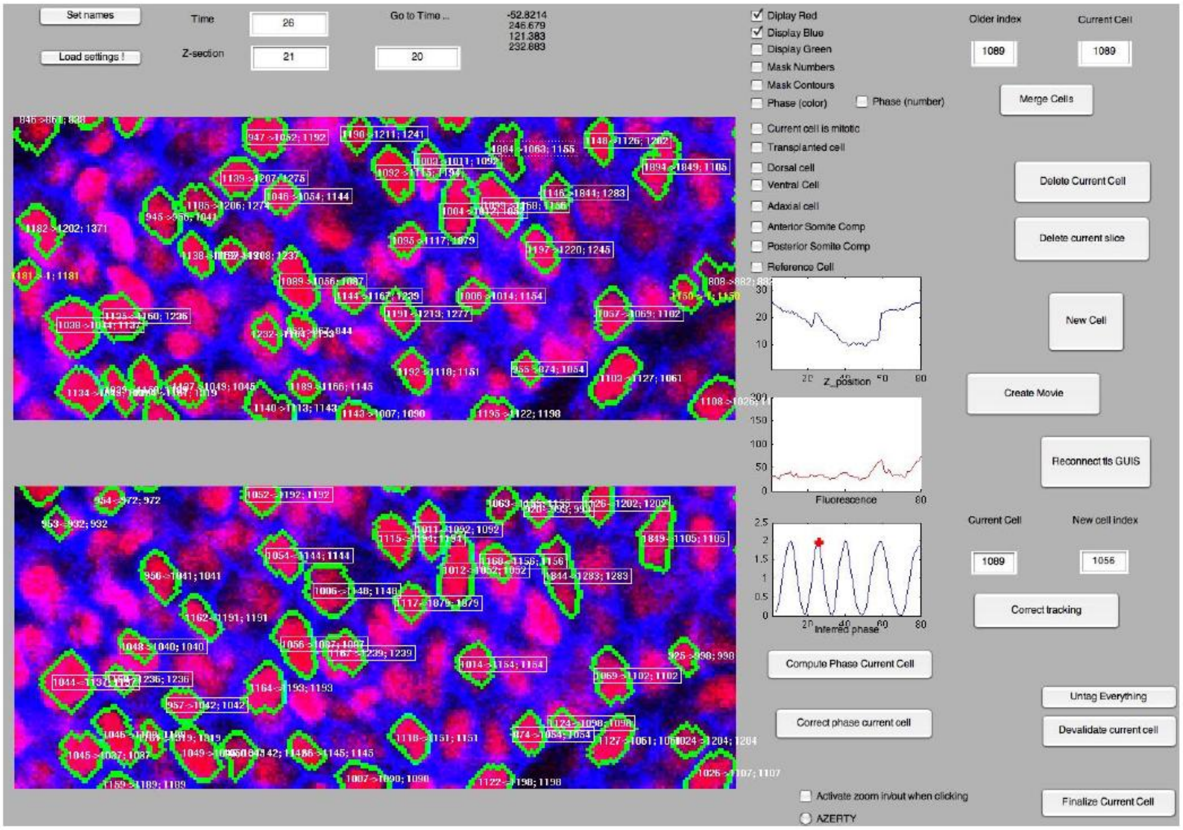

Time 26

Z-section 21

Go to Time ... 20

-52.8214
246.679
121.383
232.883

☑ Diplay Red
☑ Display Blue
☐ Display Green
☐ Mask Numbers
☐ Mask Contours
☐ Phase (color)
☐ Phase (number)
☐ Current cell is mitotic
☐ Transplanted cell
☐ Dorsal cell
☐ Ventral Cell
☐ Adaxial cell
☐ Anterior Somite Comp
☐ Posterior Somite Comp
☐ Reference Cell

Older index 1089

Current Cell 1089

Current Cell 1089

New cell index 1056

☐ Activate zoom in/out when clicking
○ AZERTY

Set names
Load settings !
Merge Cells
Delete Current Cell
Delete current slice
New Cell
Create Movie
Reconnect tls GUIS
Correct tracking
Compute Phase Current Cell
Correct phase current cell
Untag Everything
Devalidate current cell
Finalize Current Cell
30
20
10
20
40
60
80
Z_position
200
150
100
50
0
Fluorescence
80
2.5
2
1.5
1
0.5
0
20
40
60
80
Inferred phase

Figure 2.5: Graphical user interface of our MATLAB-based 3D segmentation and tracking program.

Screen shot of the graphical user interface that allowed us to rapidly correct and validate the automated tracking. On the left, the upper image is a magnified view of the current time point and the lower image is the previous time point. Various buttons are available to navigate, correct, and connect any tracked cells of interest. Green cell contours are automatically generated and can be manually deleted or added. The three small graphs on the right show z-position of the cell of interest with time (top), Her1-Venus signal with time (middle), and sine of the phase with time (bottom). See Appendix B for more extensive descriptions

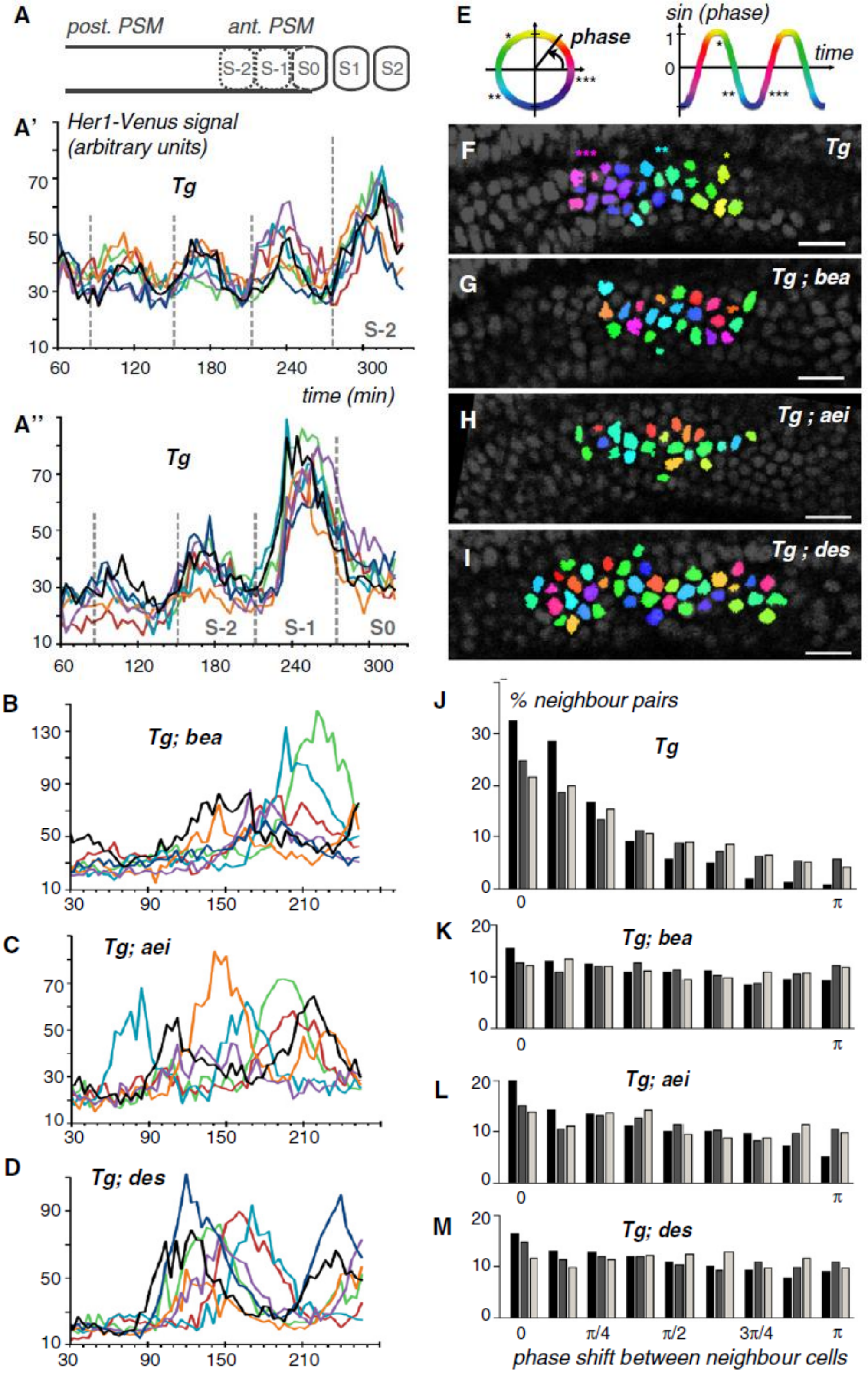
A
post. PSM
ant. PSM
S-2
S-1
S0
S1
S2
A'
Her1-Venus signal
(arbitrary units)
Tg
70
50
30
10
S-2
60
120
180
240
300
time (min)
A''
Tg
70
50
30
10
S-2
S-1
S0
60
120
180
240
300
B
Tg; bea
130
90
50
10
30
90
150
210
C
Tg; aei
70
50
30
10
30
90
150
210
D
Tg; des
90
50
10
30
90
150
210
E
phase
*
**
***
sin (phase)
1
0
time
F
Tg
G
Tg ; bea
H
Tg ; aei
I
Tg ; des
J
% neighbour pairs
Tg
30
20
10
0
0
π
K
Tg; bea
20
10
0
0
π
L
Tg; aei
20
10
0
0
π
M
Tg; des
20
10
0
0
π/4
π/2
3π/4
π
phase shift between neighbour cells

Figure 2.6: Notch Signaling Is Required for Synchronous Oscillation in Neighboring PSM Cells

(A–D) Reporter expression in six to seven neighbor cells tracked through time in wild-type (A’ and A’’), *bea* (B), *aei* (C), and *des* (D) embryos heterozygous for the *Tg(her1:her1-venus)* transgene. Dashed gray lines in A’ and A’’ indicate the time of somite boundary formation. The schematic drawing in (A) represents a lateral view of the PSM in a wild-type embryo (anterior to the right), showing newly formed (S1 and S2) and presumptive (S-2, S-1, and S0) somites. (E–I) Pseudo-coloration of cells based on the oscillation phase (E) at a single time point in wildtype (F), *bea* (G), *aei* (H), or *des* (I) mutant embryos. (J–M) Histograms of phase shift between all tracked neighbor cells at all time points for wildtype (J), *bea* (K), *aei* (L), and *des* (M) mutant embryos. Phase-shift distributions for three separate embryos (black, gray, and beige bars) are shown. A two-sample t test of wild-type embryos with each mutant indicates significant differences (two-tailed t test, $\alpha = 0.05$): WT versus aei ($t = 40.02$, $p < 10^5$), WT versus *bea* ($t = 55.68$, $p < 10^5$), and WT versus *des* ($t = 53.13$, $p < 10^5$).

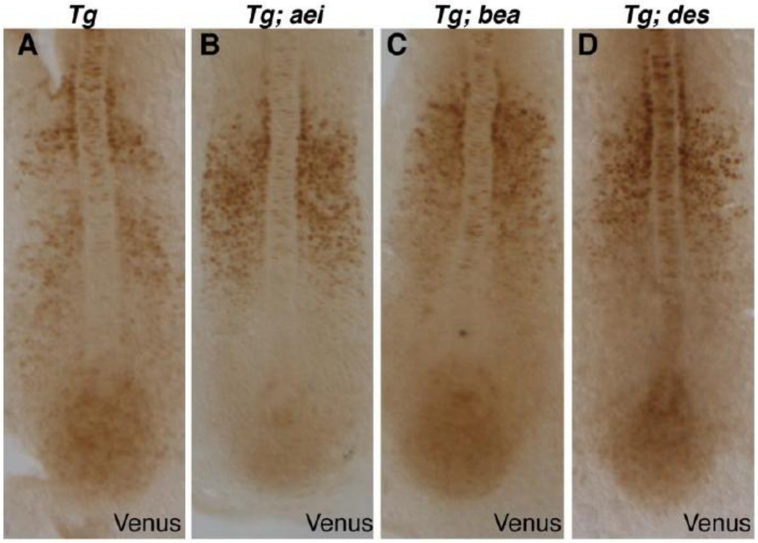
Tg
Tg; aei
Tg; bea
Tg; des
A
B
C
D
Venus
Venus
Venus
Venus

Figure 2.7: The *her1:her1-Venus* transgene is expressed in a salt-and-pepper pattern in Notch pathway mutants.

In embryos heterozygous for the *her1:her1-venus* transgene, Her1-Venus reporter protein (brown) is expressed in stripes in wild-type embryos (A), but in a salt-and-pepper pattern in *aei/deltaD* (B), *bea/deltaC* (C), and *des/notch1a* (D) Notch pathway mutants. Thus, the Her-Venus reporter is expressed similarly to endogenous cyclic genes, which also display speckled expression when Notch signaling is disrupted (Jiang *et al.*, 2000; Giudicelli *et al.*, 2007; Mara *et al.*, 2007; Riedel-Kruse *et al.*, 2007; Ozbudak and Lewis, 2008).

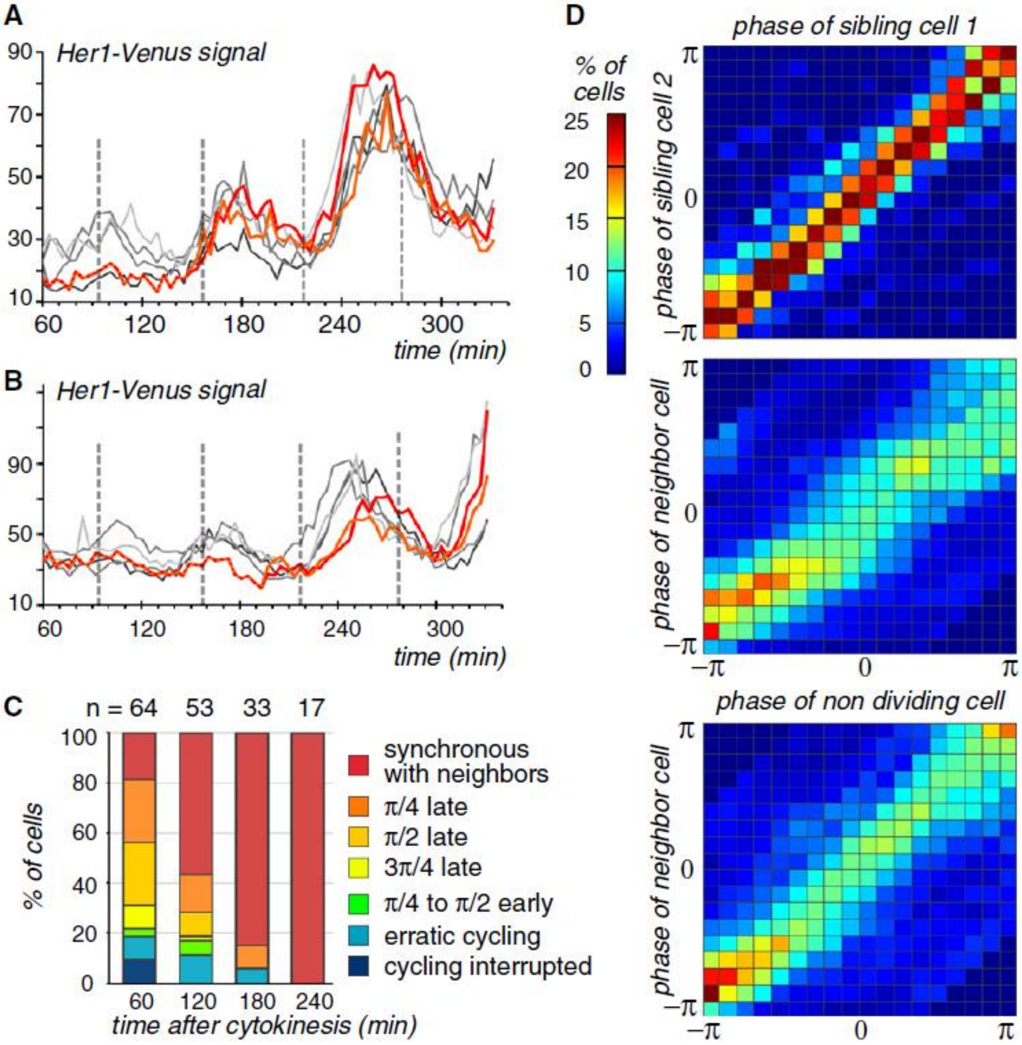
A
Her1-Venus signal
90
70
50
30
10
60
120
180
240
300
time (min)
B
Her1-Venus signal
90
50
10
60
120
180
240
300
time (min)
C
n = 64
53
33
17
100
80
60
40
20
0
% of cells
60
120
180
240
time after cytokinesis (min)
synchronous with neighbors
π/4 late
π/2 late
3π/4 late
π/4 to π/2 early
erratic cycling
cycling interrupted
D
% of cells
25
20
15
10
5
0
phase of sibling cell 1
phase of sibling cell 2
phase of neighbor cell
phase of non dividing cell
phase of neighbor cell
π
0
−π
−π
0
π

Figure 2.8: Mitosis Produces Highly Synchronized Sibling Cells that Gradually Resynchronize with Neighbors
(A and B) Reporter oscillations in a dividing cell and progeny (orange and red) and in neighbors (grayscale). Dashed lines indicate the time of somite boundary formation. Examples of maintenance of synchrony between dividing cell and neighbors before and after mitosis (A) and of initial daughter-neighbor delay with resynchronization over time (B) are shown. (C) Percentage of cells that exhibit a particular phase difference with neighbors measured at different times after mitosis. Numbers above bars indicate the number of divisions analyzed by manual inspection. Dividing cells in PSM regions where reporter oscillations were generally undetectable were excluded from the analysis. (D) MATLAB-generated two-dimensional (2D) histogram comparing the phases of recently divided cells with siblings (top) or neighbors (middle), or of random neighbor pairs (bottom), at every time point in wild-type embryos. Sibling-sibling synchrony is significantly greater than sibling-neighbor and neighbor-neighbor synchrony (two-tailed t test, $\alpha = 0.05$, $p < 10^5$).

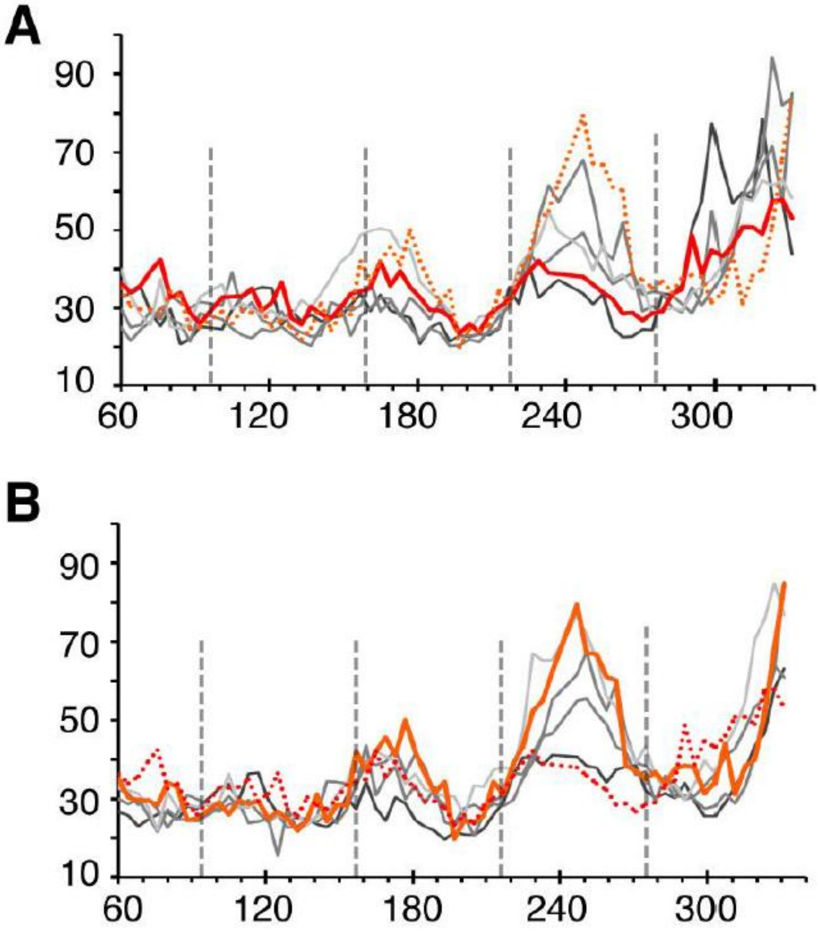
A
90
70
50
30
10
60
120
180
240
300
B
90
70
50
30
10
60
120
180
240
300

Figure 2.9: Sibling cells that drift apart from each other after division eventually re-synchronize with their local neighbors.
(A,B) Oscillations in 2 sibling cells and their neighbors. Cytokinesis giving rise to the 2 sibling cells occurred at t = 40 min (signal obtained during the first hour is not shown). For each panel, the solid colored line (red or orange) represents oscillations in one sibling cell, the grey solid lines, oscillations in its direct neighbors, and dashed colored line, oscillations in its sibling cell. Note that the neighbor population is different for each sibling cell, and the last oscillation does not begin at the same time between the two panels. Each sibling cell however oscillates in synchrony with its respective neighbors during this last oscillation.

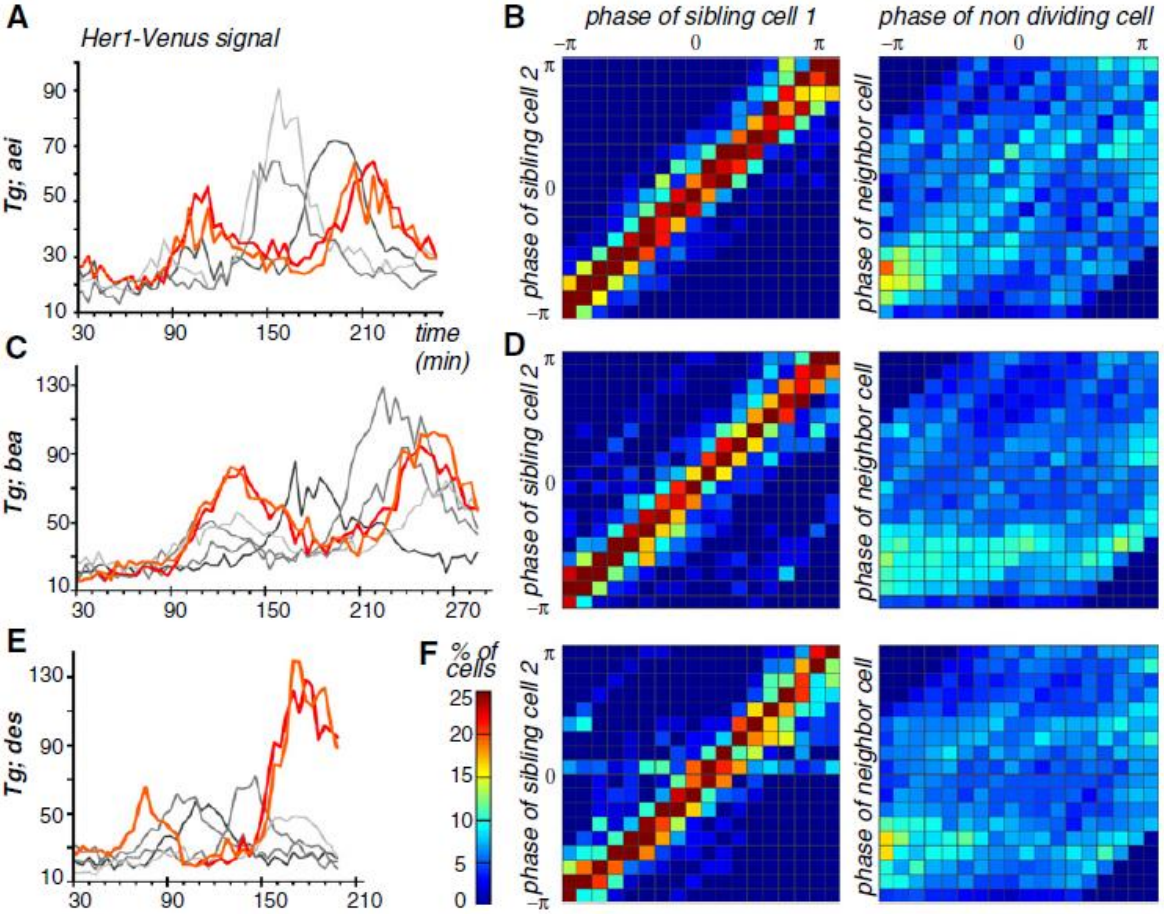
A
Her1-Venus signal
Tg; aei
90
70
50
30
10
30
90
150
210
time (min)
B
phase of sibling cell 1
phase of sibling cell 2
phase of non dividing cell
phase of neighbor cell
−π
0
π
C
Tg; bea
130
90
50
10
30
90
150
210
270
D
phase of sibling cell 2
phase of neighbor cell
E
Tg; des
130
90
50
10
30
90
150
210
F
% of cells
25
20
15
10
5
0
phase of sibling cell 2
phase of neighbor cell

Figure 2.10: After Mitosis, Sibling Cells Oscillate in Tight Synchrony in a Notch-Independent Manner
(A, C, and E) Reporter oscillations in dividing cells (orange and red) and neighbors (grayscale) in *aei/deltaD* (A), *bea/deltaC* (C), and *des/notch1a* (E) mutants. (B, D, and F) 2D histogram comparing the phases of recently divided cells with siblings or neighbors at every time point in *aei* (B), *bea* (D), and *des* (F) mutant backgrounds. Sibling-sibling synchrony is significantly greater than synchrony between random neighbors (two-tailed t test, $\alpha = 0.05$, $p < 10^5$ in all cases).

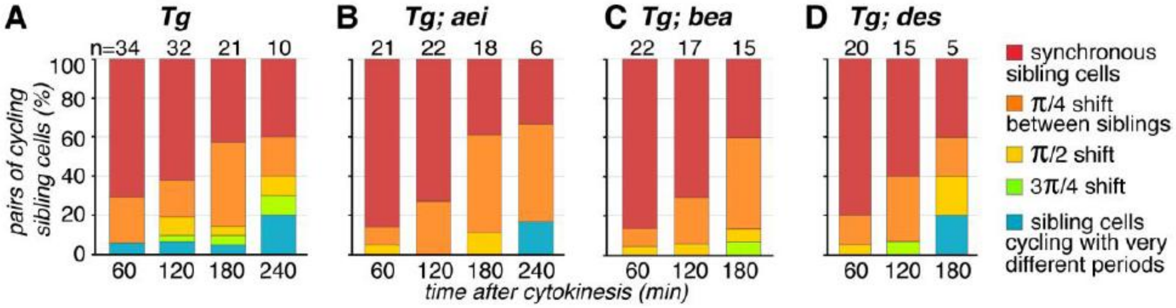
A
Tg
n=34
32
21
10
pairs of cycling sibling cells (%)
100
80
60
40
20
0
60
120
180
240
B
Tg; aei
21
22
18
6
60
120
180
240
C
Tg; bea
22
17
15
60
120
180
D
Tg; des
20
15
5
60
120
180
time after cytokinesis (min)
synchronous sibling cells
π/4 shift between siblings
π/2 shift
3π/4 shift
sibling cells cycling with very different periods

Figure 2.11: Most sibling cells remain synchronous for at least two oscillations of the clock. Phase difference between sibling cells was quantified at different times after mitosis in wild-type (A), *aei/deltaD* (B), *bea/deltaC* (C) and *des/notch1a* (D) embryos. Numbers above bars indicate number of divisions analyzed by manual inspection. Cells with undetectable oscillations were excluded from the analysis. At the temperature of these experiments, a typical oscillation cycle in the anterior PSM is about 80-100 minutes.

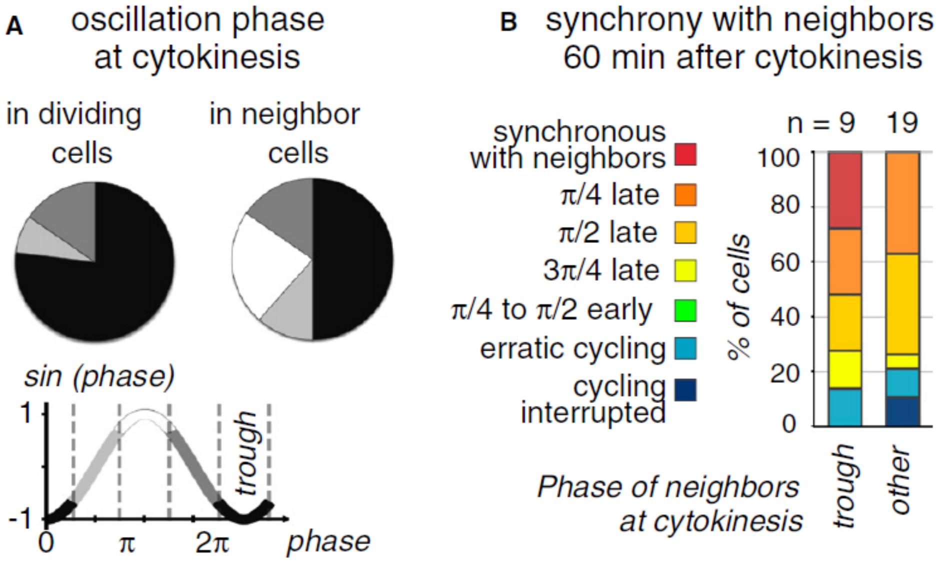
A
oscillation phase at cytokinesis
in dividing cells
in neighbor cells
sin (phase)
1
-1
0
π
2π
phase
trough
B
synchrony with neighbors 60 min after cytokinesis
synchronous with neighbors
π/4 late
π/2 late
3π/4 late
π/4 to π/2 early
erratic cycling
cycling interrupted
n = 9
19
100
80
60
40
20
0
% of cells
Phase of neighbors at cytokinesis
trough
other

Figure 2.12: Mitosis Preferentially Occurs during the Off Phase of the Her1 Oscillation Wave
(A) Oscillation phase at cytokinesis in dividing cells and their neighbors. (B) Phase difference between sibling cells and neighbors 60 min postmitosis, for cells whose neighbors were in trough or other phase (see A) when cytokinesis occurred. Numbers above bars indicate the number of divisions analyzed by manual inspection.

Chapter 3

Slowing of the Segmentation Clock Establishes a Two-Segment Periodicity in Zebrafish

Introduction

In vertebrates, the process of somitogenesis generates mesodermal blocks of tissue – called somites – from the undifferentiated presomitic mesoderm (PSM). Somites flank the notochord and eventually give rise to structures such as axial muscles and vertebrae. Somites are formed sequentially with regularity in size, periodicity, and number within each species. Segmentation is extremely resilient, being able to adjust for changes in embryo size (Lauschke *et al.*, 2013) and temperature (Schroter and Oates 2008). To account for the regularity of somite formation, Cooke and Zeeman (1976) proposed two hypothetical, interacting mechanisms behind somitogenesis: a "clock" and a "wavefront". They hypothesized that cells in the PSM would oscillate between a permissive and restrictive phase (clock), periodically forming somites based on their interaction with a positional signal (wavefront), the latter progressing posteriorly at the same rate as tailbud elongation. PSM cells in the permissive phase of the clock would respond to the wavefront by pinching off and rapidly transitioning from undifferentiated PSM cells into segmented somites. Their model informed the search for factors that might molecularly define the clock and wavefront, and forms the basis of most somitogenesis models today (reviewed in Lewis *et al.* 2009, Aulehla and Pourquié 2010, Pourquié 2011, Oates 2012).

Through experimental and theoretical data across a wide breadth of organisms, the periodicity and timing of somite formation is now thought to be controlled by a molecular network known as the segmentation clock (Palmeirim *et al.*, 1997, Holley *et al.*, 2000, Jouve *et al.*, 2000, Henry *et al.*, 2002, Oates and Ho *et al.*, 2002, Bessho *et al.*, 2003, reviewed in Oates *et al.*, 2012, Pourquié, 2011). Clock genes oscillate in individual cells within the PSM and are important to the proper formation of somites. Cells within the PSM oscillate in a coordinated fashion, with neighboring cells synchronizing their expression through the Notch pathway (reviewed in Oates *et al.*, 2012, *Pourquié*, 2011). This coupling of clock cycling generates a wave of gene expression that is propagated as a narrowing stripe from the posterior to the anterior PSM and is kinematic, produced by coordinated expression in individual cells rather than the bulk transport or transduction of molecules or cells. The periodicity of oscillatory expression of cyclic genes *in vivo* matches the rate of somite generation, with each wave of clock expression reaching the PSM-somite boundary as a new somite is formed (Aulehla et al., 2008; Masamizu et al., 2006, Oates et al., 2012, Takashima et al., 2011, Delaune et al, 2012).

A family of core clock components oscillates within the vertebrate PSM: the Hairy/Enhancer-of-split (*Hes*) transcriptional repressors (Palmerin 1997, Jouve 2000, Bessho 2001). The cycling of these *hairy*-related genes was first deduced in fixed embryos by *in situ* hybridization. By fixing the halves of each embryo at different times or exposing each half to different temperatures, stripes of gene expression would differ with a period that matched that of somite formation (Palmerim 1997, Jouve 2000, Jiang 2000). In zebrafish, *hairy/enhancer-of-split*-related (*her)* genes, *her1* and *her7,* oscillate in the PSM and are necessary for proper somite formation (Henry *et al.,* 2002, Oates and Ho *et al.*, 2002, Oates *et al.,* 2012, Pourquié, 2011). High-resolution *in situ* hybridization for *her* genes show that clock expression sweeps in a posterior-to-anterior direction: in each stripe of expression, transcripts in the more posterior edge of the stripe are localized in the cytosol, while cells in the anterior have transcripts localized in nuclear puncta (Julich 2005, Mara 2007). Recently, we directly observed waves of zebrafish cyclic gene expression using a single-cell-resolution clock reporter, *her1:her1-venus*, in which the 8.6 kb *her1* regulatory region drives expression of a transcript encoding a Her1–Venus fusion protein, flanked by *her1* 5'- and 3'-UTRs to facilitate rapid transcript turnover (Delaune and Francois *et al.*, 2012). Using this reporter, we elucidated the behavior of oscillating cells at a local level, confirming that the Notch pathway synchronizes neighboring cells and revealing that daughter cells oscillate synchronously after mitosis. The *her1:her1-venus* reporter thus provides a powerful tool to explore how segmentation clock signal is translated to pattern each forming somite.

In both fixed and live embryos, the wave of gene expression slows as it approaches the anterior of the PSM, a feature not described in the original clock and wavefront model. The function of this slowing is still unclear; recent models suggested the clock freezes as it interacts with a theoretical "arrest front," effectively stopping and stabilizing clock expression (Guidicelli *et al.* 2007, Morelli *et al.* 2009). The observed clock slowing would then account for the continuous transition from a finite period in the tail bud to an "infinite period" at the front. Importantly, transition from oscillating systems to somites does not require *a priori* a diverging period since the generic way oscillators disappear with change of parameters is via Hopf bifurcations, with a finite period at transition (François and Siggia 2012). Indeed, we have shown that the period of the clock in the anterior PSM does slow *in vivo* (Delaune and Francois *et al.*, 2012), but not at the rate predicted by fixed embryos (Guidicelli *et al.* 2007). Understanding how exactly the clock behaves in the anterior PSM may have important implications in understanding somite patterning.

Here, we follow oscillating PSM cells *in vivo* to investigate the slowing of the clock relative to somite boundary formation. We focus on cells that eventually form each somite boundary, using the *her1-venus* reporter to examine clock oscillation patterns in future boundary cells through developmental time. We find that clock oscillations gradually slow as PSM cells become anteriorly displaced, with clear increases in amplitude during the final two oscillations. The clock slows in anterior PSM cells, creating a phase distribution where cells at a one-somite distance are actually in opposite phases of clock expression. Importantly, we do not find evidence for an arrest front that causes cells to drastically increase in period and stop oscillating. Based on these results, we propose an updated interpretation of how the segmentation clock patterns somites.

Results

To understand the dynamics of clock slowing and somite formation, we followed oscillations in cells progressing anteriorly in the PSM. We tracked cells over time in the transgenic line *her1:her1-venus*, a single-cell resolution clock reporter (Delaune and Francois *et al.* 2012). Zebrafish embryos were injected at the one-cell stage with *h2b-cerulean* and *lyn-mcherry* mRNA to mark the nuclei and membranes respectively (Megason 2009; Delaune and Francois *et al.* 2012). The PSM was imaged beginning at the 10-12 somite stage for 4-6 hours and PSM cells were tracked across time using a semi-automated cell tracking software (Delaune et al. 2012). We imaged embryos at a lower temperature (23°C instead of 28.5°C) and observed that somite formation is correspondingly slowed (~60 minutes instead of 20-30 minutes), consistent with published reports that show that somite periodicity in zebrafish is temperature-dependent (Schroter *et al.*, 2008, Kimmel 1995). Each peak of expression was labeled based on the cell's approximate anterior-posterior global position in the PSM, using conventions in the field (Pourquié and Tam, 2001), with the newest, fully-formed somite named S1 and the second-newest formed named S2. The tissue constituting the newest forming somite is named S0, while tissue forming the two subsequent future somites are named S-1 and S-2, respectively. As previously noted by us and others, we observed that reporter oscillations are faster in posterior PSM cells than in anterior PSM cells (Figure 3.1A-C), and that reporter expression levels in anterior PSM cells are larger in amplitude than in posterior PSM cells (Figure 3.1B,C). We quantified the periodicity of oscillations by measuring the time between each peak of fluorescence and normalizing it to the somitogenesis period. As expected, cells in the posterior PSM (Figure 3.1D, "S-5" to "S-3") oscillate with a periodicity that closely matches somitogenesis (Guidicelli *et al.* 2007, Holley *et al.* 2000, Oates 2012). The periodicity increases in a linear fashion as cells progressed anteriorly, with a 50.7% longer period (Standard Error (S.E.) = 1.2%) by the last oscillation (Figure 3.1D). We did not see evidence of period divergence to infinity, contrary to suggestions in previous models (Guidicelli *et al.* 2007). We also observed an increase in amplitude of clock expression in the last two oscillations of anterior PSM cells (Figure 3.1E).Clock expression in the posterior PSM has little or no change in amplitude when compared to the previous oscillation (Figure 3.1E, "S-5" to "S-3"). However, we noted a 58.9% (S.E.=3.6%) increase in fluorescence in comparing the second-to-last oscillation with the third-to-last oscillation ("S-2" vs. "S-1"), and an additional 70.1% (S.E.=4.6%) increase when comparing the last oscillation with the second-to-last (Figure 3.1D, "S-1" vs. "S0"). The gradual amplification and slowing of the clock was observed in all PSM cells (4 embryos, 243 cells), regardless of a cell's final position within a formed somite.

With cells in the posterior PSM oscillating with the same periodicity as somitogenesis, one wave of clock expression is propagated through the PSM for each somite formed. As the clock slows, these waves condense into narrowing peaks of expression. Steady-state models of somitogenesis routinely position peaks of clock signal at one-somite length intervals across the entire PSM, where period eventually diverges towards infinity at the anterior PSM, with opposing levels of clock expression on either side of the forming boundary (Guidicelli 2007, Morelli *et al.*, 2009, Herrigan *et al.* 2010, Oates 2012). To determine if the rate of clock slowing changes the spacing of peaks of clock signal in the anterior PSM, we followed reporter expression over time in cells that eventually form either side of somite boundaries (Figure 3.2A, A'). Since adjacent cells can eventually end up in adjacent somites, we investigated when their behavior diverged. We found that oscillations in anterior boundary cells of the forming somite (cells circled in red, Figure 3.2A') are nearly synchronous to cells in the adjacent posterior boundary of the previously formed somite (circled in blue, Figure 3.2A', B). A prominent distinction between these two neighbor populations is that cells in S0 will oscillate one more time, while cells incorporated into S1 cease oscillations. We observed a similar pattern in boundary cells that formed the previous somite (circled as green and orange in Figure 3.2A'): synchronous oscillations (Figure 3.2D), with cells that form the future anterior S1 boundary oscillating one more time after boundary cells that form the future posterior S2 boundary have stopped (Figure 3.2D).

In models where the clock's period diverges to infinity at the arrest front, cells at a one-somite distance are phase shifted by one cycle of the clock, with that phase shift spread across the length of one presumptive somite (Morelli *et al.* 2009, Oates 2012). As expected, we find that cells in the posterior PSM oscillate in synchrony, even when at a one somite distance (Figure 3.3). However, in the anterior PSM, cells that incorporate into the anterior border of S0 have opposite levels of expression compared to cells that incorporate into anterior-most border of S1 (Figure 3.2C). That is, when presumptive anterior border S0 cells have peak expression levels, presumptive anterior border S1 cells are at the expression trough, and vice versa. This distinct anti-phase relationship is observed when comparing any two groups of anterior PSM cells separated by one somite length, including cells that incorporate into the posterior-most border (Figure 3.2E) or center of formed somites (not shown). These oscillation relationships among PSM cells were consistent at every forming somite boundary we examined (15 boundaries across 5 embryos): cells at a one-somite distance initially oscillate in synchrony in the posterior PSM, but as the clock slows in the anterior PSM, they shift into anti-phase. This spacing of clock phase is correlated with somite boundary formation. As the furrow of the somite boundary begins to form, a peak of clock expression is observed one somite-length away (Figure 3.4).

To globally compare anterior PSM oscillation phase across multiple boundaries and embryos, we quantified the synchrony of these anterior PSM cells. To counteract the stochasticity of our reporter fluorescence measurements, we used a smoothing heuristic we developed previously (Delaune and Francois *et al.* 2012) to estimate each cell's oscillations, a process validated by the Hilbert's transform (data not shown). We used these smoothed oscillations to calculate the clock phase in each cell at each timepoint; phase calculations were then used to quantify the phase difference between any two cells at any given timepoint as long as both cells were still oscillating. Tracked cells were indexed based on their final position within a developing somite, either at the anterior or posterior border. The phases of cells constituting each boundary were compared to each other in a combinatorial fashion. Cells in the same compartment exhibited a high level of synchrony with very little phase difference between cells at any given time point (35,740 comparisons across 4 embryos, Figure 3.2F). As expected, cells on either side of a somite boundary are slightly less synchronized than cells on the same side of a somite boundary (17,353 comparisons, across 4 embryos, Figure 3.2G). Across a larger distance, clock synchrony in the anterior PSM continues to decrease (15,003 comparisons across 4 embryos, Figure 3.2H), with maximum phase difference at one somite-length away (25,326 comparisons across 4 embryos, Figure 3.2I). These data validate previous observations that cells in close proximity are synchronized (Delaune and Francois *et al.*, 2012), and we show here that a somite boundary does not create an exception to that finding. Instead, a gradual phase gradient is distributed along the length of the anterior PSM, with adjacent cells oscillating in phase and cells at a one-somite distance in anti-phase.

To gain a better sense of how clock oscillations behave throughout the entire PSM, we looked to a tissue-level analysis of clock behavior. Single cells exhibited some variability in reporter intensity in their oscillations and only covered a relatively small area of the entire PSM. By broadly analyzing the waves of clock expression across space and time, we can search for repeating patterns of clock oscillations that match the repeated formation of somites. Using automated scripts, z-stacks of images at each timepoint were processed to detect the embryo's axis based on injected nuclear and membrane labels. We divided the somite and PSM tissue into sectors - with each future somite delineated into thirds (Figure 3.5A) - and measured the total fluorescence within each sector at each timepoint. The clock expression pattern in each somite recapitulated our single-cell observations: in the anterior PSM, stripes of tissue separated by a one-somite distance were in anti-phase with each other and cells that were separated at a distance of two somites were in phase with each other (two embryos shown, Figure 3.5B, C). These findings are based off the center third of each somite, to ensure fluorescence measurements were representative from only one somite.

An embryo-wide profile of clock expression dynamics generated by measuring reporter fluorescence across the entire AP axis (without individual cell tracking) resembles the spatial readout of mRNA levels using *in situ* hybridization. However, our system measures spatial expression profiles over developmental time in a single embryo, rather than at a single time point in a fixed embryo. Tissue-wide fluorescence was quantified by totaling reporter signal within each digital slice of PSM. Based on morphological furrowing of somite boundaries, we examined fluorescence reporter levels in the PSM at each moment a somite was forming more anteriorly (Figure 3.5D-D’’’, E-E’’’). At each time point, we observed peaks of expression in the forming somite (S0) and at a two-somite distance (S-2), with minimal clock expression at the S-1 position (Figure 3.5F,G). This pattern recapitulates the two stripes of expression seen in fixed embryos, with an alternating gap of gene expression between the newly forming S0 and the subsequent S-2. As the cells in S0 form a somite, cells that were previously in the S-1 position are now in S0. The pattern repeats, with cells in the new S0 and S-2 peaking in expression while S-1 cells (halfway between these two peaks) are at a minimum level of expression. The only difference between these two patterns is that peaks are shifted one-somite length posteriorly as each somite forms. Cells that end up in adjacent somites have opposite levels of clock expression in the anterior PSM, both temporally and spatially. This alternating pattern was recapitulated even when the clock was slowed using a *hes6* anti-sense morpholino, which has been previously shown to create larger somites (Schröter and Oates, 2010, Figure 3.6) This indicates that the dynamics of the phase gradient do not depend on the absolute period of the oscillators, which supports the idea that the phase gradient itself is regulated and crucial for somite formation (Lauschke *et al.* 2013)

Discussion

Since the discovery of cyclic segmentation clock genes, researchers have explored how these oscillations are translated into patterning future somites. Much of the work focuses on clock dynamics in the posterior PSM, where clock periodicity matches that of somite formation (Oates, 2012). Because a kinematic wave of clock expression narrows as it sweeps across the PSM, it is clear that the clock slows anteriorly (Guidicelli *et al.* 2007, Morelli *et al.* 2009). The gradual slowing of the clock has received less attention, largely due to the lack of tools to measure changes in expression dynamics. We investigated how the longer clock periodicity in the anterior PSM manifests in real time as the embryo develops.

Using an *in vivo* clock reporter, we examined clock expression in individual PSM cells as the embryo developed, correlating clock oscillations with morphological somite formation. We observed that segmentation clock periodicity and amplitude increases in the anterior PSM, with each wave of clock expression corresponding to a forming somite boundary. Our measurements of the clock slowing matches mathematical predictions made in mice (Niwa 2011). The increase in period and amplitude may be connected, with a longer period allowing for more protein to accumulate. Although it is not clear what regulates the change in cyclic gene expression dynamics in the anterior PSM, we know that *her1* expression in the anterior PSM is controlled by distinct regulatory elements (Gajewski *et al.* 2003, Brend *et al.* 2009), including a 500bp upstream region with binding sites for Tbx24, Su(H), and Hairy-related transcriptional regulators (Brend *et al.* 2009). Additionally, wavefront components, including FGF, Wnt, and RA (Aulehla and Pourquié 2010), likely contribute to differential *her1* regulation in the anterior versus posterior PSM.

In vivo imaging of clock dynamics confirms that clock expression in the anterior PSM slows, while also revealing that peaks of expression are separated with nearly a two-segment periodicity. The slowing of the clock creates a spatial and temporal phase gradient with expression marking two future alternating somites, with a gap of expression between them. This *in vivo* pattern mirrors previous fate maps and *in situ* data: the distance between stripes of anterior PSM *her1* expression was measured to be up to two somites in length (Muller *et al.* 1996, Holley *et al.* 2000). Recent steady-state models of clock expression assert that expression peaks are separated by only one-somite length in the anterior-most PSM (Guidicelli *et al.* 2007, Morelli *et al.* 2009). The distance between each domain of segmentation gene expression differs among arthropods, with segmentation genes expressed at a one-segment length in spiders (Damen 2007) or a two-segment length in insects such as beetles and fruit flies (Damen 2007, Sarrazin *et al.* 2012). Our analyses definitively show that peaks of clock expression are spaced at a two-segment length in the anterior PSM in vertebrates. While *her1* is expressed as a dynamic kinematic wave, it is intriguing that *her1* spatial distribution in the anterior PSM at any given time has a similar alternating segment pattern to that of the *Drosophila* pair-rule genes (Nusslein-Volhard and Wieschaus 1980, Muller *et al.* 1996).

In the original clock and wavefront model, the clock oscillates between a permissive and restrictive phase, interacting with the wavefront to mark distinct blocks of cells for somite formation (Cooke and Zeeman 1976). One issue of this model is that for each group of cells incorporated into a somite by the permissive phase of the clock, another group of cells is necessarily excluded because it is in the restrictive phase of the clock. Later models attempted to incorporate additional features, such as the slowing of the clock. A steady-state model predicted that clock periodicity increases to infinity at the PSM-somite boundary, polarizing the forming somite with high clock expression in the anterior half and no clock expression in the posterior half (Morelli *et al.* 2009, Oates 2012). These predictions were based on the width of the anterior-most stripe of *her1* transcripts in fixed embryo (Holley *et al.* 2000, Sawada *et al.* 2000) and on the spacing of stripes in the anterior PSM (Guidicelli *et al.* 2007). Our real-time imaging clearly shows that the Her-Venus clock reporter is not constantly expressed in the anterior half of the next presumptive somite. The half-somite stripe of clock expression observed in fixed embryos is probably the last portion of the kinematic wave of clock expression sweeping through the PSM. Differences in interpretation may also be due to the focus on mRNA transcripts in fixed embryos, compared to protein levels in our *in vivo* experiments (cyclic mRNA and proteins are expressed in offset domains, see Guidicelli *et al.* 2007, Delaune and Francois *et al.* 2012). We clearly see that clock expression in the anterior PSM is not restricted to any subset of cells; instead, all cells are oscillating, even at the PSM-somite boundary.

Based on our findings, we believe that the slowing of the clock in the anterior PSM creates a phase gradient of clock expression that cycles with two-somite periodicity. This phase gradient is continuous (Figure 3.7A), as observed in various real-time clock reporters (Masamizu *et al.* 2006, Aulehla *et al.* 2008, Takashima *et al.* 2011, Delaune and Francois *et al.*, 2012, Lauschke *et al.*, 2013), with no sharp breaks between any group of neighboring cells until the clock stops as cells are incorporated into somites. Continuity is expected given that these oscillations are coordinated by the Notch pathway to create a kinematic wave sweeping anteriorly in the PSM (Lewis 2003, Horikawa *et al.* 2006, Mara *et al.* 2007, Riedel-Kruse *et al.* 2007, Ozbudak *et al.* 2008). This coordination acts via a cell-to-cell contact of the Delta ligand and Notch receptor, causing delayed coupling of clock oscillations in neighboring cells (Figure 4B, Morelli *et al.* 2009, Herrigan *et al.* 2010). The synchrony generated by oscillating *her* genes and the Notch pathway is more parsimoniously explained by our phase gradient model than a steady-state model. Since the Notch pathway only communicates through adjacent cells and not the broad tissue, a steady-state model would require a separate mechanism to cause clock oscillations in half the cells in a future somite to diverge to infinity, while the other half arrest and remain off (Figure 3.7C). In a continuous phase gradient model, cells in the anterior PSM continue to oscillate in synchrony with their neighbors, regardless of future somite position (Figure 3.7C).

The increased spacing and amplitude of clock peaks in the anterior PSM could be important in defining where to make a somite boundary. The phase of the clock could be used to determine both temporal and positional information. Clock expression could be, for example, discretized into anterior-posterior fates using a downstream bistable system (Meinhardt 1982, Francois *et al.* 2007). As clock expression increases over the last two oscillations, its amplitude may reach a threshold required to permanently repress its own expression and drive differentiation of PSM cells into a somite. The spacing of these peaks of expression would also help the embryo differentiate how to respond to these increased oscillations. With peaks at a two-somite length, cells in future adjacent somites are experiencing a maximal difference in clock expression. This two-somite periodicity is preserved in the anterior PSM through the slowing of the clock, even though a wave of clock expression is generated in the posterior PSM every time one somite forms. Steady-state models contend that peaks of expression in the anterior PSM are spaced at a one-somite periodicity, but we do not observe this in our study. The two-somite periodicity that we do observe may actually not be too shocking when framed in an evolutionary context, as this two-segment spacing of segmentation genes has been observed in *Drosophila* and the beetle *Tribolium*, (Damen 2007, Sarrazin *et al.* 2012). This correlation of gene oscillations and specific morphological landmarks is a broad theme in both animal and plant development, such as *Arabidopsis* periodically expresses auxin to mark the position of lateral root formation (Moreno-Risueno *et al.* 2011).

As we continue to investigate somitogenesis, more sophisticated analytical tools will expand our understanding of the underlying mechanisms. Our findings have revealed the complex behaviors of the segmentation clock and how the clock may play a more central role in segmenting boundaries. The slowing of the clock in the anterior PSM is precise, generating separation of phase both temporally and spatially. Real-time reporters are important to capture dynamics not otherwise observable, and will continue to enhance our understanding of the segmentation clock.

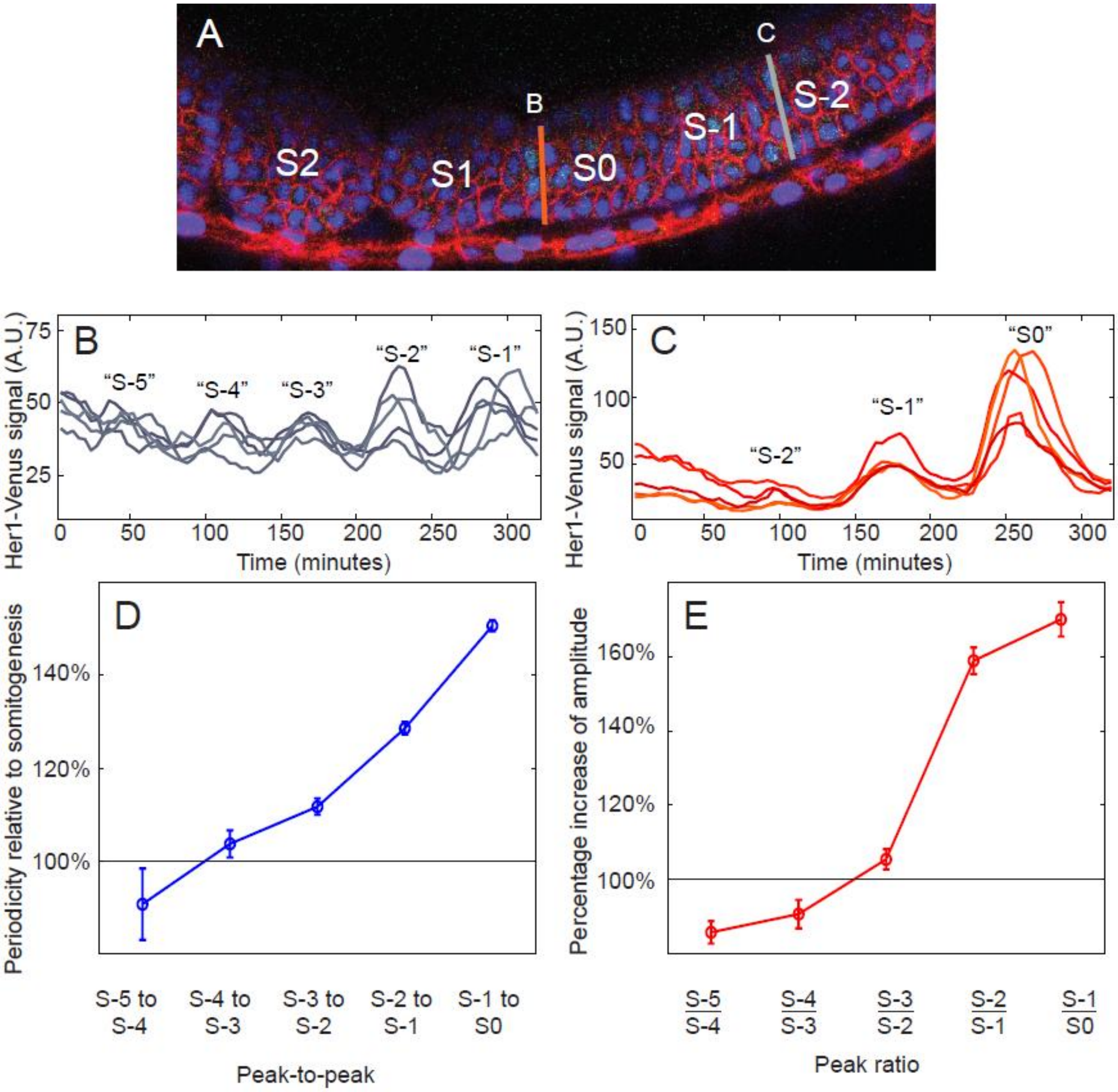
A
C
S-2
B
S-1
S2
S1
S0
B
"S-5"
"S-4"
"S-3"
"S-2"
"S-1"
Her1-Venus signal (A.U.)
75
50
25
0
50
100
150
200
250
300
Time (minutes)
C
"S0"
"S-1"
"S-2"
Her1-Venus signal (A.U.)
150
100
50
0
50
100
150
200
250
300
Time (minutes)
D
Periodicity relative to somitogenesis
140%
120%
100%
S-5 to S-4
S-4 to S-3
S-3 to S-2
S-2 to S-1
S-1 to S0
Peak-to-peak
E
Percentage increase of amplitude
160%
140%
120%
100%
S-5 / S-4
S-4 / S-3
S-3 / S-2
S-2 / S-1
S-1 / S0
Peak ratio

Figure 3.1: Clock expression slows and amplifies as it enters the anterior PSM.
(A) Example embryo indicating somite designations in PSM and developing somites, with regions delineating formed somites (S1, S2), forming somite S0, and future somites (S-1, S-2) indicated. The Her1-Venus reporter fluorescence is shown in green, and labeling of the nucleus and cell membrane is indicated by H2B-Cerulean (blue) and lyn-mCherry (red), respectively. (B,C) Single-cell clock oscillations in a group of 5 neighbors in the posterior (B) and anterior (C) PSM. Approximate position of the cell within the developing PSM is included in quotes above the expression peaks. (D) The periodicity of clock expression relative to the periodicity of somitogenesis. Periodicity of oscillations measured based on time between peaks of maximum expression (n=243 cells). (E) The change in clock expression amplitude measured in four embryos (n=243 cells), based on the ratio of periodicity change between two sequential oscillations.

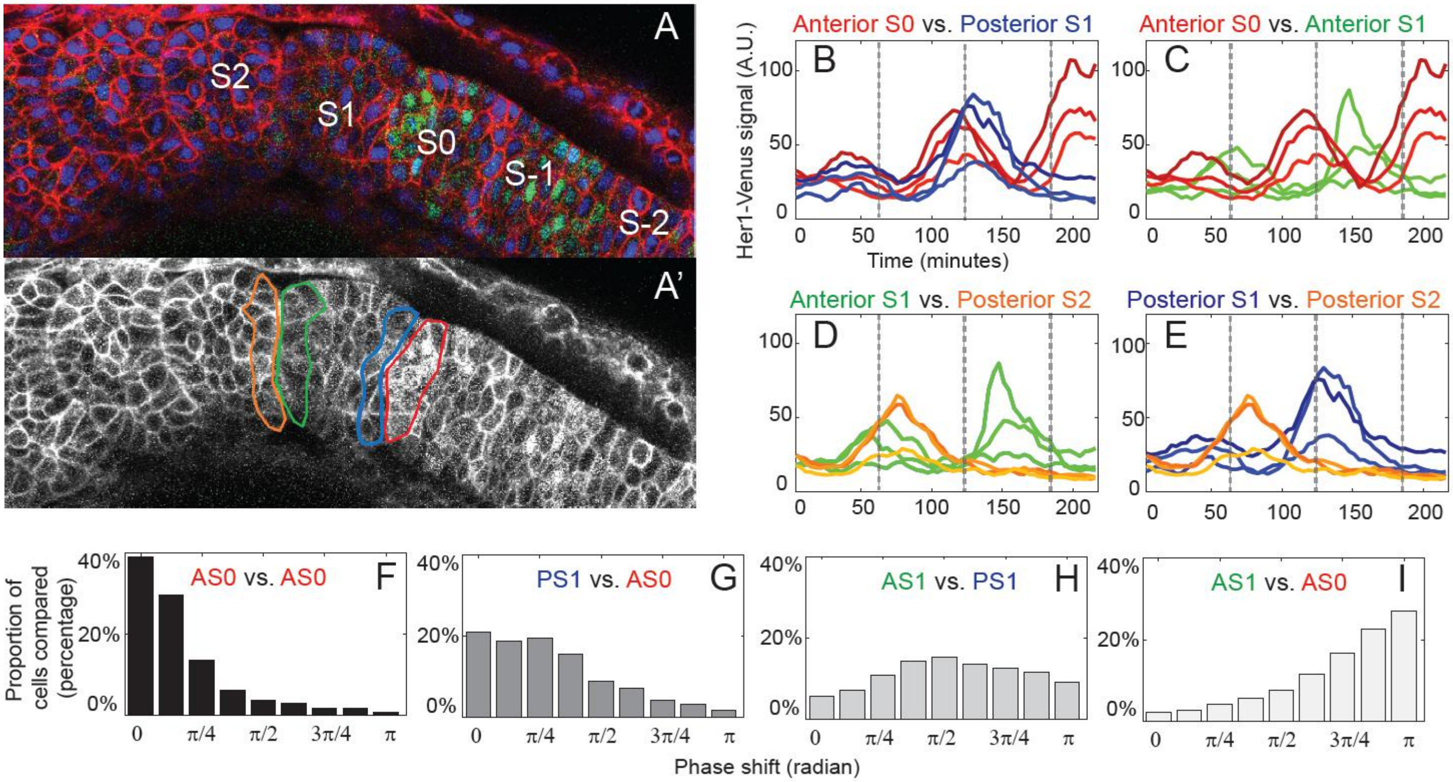
A
S2
S1
S0
S-1
S-2
A'
Anterior S0 vs. Posterior S1
B
Anterior S0 vs. Anterior S1
C
Anterior S1 vs. Posterior S2
D
Posterior S1 vs. Posterior S2
E
Her1-Venus signal (A.U.)
100
50
0
0
50
100
150
200
Time (minutes)
Proportion of cells compared (percentage)
40%
20%
0%
AS0 vs. AS0
F
PS1 vs. AS0
G
AS1 vs. PS1
H
AS1 vs. AS0
I
0
π/4
π/2
3π/4
π
Phase shift (radian)

Figure 3.2: Synchrony of anterior PSM cells depends on distance between cells
(A) Embryo at one timepoint (220 min, in B-E) during a time lapse. Her1-Venus reporter fluorescence is indicated in green, with nuclei and membrane labeled with H2B-Cerulean and lyn-mCherry, respectively. (A') Black and white image of the same embryo in A. Colored outlines indicate the cohort of cells used to represent each boundary. S0 and S1 boundary cohorts (red/blue and orange/green, respectively) were identified by retrospectively tracing actual boundary cells. (B-E) Raw reporter fluorescence levels of 3 representative cells from each boundary cohort indicated in A'. To indicate periodicity of somite formation, gray dotted lines indicate times at which somite boundaries are forming more anteriorly in the imaged embryo. (F-I) Histograms of phase differences between boundary cell cohorts. Phase differences are plotted between 0 (indicating cells are in phase) and π (indicating opposite phase). Distance between the two populations compared increase from left to right. Average phase differences are 0.75 (F), 1.12 (G), 1.59 (H), and 2.17 (I), calculated from 15003-35740 pair-wise comparisons over 4 different embryos.

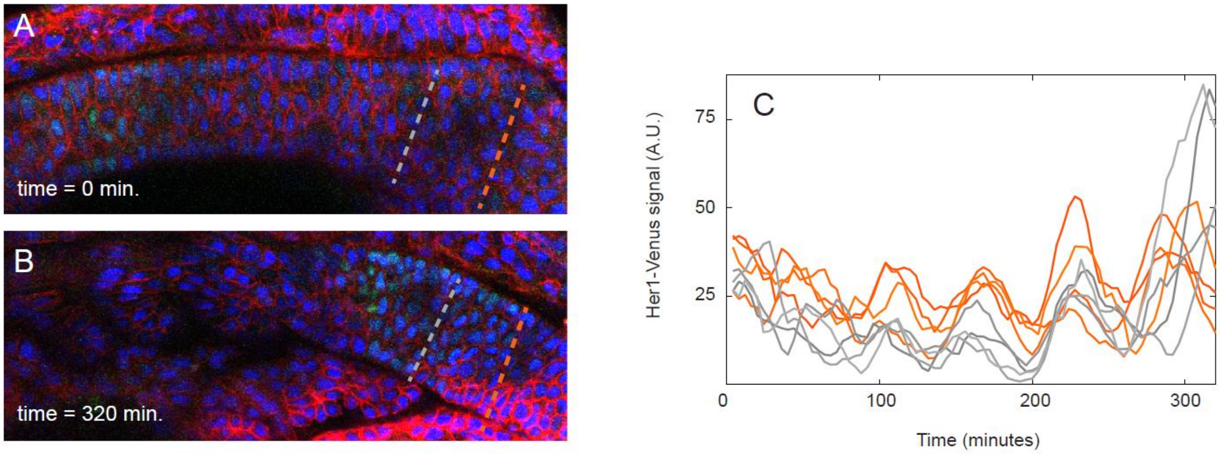
A
time = 0 min.
B
time = 320 min.
C
Her1-Venus signal (A.U.)
75
50
25
0
100
200
300
Time (minutes)

Figure 3.3: Cells in the posterior PSM oscillate in-phase with each other.
A representative embryo at the beginning (A) and end (B) of a timelapse experiment. Orange and gray dotted lines indicate position of cells that were sampled for oscillations. At t=0, the cells lie roughly at S-4 and S-5Y, respectively, and at the end of the movie, they are at approximately S-1 and S-2 (C) Oscillations of five representative cells from each region are shown here. Oscillation synchrony of these two populations clearly diverge by the last oscillation of the timelapse (t=300 minutes).

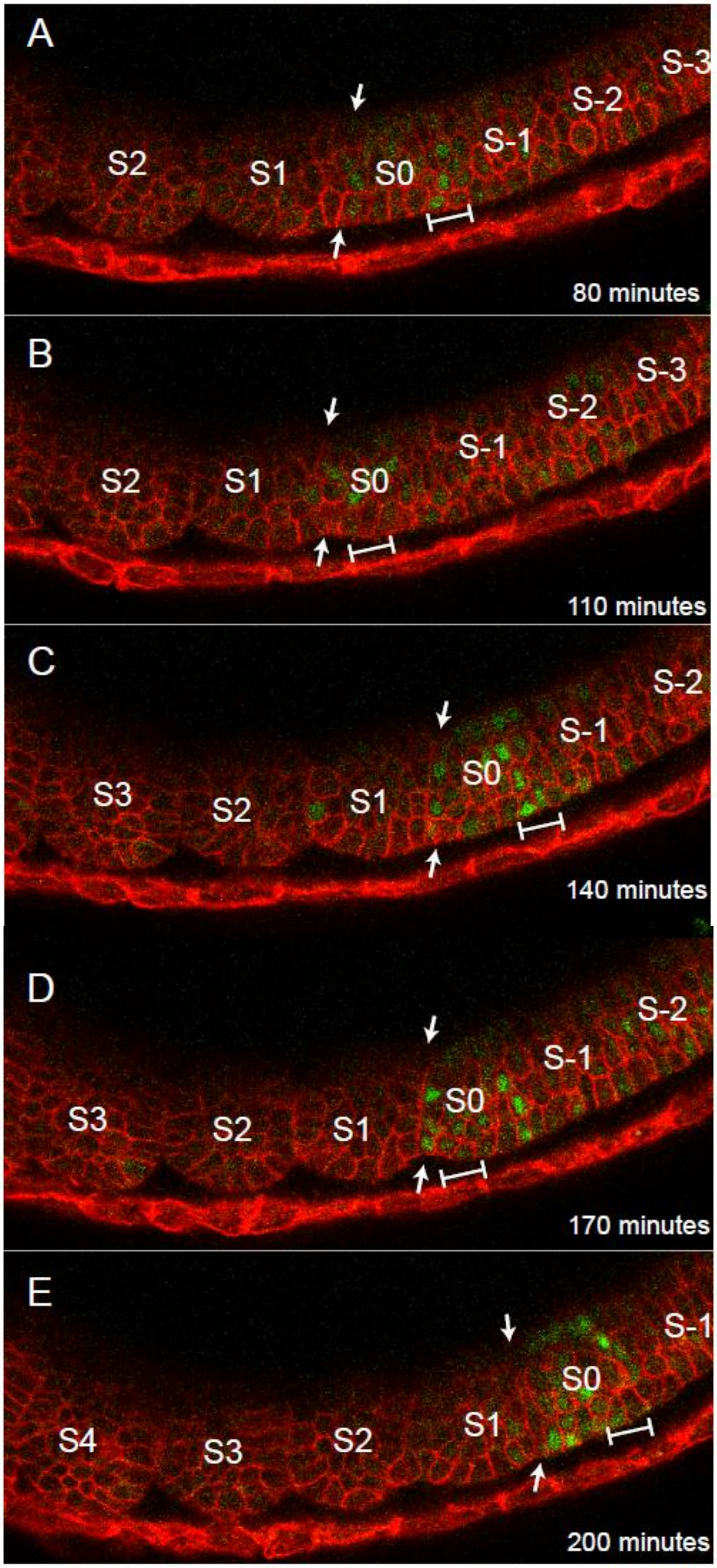
A
S2
S1
S0
S-1
S-2
S-3
80 minutes
B
S2
S1
S0
S-1
S-2
S-3
110 minutes
C
S3
S2
S1
S0
S-1
S-2
140 minutes
D
S3
S2
S1
S0
S-1
S-2
170 minutes
E
S4
S3
S2
S1
S0
S-1
200 minutes

Figure 3.4: Correlation of clock wave and somite boundary formation.
(A-E) White arrows mark the furrowing of the most recent-forming somite boundary. White brackets denote cells experiencing peak of clock expression in the anterior PSM. Somites labeled based on conventional nomenclature.

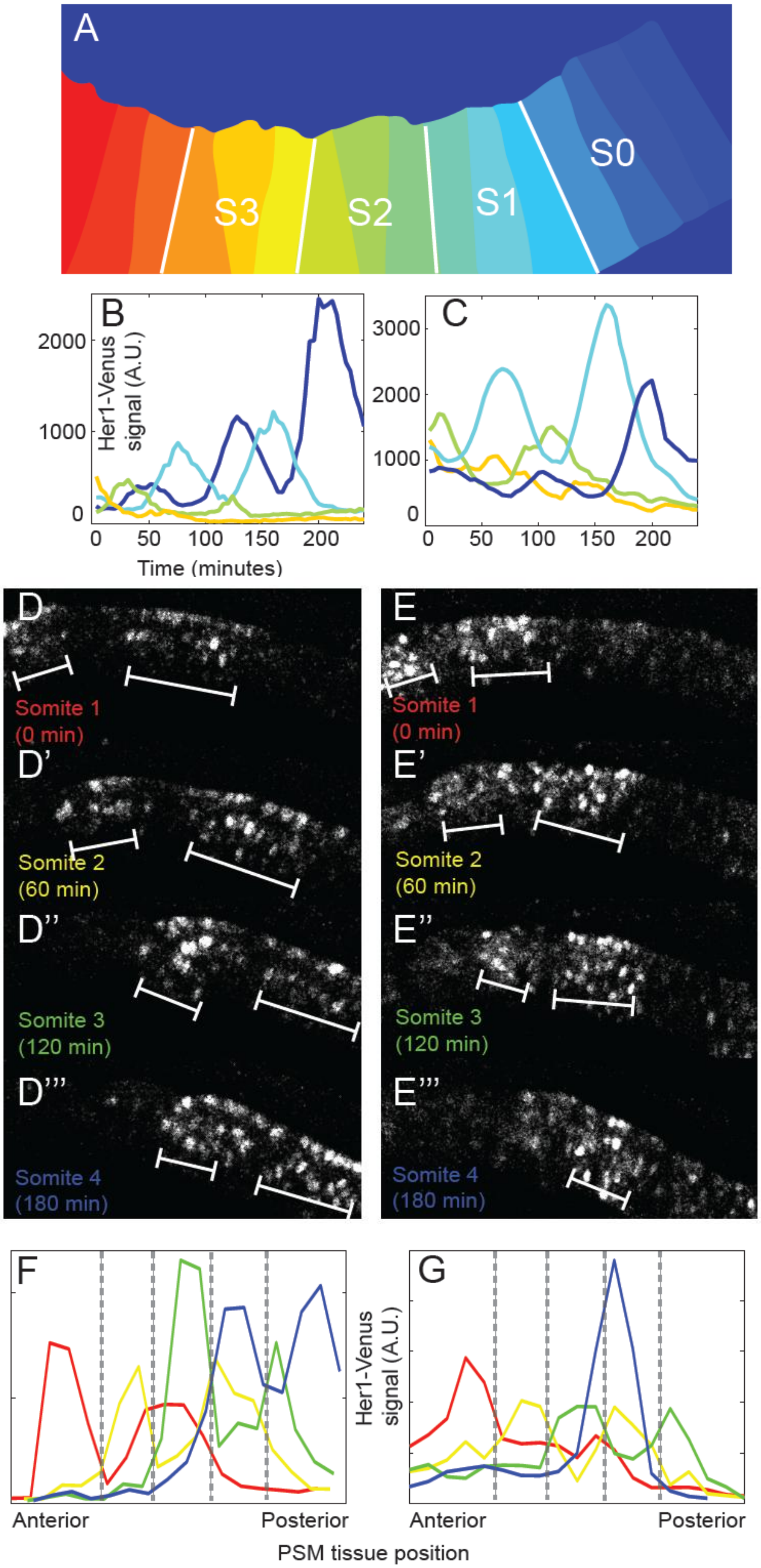
A
S3
S2
S1
S0
B
Her1-Venus signal (A.U.)
2000
1000
0
0
50
100
150
200
Time (minutes)
C
3000
2000
1000
0
0
50
100
150
200
D
Somite 1 (0 min)
D'
Somite 2 (60 min)
D''
Somite 3 (120 min)
D'''
Somite 4 (180 min)
E
Somite 1 (0 min)
E'
Somite 2 (60 min)
E''
Somite 3 (120 min)
E'''
Somite 4 (180 min)
F
Anterior
Posterior
G
Her1-Venus signal (A.U.)
Anterior
Posterior
PSM tissue position

Figure 3.5: In anterior PSM tissue, clock expression has a two-somite periodicity. (A) An example of PSM tissue separated into slices for tissue-level fluorescence measurements. White lines denote position of somite boundaries at the end of the timelapse. (B,C) Tissue-wide fluorescence quantification in two representative embryos. Total fluorescence in the center slice of each future somite and S0 is plotted through time. Line color matches stripe position in (A). (D,E) Raw fluorescence confocal image of Her1-Venus signal (a merge of 5 consecutive z-stacks) in two different embryos. Images shown are PSM "snapshots" taken just as a somite is forming more anteriorly, based on morphological landmarks. White brackets denote areas of highest clock reporter expression. (F,G) Clock reporter levels quantified across the PSM at the same timepoints shown in (D) and (E), respectively. Line color corresponds to labeling in (D) and (E). Gray dotted lines mark morphological somite boundaries (that appear later).

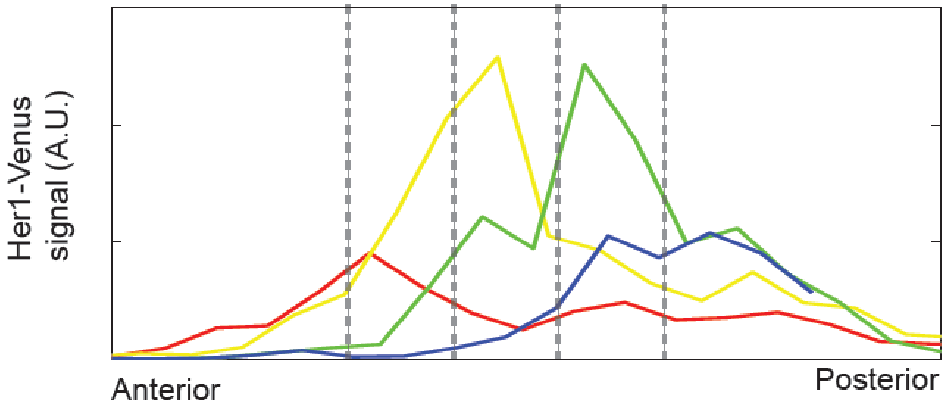
Her1-Venus
signal (A.U.)
Anterior
Posterior

Figure 3.6: Clock gene oscillations in hes6 MO-injected embryos show the same two-segment periodicity in the anterior PSM as in wildtype.
The reporter fluorescence across the entire embryo axis is shown at four different timepoints, at the moment a somite forms more anteriorly. Gray lines denote position of future morphological somite boundaries.

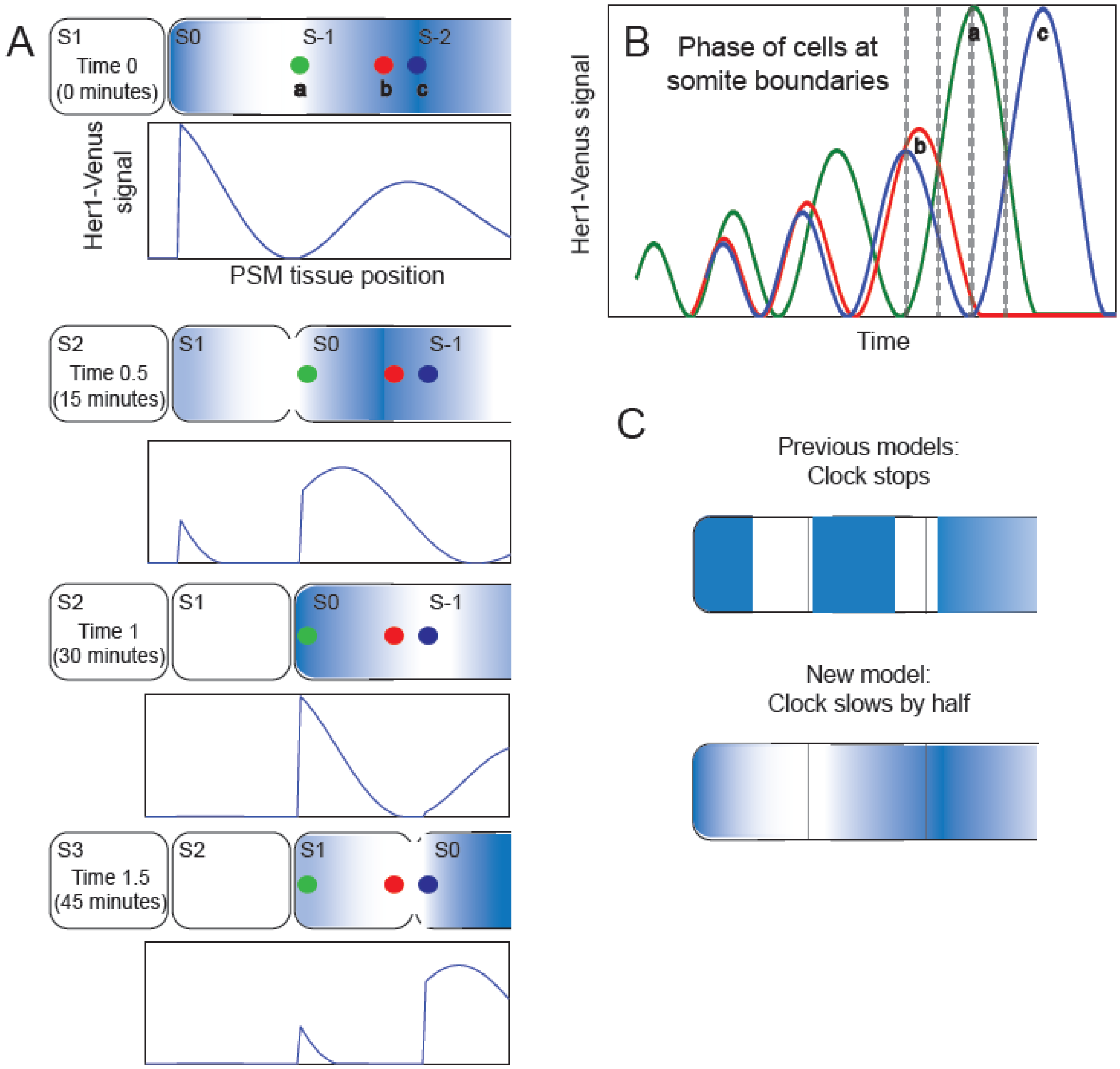
A
S1
Time 0
(0 minutes)
S0
S-1
S-2
a
b
c
Her1-Venus signal
PSM tissue position
S2
Time 0.5
(15 minutes)
S1
S0
S-1
S2
Time 1
(30 minutes)
S1
S0
S-1
S3
Time 1.5
(45 minutes)
S2
S1
S0
B
Phase of cells at somite boundaries
a
b
c
Her1-Venus signal
Time
C
Previous models:
Clock stops
New model:
Clock slows by half

Figure 3.7: A modified model of segmentation clock expression.
Idealized instantaneous phase of clock expression, with two timepoints for each somite formed. Blue shading indicates clock expression intensity, while white represents little or no clock expression. Diagrams under each embryo schematic show expression pattern of the entire embryo at that timepoint. Colored dots represent anterior boundary (green and blue) and posterior boundary (red) cells. (**B**) Clock expression of individual cells over time. Line color corresponds to cell position in (A). Dotted lines indicate the timepoints shown in (A – A’’’). (**C**) Comparison of instantaneous phase pattern between previous models and our new model of somitogenesis.

Chapter 4

Asymmetric Segmentation Clock Signaling as a Mechanism to Pattern Somite Polarity

Introduction

In vertebrates, semi-repetitive epithelial blocks, called somites, are formed sequentially from the elongating tailbud and presomitic mesoderm (PSM). Somites eventually give rise to repeated structures in the body, such as vertebrae and axial muscles. The segmentation clock controls the periodicity of somite formation, pacing a regular rate of somite formation within a given species of vertebrates. The clock was originally proposed to oscillate PSM cells between a permissive and restrictive phase with a periodicity that matched that of somite formation (Cooke and Zeeman, 1976). Elucidation of the molecular mechanisms behind the clock revealed a sweeping, kinematic wave of gene expression that begins in the tailbud and sweeps through the PSM with a periodicity that matches that of somite formation (Holley 2007, Lewis 2009, Pourquié 2011, Oates 2012). Several genes have been shown to oscillate in the PSM, including components of the FGF, Wnt, and Notch pathway. One family of transcriptional repressors, *hairy/enhancer-of-split-related* (known as *her* in zebrafish) genes, has been shown to oscillate in a broad range of vertebrates, including zebrafish, chicks, and mice. Each somite forms as a kinematic wave of *her* expression reaches the somite-PSM boundary. These clock genes are clearly pacing the rate of somitogenesis, but their role in doing so is unclear.

Formed somites are clearly separated into rostral and caudal portions, with unique gene expression profiles for each half. How exactly these two compartments are distinguished is still being investigated, though the *mesoderm posterior* (*mesp*) genes have been implicated to play an important role. The loss of *Mesp2* in mice causes caudalization of somites, while overexpression of *Mesp2* causes somites to acquire a rostral fate (Saga *et al.* 1997). There is also evidence of genetic interactions of Mesp genes with oscillating Notch components, including cylic *her* expression. In zebrafish, *mespb* expression localizes just rostrally of *her1* expression in zebrafish (Sawada *et al.* 2000), and slight perturbations of clock expression have resulted in a similar perturbation in *mespa* expression (Delaune and Francois *et al.*, 2012). Recent work has shown that the oscillations of the clock gene *her1* slows and amplifies in anterior PSM cells, the same region where *mesp* genes are expressed (Shih 2014). Given that *her* signaling begins earlier in the PSM than *mesp*, could *her* genes be playing a role in both determining somite formation and signaling somite polarity factors?

Here, we demonstrate that waves of segmentation clock expression can be sufficient to signal the initiation of polarity definition of each somite. We show that the sweeping waves of clock expression are asymmetrically expressed within each forming somite: signal gradually increases in amplitude in the caudal region of the presumptive somite before sharply dropping off at the forming somite boundary. We also generate simulations of this behavior, and show that the specific rates of clock slowing and amplification are necessary to drive the asymmetries we observe.

Results and Discussion

Using the *her1-venus* reporter, we observe that the slowing and amplification of segmentation clock signal is theoretically sufficient to pattern and polarize forming somites. We imaged *her1-venus* transgenic zebrafish embryos for 4-6 hours, with a z-stack taken approximately every 4 minutes, as described in previous work (Delaune and Francois *et al.*, 2012, Shih *et al.* 2014). An automated axis detection script defined the curvature of the developing embryo at each timepoint, digitally dividing the tissue into discrete slices (three slices per presumptive somite, Shih *et al.* 2014). We recorded reporter signal within each slice and plotted clock expression detected throughout the embryo for each time point. As reported in previous work, the anterior PSM has increased clock expression that is reliably detectable. The overlay of clock expression at each timepoint reveals a peak in clock expression for each forming somite (Figure 4.1A). Interestingly, each peak is asymmetric across the presumptive somite, with a gradual increase in clock expression in the caudal portion of the presumptive somite followed by a sudden drop of expression at the rostral boundary of the forming somite. These asymmetric peaks of segmentation clock expression generate a sawtooth pattern, a possible mechanism for polarizing each developing somite. We observe that as each kinematic wave of clock expression sweeps through the developing PSM, cells fated for the caudal half portion of the presumptive somite stop oscillating before cells fated for the rostral half of the somite. This provides a temporal distinction between rostral and caudal cell clock signal. Combined with the spatial asymmetries generated from the sawtooth increase of clock expression, each somite can be defined and polarized using the clock signal.

We were able to recreate this sawtooth behavior through a simulation of clock expression based on empirical values of clock slowing and amplification as measured in previous work (Shih *et al.* 2014, Figure 4.1A-D). In our simulations, we estimated the clock slows by 1.5-2 fold, consistent with previous predicted and measured values (Niwa *et al.* 2011, Shih *et al.* 2014). We also included in our model the increased amplitude in the last two oscillations of the clock (Shih *et al.* 2014). The increase of amplitude is an essential characteristic of defining a somite; without appreciable increases in clock expression, we found that the position of the somites cannot be distinguished (Figure 4.1E,F). We also found that the rate of clock slowing is critical in maintaining the sawtooth pattern. The original clock and wavefront model of somitogenesis predicted that the segmentation clock oscillates throughout the PSM, with every cell oscillating with a periodicity that matches that of somite formation (Cooke and Zeeman, 1976; Oates 2012). We found that the lack of clock slowing in the anterior PSM would still generate a sawtooth pattern in each forming somite, but decrease the amplitude of clock expression in each forming somite (Figure 4.2A). A substantial increase in amplitude may be necessary to activate downstream signals of somite differentiation. We also modeled how clock expression changes if the clock slows 3-fold or diverges to infinity, the latter predicted in a previous model of somitogenesis (Morelli *et al.* 2009). When we increased the rate of clock slowing, the differences in amplitude increase, but the spatial maxima of clock expression becomes less sawtooth and more symmetrical (Figure 4.2B). The divergence of the clock to a steady state creates a completely symmetrical peak of clock amplitude at the center of the somite (Figure 4.2C). Only at an intermediate value of clock slowing, with the maximum periodicity twice that of the periodicity of somitogenesis, do segmentation clock patterns retain a sawtooth pattern and an appreciable increase in expression amplitude (Figure 4.2D).

The rate of segmentation clock slowing has important implications in understanding how the clock patterns each forming somite. Known segment polarity genes such as *mespa* and *mespb* have been shown to be dependent on proper clock expression (Sawada *et al.* 2000), and here we argue that *her1* expression is theoretically sufficient to generate this polarity. Based on rates of clock slowing and amplification measured in previous work, we find that clock expression can spatially and temporally distinguish the somite boundaries and rostral-caudal axis of each forming somite. The values we measured of clock slowing match predictions made in mice

(Niwa *et al.* 2011), despite the differences in how the segmentation clock behaves in zebrafish. Importantly, the slowing of the clock in the anterior PSM is precise, slowing to 1.5 to 2 times the periodicity of somitogenesis in both organisms (Niwa *et al.* 2011, Shih *et al.* 2014). This slowing generates a phase gradient in the anterior PSM, where peaks of clock expression are separated with a two-somite periodicity (Lauschke *et al.* 2013, Shih *et al.* 2014). This phase gradient is more prominent in zebrafish due to the shorter periodicity of somitogenesis, resulting in several kinematic waves of clock expression in the PSM at any given time (rather than just the one wave in mice). This spatial separation of phase is further accented by the increasing amplitude of clock expression in the anterior PSM, a phenomenon only recently observed in a single-cell segmentation clock reporter in zebrafish (Shih *et al.* 2014). Finally, the final oscillations of cells incorporated in the caudal region of a somite oscillate earlier than cells incorporated into the rostral region, providing a timing component to the polarization process.

Taken together, we contend that the spatial distribution of the phase gradient, sawtooth amplitude of clock expression within each forming somite, and temporal separation of final oscillations all contribute to properly patterning and polarizing forming somites. The dynamic expression pattern of the segmentation clock is more than just a pacesetter for somitogenesis; its behavior suggests a much more integral role in somite pattern. The caudal portion and forming boundary of each somite is distinguished with a peak of clock signal, while the rostral portion is patterned at a later time with a higher peak of clock signal. The time between each population’s peak of expression has a periodicity that matches somitogenesis, even though both sets of cells individually oscillate with a periodicity of twice that of somitogenesis. The phase gradient set up by the segmentation clock provides a simple mechanism to segment and polarize each somite. The increase in amplitude, slowing of the clock, and two-segment periodicity all act to maximize distinctions between and within each somite.

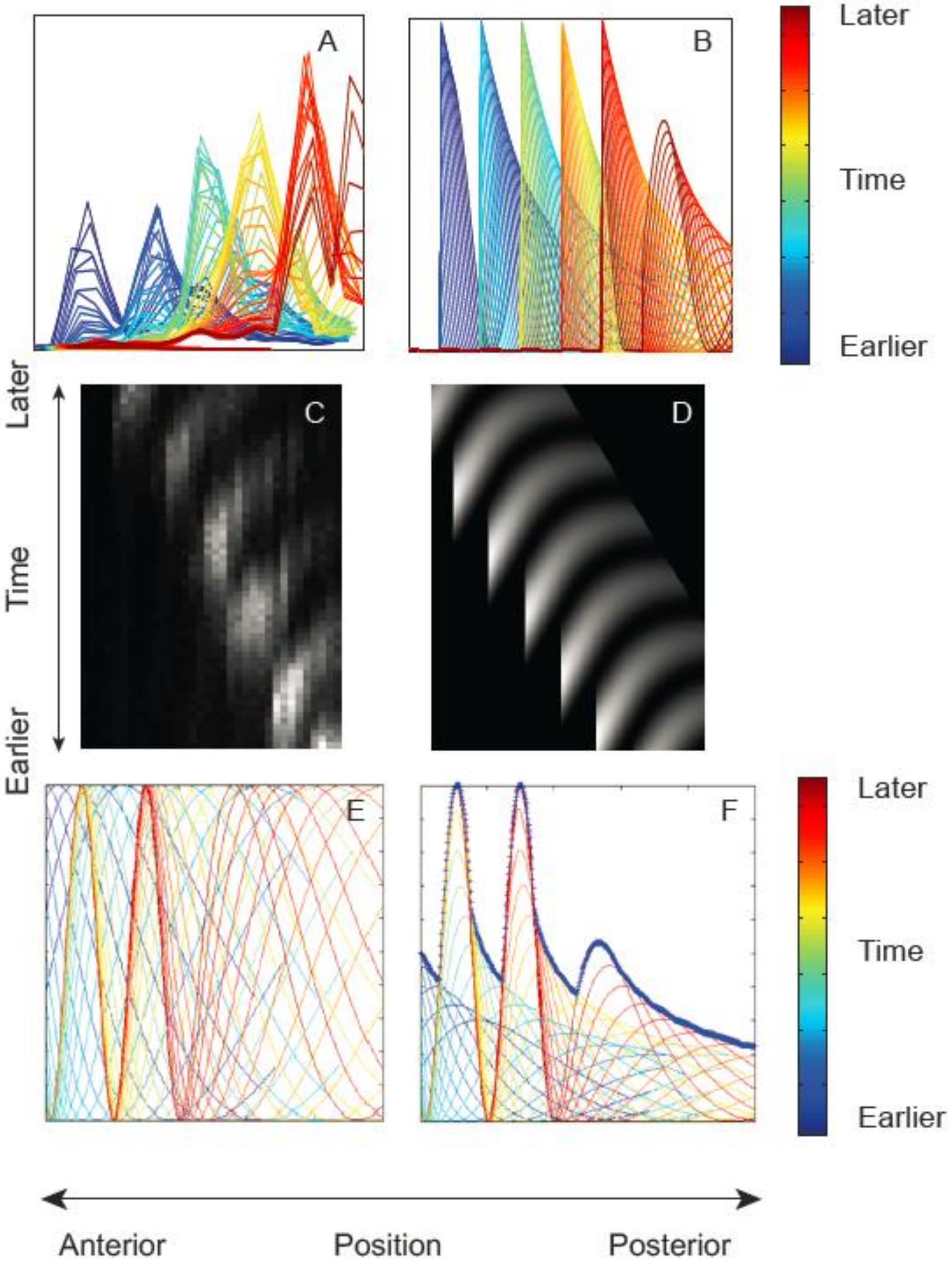
A
B
Later
Time
Earlier
Later
Time
Earlier
C
D
E
F
Later
Time
Earlier
Anterior
Position
Posterior

Figure 4.1: Experimental and theoretical examples of the segmentation clock generating a sawtooth pattern

(A) Overlay of segmentation clock reporter spatial fluorescence throughout the PSM. Each color represents an individual timepoint taken every four minutes throughout a 4 hour movie. (B) A simulation to recreate the pattern generated in (A). (C,D) Kymographs of the same data used to generate the experimental (A) and simulated (B) spatial expression patterns. (E,F) Comparison of spatial pattern if amplitude is not factored into the simulation (E) versus when amplitude is factored into the simulation (F).

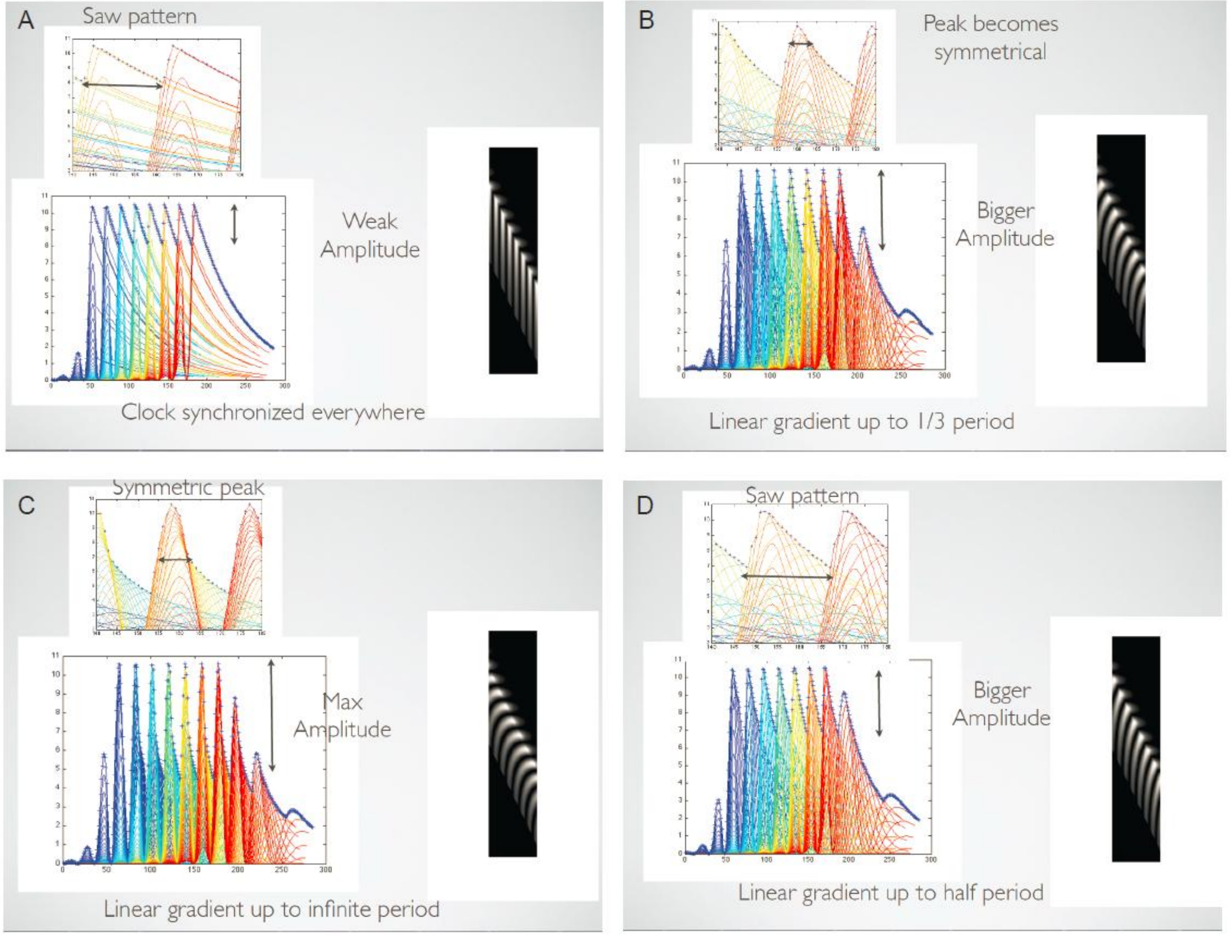

Saw pattern

Weak Amplitude

Clock synchronized everywhere

Peak becomes symmetrical

Bigger Amplitude

Linear gradient up to 1/3 period

Symmetric peak

Max Amplitude

Linear gradient up to infinite period

Saw pattern

Bigger Amplitude

Linear gradient up to half period

Figure 4.2: The slowing of the segmentation clock affects amplitude and symmetry of clock expression

Spatial fluorescence patterns and kymographs are shown for different rates of the clock slowing. Full spatial patterns shown on bottom of each subfigure, zoomed in version on the top; to the right, a kymograph this spatial pattern, with space on the x-axis and time on the y-axis. Different rates of clock slowing shown here are: (A) clock does not slow, (B) clock slows to 1/3 periodicity of segmentation, (C) Clock slows to a stop, and (D) clock slows to ½ periodicity of segmentation.

Chapter 5

Future Directions and Closing Remarks

Depletion of *pnrc2* activity may reduce clock reporter expression levels

The *tortuga* mutation in zebrafish causes *her1* transcript to persist for longer than its normal lifespan, disrupting the oscillatory nature of *her1* clock expression (Dill and Amacher 2005). Recent work in the lab has identified the genomic deletion responsible for the phenotypes observed in *tortuga* mutants, with the deletion encompassing ~20 genes. Of these genes, *proline-rich nuclear receptor coactivator 2* (*pnrc2*) has emerged as the best candidate for regulating the turnover of *her1* transcripts. *pnrc2* has been implicated in nonsense-mediated decay (Cho *et al.* 2009), the process of degrading aberrant mRNA transcripts and in Staufen-mediated decay, the process of degrading a subset of normal, but rapidly degraded, transcripts (Cho 2012). Because of its role in degrading mRNA and location in the zebrafish genome, we suspect it could play a role in regulating transcripts more broadly. When *pnrc2* activity is depleted with morpholinos, *her1* transcripts persist (Amacher lab, unpublished data). This recapitulates the pattern observed in *tortuga* mutants.

These data led us to ask how this *pnrc2* depletion would affect the segmentation clock in real time. If the transcript was persisting for a longer duration than usual, the protein might also persist for a longer duration, accumulating in PSM cells rather than oscillating in a normal fashion. I made several attempts to observe the effect of *pnrc2* depletion on clock oscillations. I injected *pnrc2* morpholinos into heterozygous *her1-venus* embryos and imaged them at the 10-16 somite stage. The morpholino was co-injected with *h2b-cerulean* and *lyn-mcherry* mRNA to mark the cell nuclei and membranes, allowing us to visualize which cells were exposed to our injection solution. Some injections were not completely efficient in labeling every single cell, resulting in mosaic expression of the fluorescent cellular markers. Surprisingly, cells with little or no fluorescent membrane/nuclear signal also expressed higher levels of the *her1-venus* reporter (Figure 5.1). If the injected mRNA and morpholino localized to the same cells, then cells with less *pnrc2* knockdown had higher clock expression from our reporter. Embryos not expressing fluorescent subcellular markers in the PSM expressed levels of Her1-Venus comparable to that of wildtype, while embryos with ubiquitous expression of these fluorescent cellular markers had little or no clock expression within the PSM. So while endogenous *her1* transcript tends to persist in these *pnrc2*MO-injected embryos, Her1-Venus reporter protein levels are diminished.

Since the clock reporter employs the *her1* 8.6kb regulatory region, *her1* UTRs, and Her1 protein, the persistence of endogenous *her1* must be affecting these components. The auto-regulatory behavior of *her1* could diminish clock reporter expression in these *pnrc2* depleted embryos. The loss of *pnrc2* could cause endogenous *her1* transcripts to persist, and this in turn could lead to an overexpression of Her1 protein. Previous work showed that overexpressing *her1* would temporarily repress clock oscillations (Guidicelli 2007), since *her* genes directly target the 8.6kb upstream of *her1* (Lewis 2003, Brend 2009). The extended persistence of *her1* in our *pnrc2* depleted embryos could cause a similar effect, targeting the *her* binding sites upstream of both the endogenous *her1* and the clock reporter. If there is a constant presence of Her1 protein, it could continuously repress clock reporter expression.

This work is promising, but more careful analyses must be done to properly quantify the intensity of clock expression in wildtype and *pnrc2* depleted embryos. Of the seven embryos imaged, one embryo actually seemed to have clock reporter fluorescence comparable to that of wildtype. This embryo was imaged in a different experimental session than the other six, and this result may be due to too little morpholino included in the injection mix (the morpholino stock solution was not properly heated and mixed before use). Careful injections and quantification of fluorescence is especially important since clock expression maximums differ between cells within the same PSM (Figure 5.2) and each cell is oscillating in expression throughout time. Imaging multiple embryos across at least one period of somite formation should account for the oscillating gene expression, and standardizing fluorescence detection sensitivity on the microscope will help with inter-embryo comparisons. Double i*n situ* assays for *her1* and *venus* could also help determine whether the persistence of *her1* coincides with a depletion or overexpression of *venus* transcripts. The use of the *in vivo* clock reporter will be useful to define the role of *pnrc2* in regulating *her* transcript degradation and expression.

Attempts to develop a clock reporter that does not affect the segmentation clock

The current segmentation clock reporter includes the Her1 protein, and some evidence suggests that this could slow segmentation clock periodicity (Delaune and Francois, *et al.* 2012). Embryos homozygous for the *her1-venus* reporter formed segments at a slower rate, resulting in fewer vertebrae than wildtype or heterozygous zebrafish (Delaune and Francois *et al.* 2012). This slowing of segmentation matches data from other studies, which have shown that the loss of Notch signaling or *hes6* transcripts would slow the rate of segment formation and cause larger segments to form (Schroter and Oates 2010, Herrgen *et al.* 2010). I also observe this reduction of vertebrae number in Notch pathway mutants such as *deltaC* and *deltaD*, but not in *her1* and *her7* (Figure 5.3). Vertebrae counts for *notch1a* were not done because the embryos would die before 21 dpf. The lack of segment number differences is consistent with published work (Hanisch *et al.* 2013). One possible reason we observe fewer segments in our embryos is because the extra copies of *her1* may disrupt the timing of clock oscillations. Our reporter has *venus* fused to the C-terminus of *her1*, and this could block the activity of the WRPW domain, a known repressor of gene activity (Fisher *et al.* 1996). The Her1 in the clock reporter may still be able to dimerize with other Her proteins and bind DNA, but not act with normal repressive functions. For these reasons, we sought to develop a modified clock reporter that would not interfere with clock activity.

The first modified reporter we attempted to make introduces two point mutations in *her1* that would knockout the transcription factor's ability to dimerize and bind to DNA. Previous work in flies has demonstrated that two highly conserved residues are necessary for DNA binding and dimerization (Wainwright *et al.* 1992). By mutating these two sites – E21V and R27C – I expected to eliminate the reporter's transcription factor activity without affecting its stability. Embryos injected with this mutated *her1-venus* plasmid displayed some transgenesis (12/43), though no germline transmission has yet to be observed. Another strategy to successfully generate a line would be to inject the embryos and then image them using a confocal microscope. Embryos showing fluorescence could be grown up to screen for germline transmission.

The second attempt at a modified reporter circumvents the Her1 protein entirely, instead fusing an ubiquitin moiety, a nuclear localization signal, and Venus fluorophore together. This reporter was designed based on work in mice (Masamizu *et al.* 2006), in which one or two ubiquitin moieties were fused to luciferase and shown to oscillate *in vivo*. Unpublished work by Emilie Delaune has demonstrated that a single ubiquitin fused with Venus is too diffuse for quantification, while two ubquitins cannot be detected by a microscope at all. The addition of the nuclear localization signal could help concentrate reporter fluorescence to cell nuclei, making it easier to quantify lower levels of expression. Out of 25 potential founders of this nuclear localizing, single-ubiquitin reporter, only two displayed any *venus* transcripts when assayed through *in situ* hybridization. One founder had a very weak stripe of *venus* expression in the anterior PSM, but not the posterior PSM (7/25 embryos). The second founder had expression that recapitulated *her1* expression more faithfully (12/66 embryos) but had extremely weak signal, requiring two hours of coloration to detect compared to just 10 minutes with the current *her1-venus* reporter. Future attempts to generate this transgenic line should use confocal microscopy when screening for founders, which can faster process embryos and ensure the functionality of these modified reporter lines. A non-disruptive reporter can probably be imaged in a homozygous condition, which would increase the signal strength.

At this point, it would be more efficient to re-inject embryos with these modified reporter plasmids and to screen anew. Much of this screening has been done by *in situ* hybridization, though this may not be the most efficient strategy. PCR for the presence of *venus* transgene in fin clips or sperm preps may be a quicker, broader method of isolating potential founders. Screening for actual founders may be better done through live imaging, so that founders can be kept and grown up. A modified reporter will be useful to counteract the potential off-target effects of the current *her1-venus* reporter. The usefulness of any next-generation reporters should be tested by looking for differences in segmentation periodicity, somite size, and segment count compared to both wildtype and *her1-venus* embryos. A less disruptive reporter would allow for more sensitive analyses, such as searching for regulatory binding sites in the 8.6kb upstream of *her1*.

The 300bp regulatory region upstream of *mespb* is insufficient to mimic the endogenous expression pattern

There is evidence that PSM cells commit to their somitic fates at a determination front, approximately two somite lengths from the somite-PSM boundary (Aulehla and Pourquié, 2010). In order to visualize the interaction of this front with the segmentation clock, we attempted to generate a wavefront reporter. One potential candidate is the *mesp* family of genes, which localizes as two stripes of expression at approximately S-2 (Sawada *et al.* 2000). Two *mesp* genes have been characterized in zebrafish, *mespa* and *mespb*. The expression of both genes is affected by T-box transcription factors, with the loss of *tbx6* (in the mutant *fused somites*) and binding sites within the 300bp upstream of their transcriptional start site (Sawada *et al.* 2000, unpublished work from Aaron Garnett). Transient expression from these 300bp regulatory regions showed some specificity, with the *mespb* driving mosaic expression in the anterior PSM and the *mespa* reporter causing scattered expression throughout the PSM (Garnett thesis).

We attempted to use this regulatory domain to establish a stable transgenic wavefront reporter. Using the *mespb* plasmid generated from previous work, we removed the ubiquitous *pXex:GFP* and added a PEST destabilization element to the end of to the original *mcherry* fluorophore, a strategy previously successful in rapidly turning over *luciferase* in a mouse clock reporter (Aulehla 2008). The wavefront reporter was injected into embryos and screened by *in situ* for transient expression. Surprisingly, embryos either exhibited no expression or a global, diffuse expression. This may have been due to the probe used in to detect transcript, so we circumvented this technical difficulty by imaging injected embryos using the confocal microscope. We found that 80 out of 131 embryos exhibited some mCherry expression in the anterior PSM (Figure 5.4A). We grew up these embryos and screened them for reporter expression at the position of the wavefront. Out of 18 founders screened, only one showed mCherry expression. Out of the progeny 75 progeny screened from male #2 (S1267.1), 75 showed mCherry expression in the somites, throughout the PSM, and in the tailbud (Figure 5.4B). Varying levels of intensity were observed from cell to cell, suggesting stochasticity in amplitude similar to that seen in the *her1-venus* transgenic.

A couple of explanations could account for this broad expression pattern domain. For the expression in the somites, the reporter may not have been properly destabilized, either due to the persistence of the transcript or lack of destabilizing capacity of the PEST sequence. Previous work in mice showed that PEST was destabilizing enough to image the dynamic expression of *lfng* expression (Aulehla *et al.* 2008), but the persistence of mRNA may be a problem with my current *mespb* reporter. No endogenous *mespb* was used in the construct of the *mespb* reporter, and this may cause the reporter transcript to have a longer lifespan than the *mespb* counterpart. The expression of *mespb* throughout the posterior PSM and tailbud is aberrant, as *mespb* is only expressed in the anterior PSM. This may be due to another regulatory domain that is not included in the 300 bp used to drive reporter expression. This missing regulatory domain could be responsive to Wnt or FGF signals, with the role of repressing posterior PSM expression of *mespb*. Future work on this reporter could focus on using a bacterial artificial chromosome to preserve the endogenous regulatory regions and UTRs. Fusing a fluorophore in frame with the endogenous *mespb* could also help confer proper instability to the reporter. Future stable transgenic lines should be validated by imaging the expression pattern for a long duration, perhaps in concert with the *her1-venus* clock reporter. *mespb* expression should have a temporal dynamic similar to the *her1* reporter, with spatial expression slightly off-set anteriorly, as described by Sawada *et al*. (2000). Expression should also be periodic, as seen in the live mouse reporter for *Mesp2* (Niwa *et al.* 2011). Another potential candidate for a determination front reporter would be *gadd45b*, which is not expressed in concert with *her* genes, but as a broader domain around the S-2 domain (see Katherine Brown's thesis). A functional wavefront reporter would be extremely useful as a marker for determination front activation. Manipulation of FGF and RA gradients could potentially shift the front, supporting evidence that the reporter would be responsive to the wavefront. A wavefront reporter could also help us further clarify how the polarity of somites is determined, as *mespb* is thought to mark the anterior boundary of the developing embryo.

Generating a *her1* and *her7* double mutant will to explore more comprehensive clock knockdown

At least two *her* genes oscillate in the PSM, *her1* and *her7*. Both oscillate in the tailbud and posterior PSM, but *her1* has an additional expression domain in the anterior PSM. The knockout of either of these genes causes mild segmentation defects, in anterior somites for the *her1* mutants, and in posterior somites for the *her7* mutants (Oates and Ho 2002; Henry *et al.* 2002). Previous work has shown that the deletion of both causes the embryo to not make somite boundaries, but that deletion was due to a large genomic deletion, which encompasses other genes besides *her1* and *her7* (Henry *et al.* 2002). The two genes sit 12kb away from each other in the genome, so generating a double mutant through a cross-over event is a difficult strategy. Recent genomic editing technologies have allowed researchers to target specific genes in the genomic and knock them out using zinc finger nucleases (Doyon *et al.* 2008, Meng *et al.* 2008, McCammon *et al.* 2010, Jasmine McCammon's thesis). Other genome editing technologies are also being developed, including TALENs (Huang *et al.* 2011, Sander *et al.* 2011) and the CRISPR–Cas9 system (Hwang *et al.* 2013, Chang *et al.* 2013).

We attempted to generate a *her1*/*her7* double mutant by injecting *her7* ZFNs into *her1*^{hu2124} mutant embryos. Transcripts for both arms of the ZFNs were transcribed off the same plasmid, generated by John Young and Jasmine McCammon (see Jasmine's thesis). Embryos were injected at the one-cell stage and grown for two days. These embryos were processed for genomic sequencing. The challenge of genotyping for a *her7* lesion is that no accessible restriction enzyme site exists, so clones of DNA had to be generated and sequenced individually for lesions. Not surprisingly, this strategy did not detect any mutations in the *her7* gene. We adjusted our strategy, injecting embryos and then growing them to sexual maturity. These fish were then fin-clipped and screened by high resolution melt analysis (Dahlem *et al.* 2012). All sixteen fish showed evidence of lesions, with five of them with having more pronounced lesions (Figure 5.5). These five lines were crossed to try to isolate the double mutant, and are currently being grown up for screening. This double mutant will be useful as a background to explore the loss of clock function. An interesting experiment would be to cross a clock reporter into this double mutant background and examine how the reporter behaves. Cyclic *her1/her7* signal is important to auto-regulate clock expression, so it would be interesting to see how the clock behaved without this cyclic signal. One possibility is that the reporter would be expressed more broadly and persistently due to the lack of cyclic repression.

It may be possible to dissect the 8.6kb upstream of *her1* for core regulatory regions

Some work has previously been done to analyze the 8.6kb upstream of *her1* (Gajewski *et al.* 2003, Brend *et al.* 2009). Only two real domains have been analyzed, the large 5kb domain responsible for posterior PSM expression and the 500bp region responsible for anterior PSM expression. There may be key regulatory regions within the 5kb domain, and undergraduate Paul Wang and I spent a summer trying to dissect this region. We aimed to use the *her1-venus* reporter as the template for this promoter bashing experiment, deleting large blocks of the 8.6 kb regulatory region and assaying for Venus expression. This project was largely unsuccessful, as cloning techniques relied on amplifying large regions of the *her1:her1-venus* plasmid. This strategy had a large chance of causing PCR-based mutations, even using a high fidelity polymerase. We were unable to generate large deletion fragments due to the large size of the plasmid we were targeting, and abandoned the project after several months. Future attempts may be more successful by amplifying 1kb, overlapping regions of regulatory region and inserting these in front of a *her1-venus* reporter plasmid. Expression of the reporter could then be assayed in transgenic embryos both through *in situ* and live imaging. Finding key regulatory regions would be useful to determine which binding sites are essential to *her1* expression. A bioinformatic search for binding sites has revealed potential sites responsive to Wnt, T-box factors, Notch, and retinoic acid (Figure 5.6, Garnett thesis). Future work could also mutate specific binding sites to determine how various factors control clock oscillations.

Closing Remarks

An *in vivo* segmentation clock reporter is a powerful tool in analyzing the dynamics of the segmentation clock. Much work on the clock has been done by assaying transcripts in fixed embryos, but the utility of this type of analysis is limiting, as it only examines a single timepoint for each embryo. For a process that is constantly in flux, looking at single timepoints does not allow one to examine oscillatory behavior over time, or how a single cell responds to a perturbation. The development of live reporters in mice and zebrafish has opened up new opportunities in exploring the segmentation clock, and I have spent my graduate career exploring these possibilities. Not only did we provide the first direct evidence that the Notch pathway synchronized cell oscillations in zebrafish, but we also characterized the effect of mitosis on cyclic expression and analyzed the dynamics of the clock slowing in the anterior PSM. The slowing of the clock, in particular, is an unexpected dynamic that we are only beginning to understand. Models based on fixed embryos make predictions that do not match what we observe *in vivo*; the clock slows in the anterior PSM, but oscillations do not stop. The gradual slowing and amplification of the clock is a likely response of the catastrophic changes PSM cells undergo as they interact with the determination front, but this has yet to be directly tested. Development of less invasive, more sensitive clock reporters will forward our analyses of the mechanisms that drive somitogenesis. Generating appropriate wavefront reporters will also be useful to examine the dynamics between the two processes.

Generating a live clock reporter was an important step along the way in uncovering the underlying mechanisms of the segmentation clock. There has been some debate in what the central oscillator of the clock is, especially in mice where FGF components appear to oscillate upstream of Wnt and Notch. In zebrafish, there seem to be somewhat different mechanisms at work, as the majority of oscillating genes discovered so far are part of the Notch pathway. A distinct possibility is that there is no master oscillator; the pacing of the segmentation clock may be simply the interactions between various oscillating (and non-oscillating) genes influencing each other, generating an emergent property that drives the periodicity and regularity of somitogenesis. This is a particularly intriguing idea given that genomic microarrays have already been performed on oscillating PSM tissue, although the microarray analyses performed in the zebrafish were not as extensive as those in chick and mouse, nor did the available arrays survey every gene (Krol *et al*. 2011). Any clear oscillators should be easily detected by this kind of analysis, as long as they oscillate at the transcript level. For such an integral process in development, it would not be surprising that oscillations are robust and redundant. We may not be able to isolate these components via traditional genetic screens because: (1) knockout of certain clock components might have earlier effects that mask later functions in somitogenesis thus precluding their detection, or (2) their functions may be compensated for in other ways, such as how Notch pathway mutants in zebrafish manage to recover after 48 hpf (van Eeden *et al.* 1996; Henry *et al.* 2005). It will be exciting to see how these various clock and wavefront components will be teased apart, and what implications each component has on the system as a whole.

Working with the *her1-venus* clock reporter has led me down a path I did not expect at the beginning of graduate school. The developmental biology experiments I learned about as an undergraduate were classic, and I was not fully prepared for how far the field had come. The immense power of high-resolution confocal imaging and computational quantification of gene expression truly staggered me. My graduate work really emphasizes the use of cutting edge technology to explore developmental questions. I was fortunate to have the UC Berkeley Molecular Imaging Center as a resource, providing excellent support for a transgenic reporter that was very difficult to detect. Not all microscopes are created equal; after trying to detect the reporter on a plethora of microscopes, only four were successful: the Leica SP5, Zeiss Lightsheet Z.1, Olympus FV1000 and the Zeiss 780 (Figure 5.7). Of these, the Lightsheet Z.1 has the highest resolution and fastest imaging time (Figure 5.7B). My growth as a scientist also greatly benefited from excellent collaborations, including the creation of a *de novo* cell tracking software. The quantification of clock oscillations provides an explanatory power not possible with only qualitative observations. An emphasis on understanding developmental biology in the context of theoretical physics helps introduce new ideas on both sides. Continuing this collaboration would be greatly beneficial to our understanding of the segmentation clock and development in general. Finally, the discoveries I have made in my graduate work would not have been possible without excellent mentorship. I am extremely grateful for the direction and professional development provided by my mentor and colleagues. I am eager to see how the clock reporter will continue to advance our understanding of somitogenesis, and look forward to following the field for years to come.

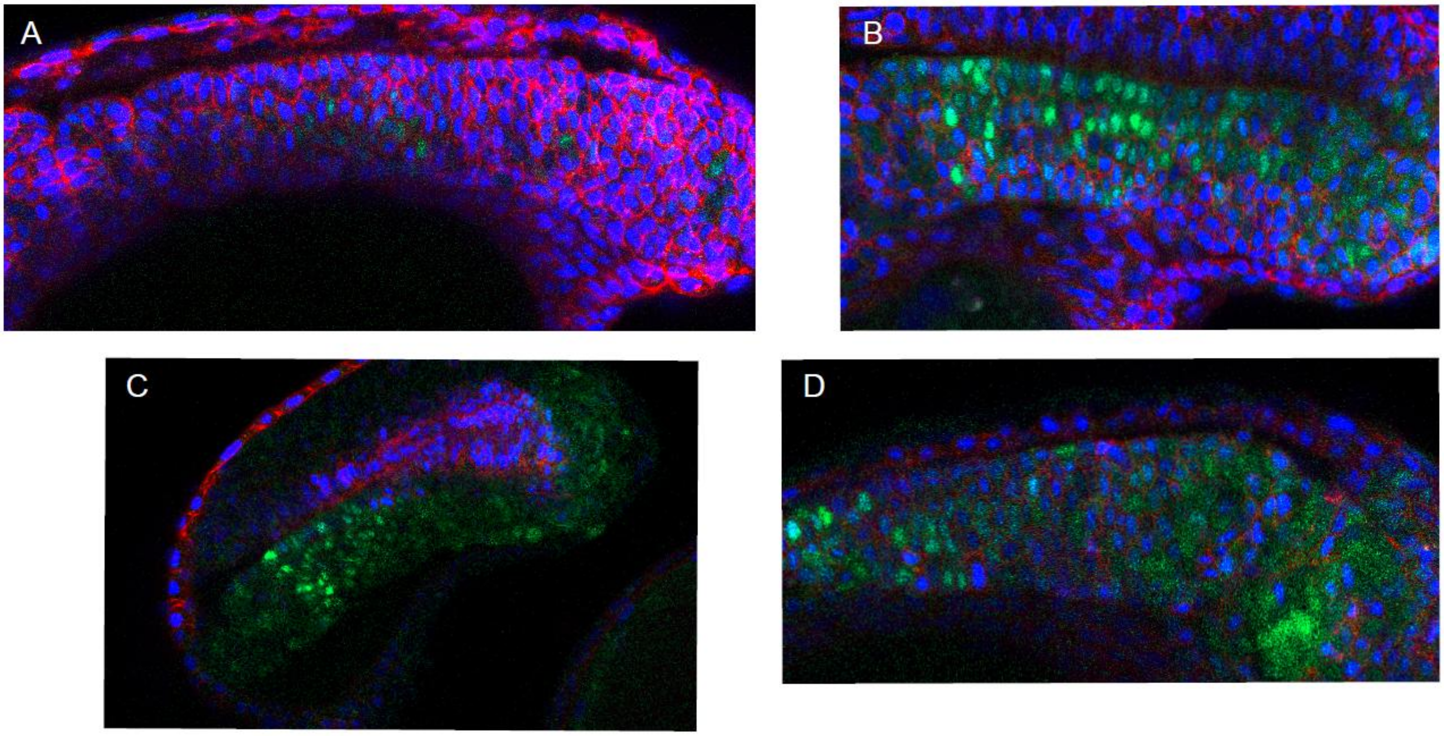
A
B
C
D

Figure 5.1: *pnrc2* morpholino, H2B-cerulean mRNA, and lyn-mCherry mRNA co-injected into a *her1-venus* heterozygous embryo.
Four examples of injected embryos are shown, with varying degrees of mosaicism of the injected compounds. Clock expression appears elevated in cells that are not expressing membrane/nuclear fluorescent markers. Anterior to the left, dorsal is up. Embryos imaged at 12-16 somite stage

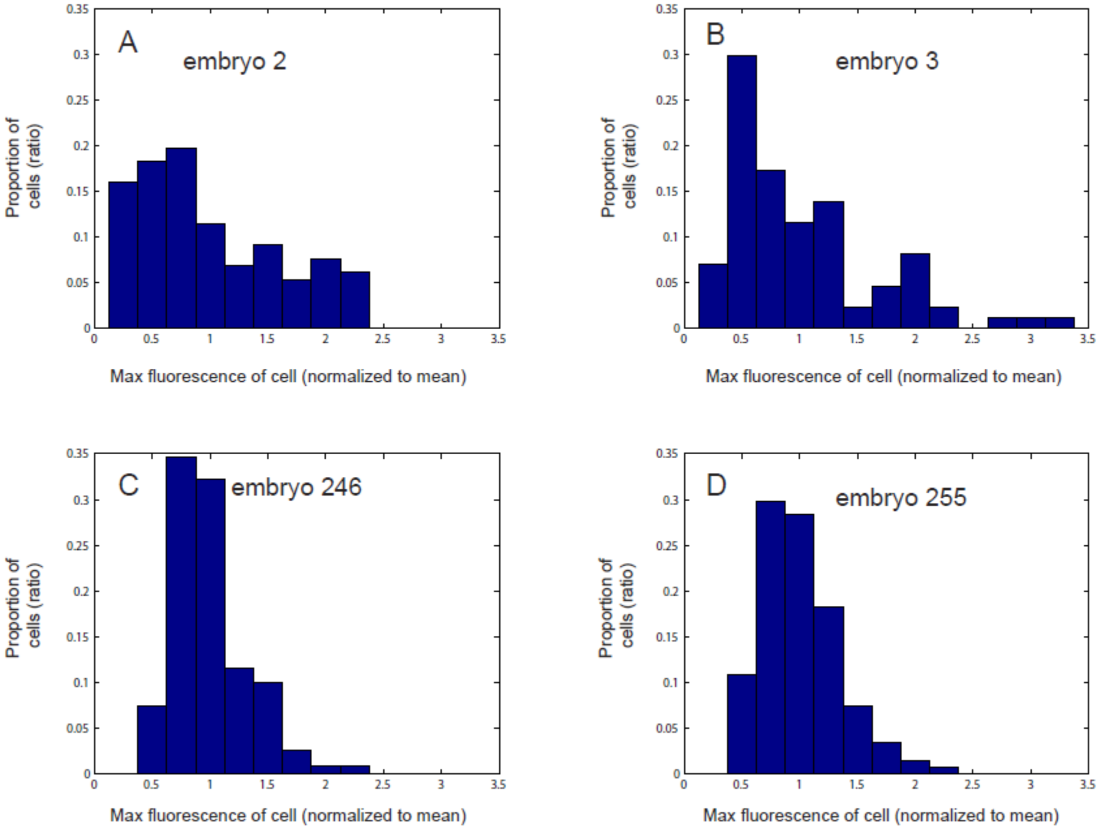
A
embryo 2
B
embryo 3
C
embryo 246
D
embryo 255
Proportion of cells (ratio)
Max fluorescence of cell (normalized to mean)
0
0.05
0.1
0.15
0.2
0.25
0.3
0.35
0
0.5
1
1.5
2
2.5
3
3.5

Figure 5.2: Variability of maximum fluorescence in cells tracked in four embryos. The maximum fluorescence of each tracked cell in the embryo is normalized to the mean maximum fluorescence of all tracked cells. A histogram of the distribution of maximum fluorescence is made for four tracked embryos: (A) and (B) represent the two embryos imaged with the Zeiss 780, while (C) and (D) represent two embryos imaged with the Olympus FV1000.

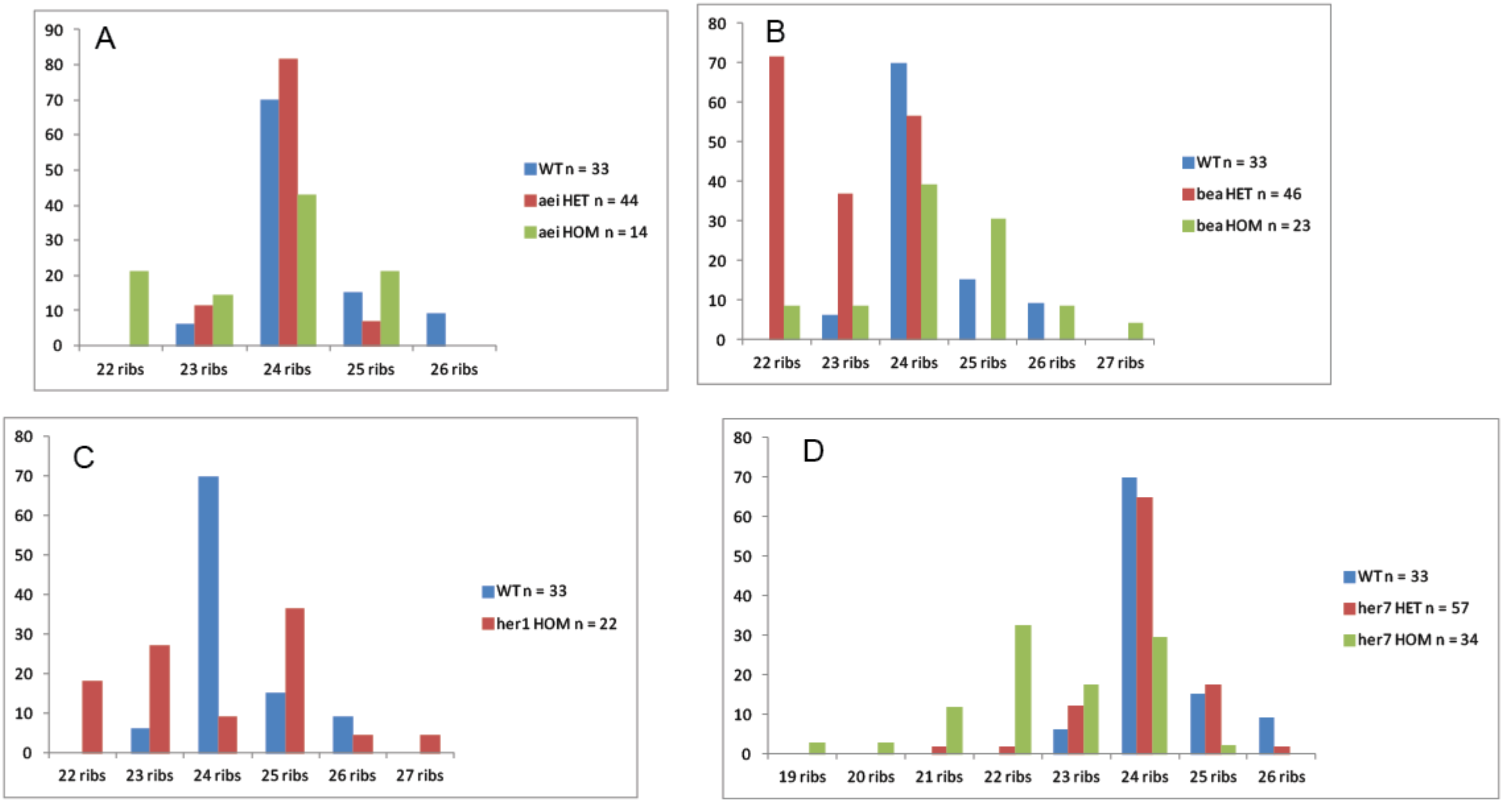
A
90
80
70
60
50
40
30
20
10
0
22 ribs
23 ribs
24 ribs
25 ribs
26 ribs
WT n = 33
aei HET n = 44
aei HOM n = 14
B
80
70
60
50
40
30
20
10
0
22 ribs
23 ribs
24 ribs
25 ribs
26 ribs
27 ribs
WT n = 33
bea HET n = 46
bea HOM n = 23
C
80
70
60
50
40
30
20
10
0
22 ribs
23 ribs
24 ribs
25 ribs
26 ribs
27 ribs
WT n = 33
her1 HOM n = 22
D
80
70
60
50
40
30
20
10
0
19 ribs
20 ribs
21 ribs
22 ribs
23 ribs
24 ribs
25 ribs
26 ribs
WT n = 33
her7 HET n = 57
her7 HOM n = 34

Figure 5.3: Rib counts of various *delta* and *her* mutants in 21 dpf larvae
The number of ribs in wildtype, heterozygous, and homozygous for various mutants are shown as bar graphs. (A) *aei/deltaD*, (B) *bea/deltaC*, (C) *her1*, (D) *her7*.

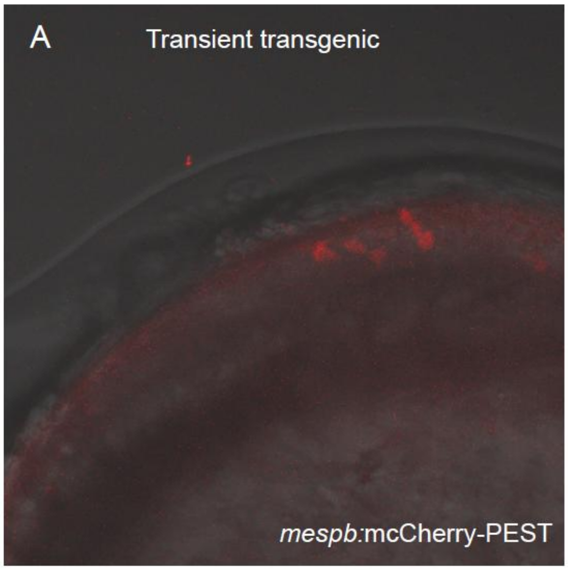
A
Transient transgenic
mespb:mcCherry-PEST

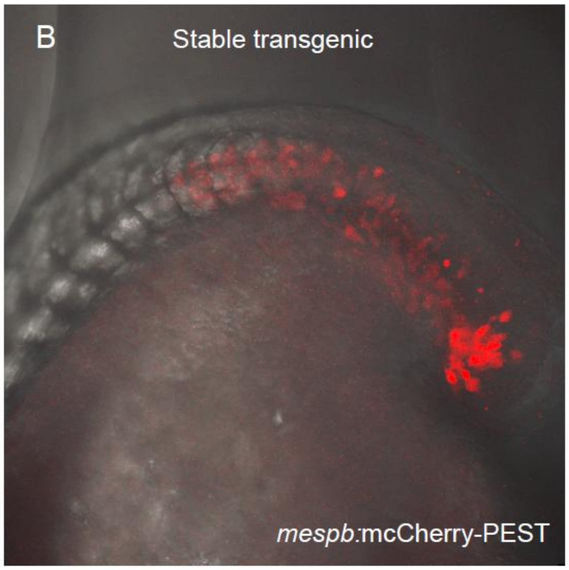
B
Stable transgenic
mespb:mcCherry-PEST

Figure 5.4: Confocal images of the *mespb:venus-PEST* reporter line.
Confocal images taken using the Zeiss 780. (A) An example of the transient expression of the wavefront reporter in an injected embryo. (B) Stable transgenic expression of reporter in the progeny of a *mespb:venus-PEST* founder. Image is a maximum projection of 45 stacks, taken at 1.5 microns each. Expression is visible in the somites, PSM, and tailbud.

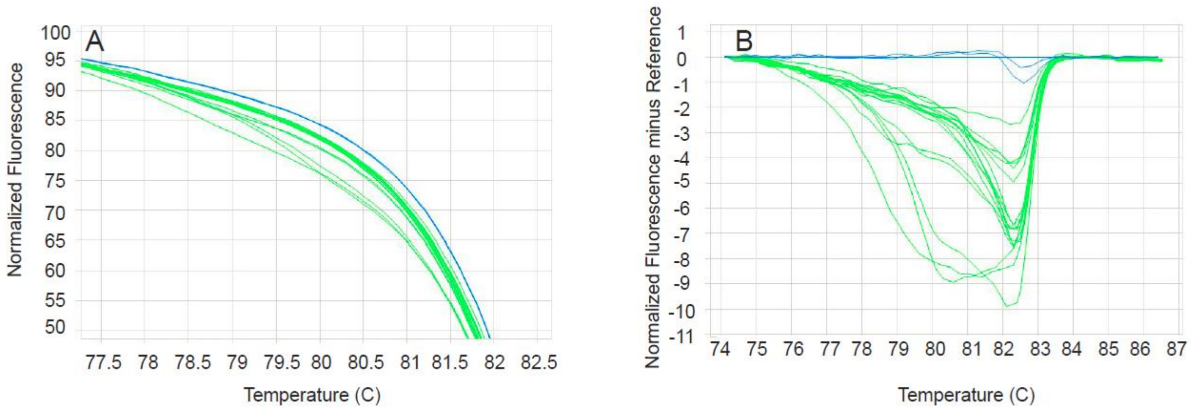
A
Normalized Fluorescence
100
95
90
85
80
75
70
65
60
55
50
77.5
78
78.5
79
79.5
80
80.5
81
81.5
82
82.5
Temperature (C)
B
Normalized Fluorescence minus Reference
1
0
-1
-2
-3
-4
-5
-6
-7
-8
-9
-10
-11
74
75
76
77
78
79
80
81
82
83
84
85
86
87
Temperature (C)

Figure 5.5: High-resolution melt analysis of *her7* ZFN-injected embryos compared to wildtype.
(A) Melt curves of normalized fluorescence for wildtype *her7* (blue) compared to 16 different founders injected with the *her7* ZFN (green). (B) Melt curves plotting the normalized difference between the wildtype *her7* sequences (blue) compared to the 16 different founders injected with *her7* ZFNs (green). Negative values represent differences of strand annealing temperature compared to wildtype.

Predicted binding sites on the 8.6 kb *her1* enhancer

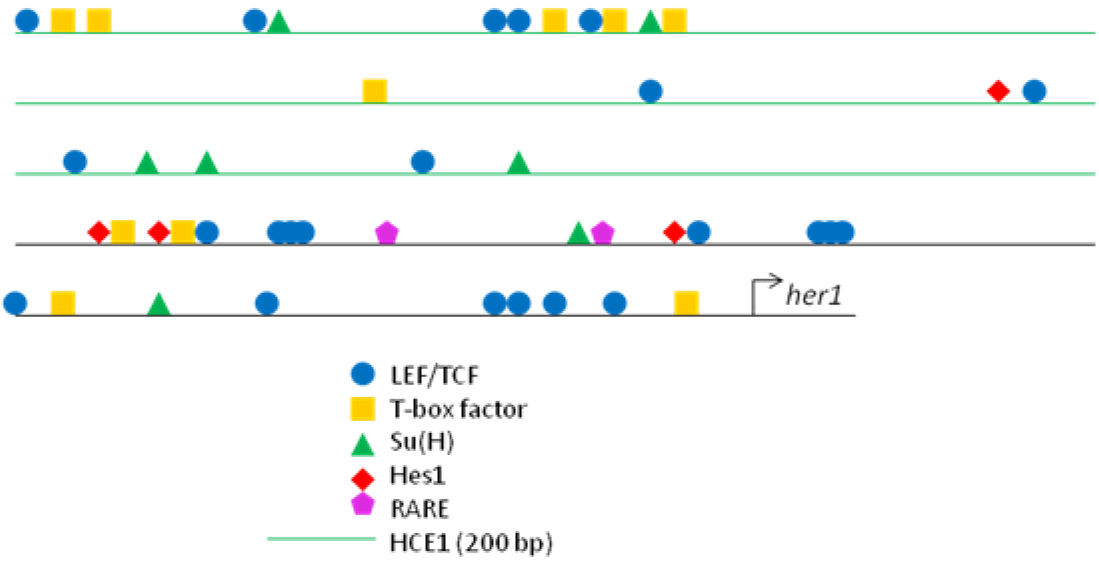
her1
● LEF/TCF
■ T-box factor
▲ Su(H)
◆ Hes1
⬟ RARE
HCE1 (200 bp)

Figure 5.6: Distribution of bioinformatically-predicted binding sites of the 8.6kb upstream of *her1*.
Binding sites based on predictions made by Aaron Garnett. HCE1 is labeled as a green line, and is requirede for posterior *her1* expression (Gajewski *et al.* 2003; Brend *et al.* 2009; Delaune and Francois *et al.* 2012).

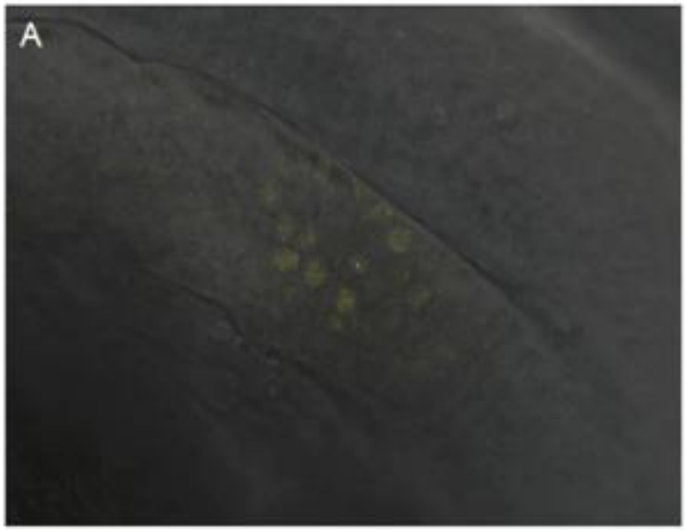
A

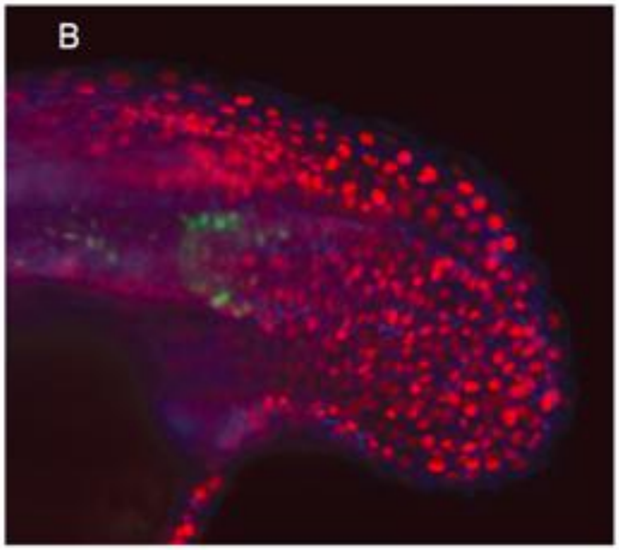
B

Figure 5.7: Examples of imaging the *her1-venus* reporter line using different confocal microscopes.
(A) Composite of brightfield and Venus fluorescence using the Leica SP5 with resonance scanner. (B) Composite of Venus (green), membrane mCherry (blue), and H2B-Cerulean (red) fluorescence on the Lightsheet Z.1 LSFM, with 6 laser lines (405, 455, 488, 515, 561, and 638nm)

References

Aulehla A., R. L. Johnson, Dynamic expression of lunatic fringe suggests a link between notch signaling and an autonomous cellular oscillator driving somite segmentation. *Dev Biol* **207**, 49-61 (1999)

Aulehla A., O. Pourquié, Signaling gradients during paraxial mesoderm development. *Cold Spring Harb Perspect Biol* **2**, a000869 (2010)

Aulehla A., C. Wehrle, B. Brand-Saberi, R. Kemler, A. Gossler, B. Kanzler, B. G. Herrmann, Wnt3a plays a major role in the segmentation clock controlling somitogenesis. *Dev Cell* **4**, 395-406 (2003)

Aulehla A., W. Wiegraebe, V. Baubet, M. B. Wahl, C. Deng, M. Taketo, M. Lewandoski, O. Pourquié, A beta-catenin gradient links the clock and wavefront systems in mouse embryo segmentation. *Nat Cell Biol* **10**, 186-193 (2008)

Ay A., S. Knierer, A. Sperlea, J. Holland, E. M. Ozbudak, Short-lived Her proteins drive robust synchronized oscillations in the zebrafish segmentation clock. *Development* **140**, 3244-3253 (2013)

Bard J., I. Lauder, How well does Turing's theory of morphogenesis work? *J Theor Biol* **45**,501-531 (1974)

Bessho Y., H. Hirata, Y. Masamizu, R. Kageyama, Periodic repression by the bHLH factor Hes7 is an essential mechanism for the somite segmentation clock. *Genes Dev* **17**, 1451-1456 (2003)

Bessho Y., G. Miyoshi, R. Sakata, R. Kageyama, Hes7: a bHLH-type repressor gene regulated by Notch and expressed in the presomitic mesoderm. *Genes Cells* **6**, 175-185 (2001)

Bessho Y., R. Sakata, S. Komatsu, K. Shiota, S. Yamada, R. Kageyama, Dynamic expression and essential functions of Hes7 in somite segmentation. *Genes Dev* **15**, 2642-2647 (2001)

Branicky R., S. Hekimi, What keeps *C. elegans* regular: the genetics of defecation. *Trends Genet* **10**, 571-579 (2006)

Brend T., S. A. Holley, Expression of the oscillating gene her1 is directly regulated by Hairy/Enhancer of Split, T-box, and Suppressor of Hairless proteins in the zebrafish segmentation clock. *Dev Dyn* **238**, 2745-2759 (2009)

Caneparo L., P. Pantazis, W. Dempsey, S. E. Fraser, Intercellular bridges in vertebrate gastrulation. *PLoS One* **6**, e20230 (2011)

Cerny A. C., G. Bucher, R. Schroder, M. Klingler, Breakdown of abdominal patterning in the Tribolium Kruppel mutant jaws. *Development* **132**, 5353-5363 (2005)

Chang N., C. Sun, L. Gao, D. Zhu, X. Xu, X. Zhu, J. W. Xiong, J. J. Xi, Genome editing with RNA-guided Cas9 nuclease in zebrafish embryos. *Cell Res* **23**, 465-472 (2013)

Chen J., L. Kang, N. Zhang, Negative feedback loop formed by Lunatic fringe and Hes7 controls their oscillatory expression during somitogenesis. *Genesis* **43**, 196-204 (2005)

Chipman A. D., W. Arthur, M. Akam, A double segment periodicity underlies segment generation in centipede development. *Curr Biol* **14**, 1250-1255 (2004)

Chipman A. D., A. Stollewerk, Specification of neural precursor identity in the geophilomorph centipede Strigamia maritima. *Dev Biol* **290**, 337-350 (2006)

Cho H., K. M. Kim, Y. K. Kim, Human proline-rich nuclear receptor coregulatory protein 2 mediates an interaction between mRNA surveillance machinery and decapping complex. *Mol Cell* **33**, 75-86 (2009)

Cho H., K. M. Kim, S. Han, J. Choe, S. G. Park, S. S. Choi, Y. K. Kim, Staufen1-mediated mRNA decay functions in adipogenesis. *Mol Cell* **46**, 495-506 (2012)

Choe C. P., S. J. Brown, Evolutionary flexibility of pair-rule patterning revealed by functional analysis of secondary pair-rule genes, paired and sloppy-paired in the short-germ insect, Tribolium castaneum. *Dev Biol* **302**, 281-294 (2007)
Choe C. P., S. C. Miller, S. J. Brown, A pair-rule gene circuit defines segments sequentially in the short-germ insect Tribolium castaneum. *Proc Natl Acad Sci U S A* **103**, 6560-6564 (2006)
Choorapoikayil S., B. Willems, P. Strohle, M. Gajewski, Analysis of her1 and her7 mutants reveals a spatio temporal separation of the somite clock module. *PLoS One* **7**, e39073 (2012)
Cohen B., A. Bashirullah, L. Dagnino, C. Campbell, W. W. Fisher, C. C. Leow, E. Whiting, D. Ryan, D. Zinyk, G. Boulianne, C. C. Hui, B. Gallie, R. A. Phillips, H. D. Lipshitz, S. E. Egan, Fringe boundaries coincide with Notch-dependent patterning centres in mammals and alter Notch-dependent development in Drosophila. *Nat Genet* **16**, 283-288 (1997)
Conlon R. A., A. G. Reaume, J. Rossant, Notch1 is required for the coordinate segmentation of somites. *Development* **121**, 1533-1545 (1995)
Cooke J., E. C. Zeeman, A clock and wavefront model for control of the number of repeated structures during animal morphogenesis. *J Theor Biol* **58**, 455-476 (1976)
Copf T., N. Rabet, S. E. Celniker, M. Averof, Posterior patterning genes and the identification of a unique body region in the brine shrimp Artemia franciscana. *Development* **130**, 5915-5927 (2003)
Dahlem T. J., K. Hoshijima, M. J. Jurynec, D. Gunther, C. G. Starker, A. S. Locke, A. M. Weis, D. F. Voytas, D. J. Grunwald, Simple methods for generating and detecting locus-specific mutations induced with TALENs in the zebrafish genome. *PLoS Genet* **8,** e1002861 (2012)
Dahmann C., A. C. Oates, M. Brand, Boundary formation and maintenance in tissue development. *Nat Rev Genet* **12**, 43-55 (2011)
Dale J. K., P. Malapert, J. Chal, G. Vilhais-Neto, M. Maroto, T. Johnson, S. Jayasinghe, P. Trainor, B. Herrmann, O. Pourquié, Oscillations of the snail genes in the presomitic mesoderm coordinate segmental patterning and morphogenesis in vertebrate somitogenesis. *Dev Cell* **10**, 355-366 (2006)
Damen W. G., Evolutionary conservation and divergence of the segmentation process in arthropods. *Dev Dyn* **236**, 1379-1391 (2007)
Damen W. G., R. Janssen, N. M. Prpic, Pair rule gene orthologs in spider segmentation. *Evol Dev* **7**, 618-628 (2005)
Davis R. L., D. L. Turner, Vertebrate hairy and Enhancer of split related proteins: transcriptional repressors regulating cellular differentiation and embryonic patterning. *Oncogene* **20**, 8342-8357 (2001)
Delaune E. A., P. Francois, N. P. Shih, S. L. Amacher, Single-cell-resolution imaging of the impact of Notch signaling and mitosis on segmentation clock dynamics. *Dev Cell* **23**, 995-1005 (2012)
Delfini M. C., J. Dubrulle, P. Malapert, J. Chal, O. Pourquié, Control of the segmentation process by graded MAPK/ERK activation in the chick embryo. *Proc Natl Acad Sci U S A* **102**, 11343-11348 (2005)
Dequeant M. L., E. Glynn, K. Gaudenz, M. Wahl, J. Chen, A. Mushegian, O. Pourquié, A complex oscillating network of signaling genes underlies the mouse segmentation clock. *Science* **314**, 1595-1598 (2006)
Dequeant M. L., O. Pourquié, Segmental patterning of the vertebrate embryonic axis. *Nat Rev Genet* **9**, 370-382 (2008)
Diez del Corral R., I. Olivera-Martinez, A. Goriely, E. Gale, M. Maden, K. Storey, Opposing

FGF and retinoid pathways control ventral neural pattern, neuronal differentiation, and segmentation during body axis extension. *Neuron* **40**, 65-79 (2003)

Dill K. K., S. L. Amacher, tortuga refines Notch pathway gene expression in the zebrafish presomitic mesoderm at the post-transcriptional level. *Dev Biol* **287**, 225-236 (2005)

Dodd A. N., N. Salathia, A. Hall, E. Kevei, R. Toth, F. Nagy, J. M. Hibberd, A. J. Millar, A. A. Webb, Plant circadian clocks increase photosynthesis, growth, survival, and competitive advantage. *Science* **309**, 630-633 (2005)

Doyon Y., J. M. McCammon, J. C. Miller, F. Faraji, C. Ngo, G. E. Katibah, R. Amora, T. D. Hocking, L. Zhang, E. J. Rebar, P. D. Gregory, F. D. Urnov, S. L. Amacher, Heritable targeted gene disruption in zebrafish using designed zinc-finger nucleases. *Nat Biotechnol* **26**, 702-708 (2008)

Draper B. W., D. W. Stock, C. B. Kimmel, Zebrafish fgf24 functions with fgf8 to promote posterior mesodermal development. *Development* **130**, 4639-4654 (2003)

Dubrulle J., M. J. McGrew, O. Pourquié, FGF signaling controls somite boundary position and regulates segmentation clock control of spatiotemporal Hox gene activation. *Cell* **106**, 219-232 (2001)

Dubrulle J., O. Pourquié, fgf8 mRNA decay establishes a gradient that couples axial elongation to patterning in the vertebrate embryo. *Nature* **427**, 419-422 (2004)

Dunty W. C., Jr., K. K. Biris, R. B. Chalamalasetty, M. M. Taketo, M. Lewandoski, T. P. Yamaguchi, Wnt3a/beta-catenin signaling controls posterior body development by coordinating mesoderm formation and segmentation. *Development* **135**, 85-94 (2008)

Dunwoodie S. L., M. Clements, D. B. Sparrow, X. Sa, R. A. Conlon, R. S. Beddington, Axial skeletal defects caused by mutation in the spondylocostal dysplasia/pudgy gene Dll3 are associated with disruption of the segmentation clock within the presomitic mesoderm. *Development* **129**, 1795-1806 (2002)

Fisher A. L., S. Ohsako, M. Caudy, The WRPW motif of the hairy-related basic helix-loop-helix repressor proteins acts as a 4-amino-acid transcription repression and protein-protein interaction domain. *Mol Cell Biol* **16**, 2670-2677 (1996)

Fisher A., M. Caudy, The function of hairy-related bHLH repressor proteins in cell fate decisions. *Bioessays* **20**, 298-306 (1998)

Fisher D. A., S. Kivimae, J. Hoshino, R. Suriben, P. M. Martin, N. Baxter, B. N. Cheyette, Three Dact gene family members are expressed during embryonic development and in the adult brains of mice. *Dev Dyn* **235**, 2620-2630 (2006)

Forsberg, H., F. Crozet, N. A. Brown, Waves of mouse Lunatic fring expression, in four-hour cycles at two-hour intervals, precede somite boundary formation. *Curr Biol* **18**, 1027-1030 (1998)

Francois P., V. Hakim, E. D. Siggia, Deriving structure from evolution: metazoan segmentation. *Mol Syst Biol* **3,** 154 (2007)

Francois P., E. D. Siggia, Phenotypic models of evolution and development: geometry as destiny. *Curr Opin Genet Dev* **22**, 627-633 (2012)

Fujioka M., J. B. Jaynes, T. Goto, Early even-skipped stripes act as morphogenetic gradients at the single cell level to establish engrailed expression. *Development* **121**, 4371-4382 (1995)

Gajewski M., D. Sieger, B. Alt, C. Leve, S. Hans, C. Wolff, K. B. Rohr, D. Tautz, Anterior and posterior waves of cyclic her1 gene expression are differentially regulated in the presomitic mesoderm of zebrafish. *Development* **130**, 4269-4278 (2003)

Giudicelli F., E. M. Ozbudak, G. J. Wright, J. Lewis, Setting the tempo in development: an investigation of the zebrafish somite clock mechanism. *PLoS Biol* **5**, e150 (2007)

Godinho S. I., E. S. Maywood, L. Shaw, V. Tucci, A. R. Barnard, L. Busino, M. Pagano, R. Kendall, M. M. Quwailid, M. R. Romero, J. O'Neill, J. E. Chesham, D. Brooker, Z. Lalanne, M. H. Hastings, P. M. Nolan, The after-hours mutant reveals a role for Fbxl3 in determining mammalian circadian period. *Science* **316**, 897-900 (2007)

Gomez C., E. M. Ozbudak, J. Wunderlich, D. Baumann, J. Lewis, O. Pourquié, Control of segment number in vertebrate embryos. *Nature* **454**, 335-339 (2008)

Gonzalez A., I. Manosalva, T. Liu, R. Kageyama, Control of Hes7 expression by Tbx6, the Wnt pathway and the chemical Gsk3 inhibitor LiCl in the mouse segmentation clock. *PLoS One* **8**, e53323 (2013)

Gwinner E., Photoperiod as a modifying and limiting factor in the expression of avian circannual rhythms. *J Biol Rhythms* **5**, 237-250 (1989)

Hanisch A., M. V. Holder, S. Choorapoikayil, M. Gajewski, E. M. Ozbudak, J. Lewis, The elongation rate of RNA polymerase II in zebrafish and its significance in the somite segmentation clock. *Development* **140**, 444-453 (2013)

Harima Y., Y. Takashima, Y. Ueda, T. Ohtsuka, R. Kageyama, Accelerating the tempo of the segmentation clock by reducing the number of introns in the Hes7 gene. *Cell Rep* **3**, 1-7 (2013)

Henry C. A., I. M. McNulty, W. A. Durst, S. E. Munchel, S. L. Amacher, Interactions between muscle fibers and segment boundaries in zebrafish. *Dev Biol* **287**, 346-360 (2005)

Henry C. A., M. K. Urban, K. K. Dill, J. P. Merlie, M. F. Page, C. B. Kimmel, S. L. Amacher, Two linked hairy/Enhancer of split-related zebrafish genes, her1 and her7, function together to refine alternating somite boundaries. *Development* **129**, 3693-3704 (2002)

Herrgen L., S. Ares, L. G. Morelli, C. Schroter, F. Julicher, A. C. Oates, Intercellular coupling regulates the period of the segmentation clock. *Curr Biol* **20**, 1244-1253 (2010)

Hilgers V., O. Pourquié, J. Dubrulle, In vivo analysis of mRNA stability using the Tet-Off system in the chicken embryo. *Dev Biol* **284**, 292-300 (2005)

Hirata H., Y. Bessho, H. Kokubu, Y. Masamizu, S. Yamada, J. Lewis, R. Kageyama, Instability of Hes7 protein is crucial for the somite segmentation clock. *Nat Genet* **36**, 750-754 (2004)

Hirata H., S. Yoshiura, T. Ohtsuka, Y. Bessho, T. Harada, K. Yoshikawa, R. Kageyama, Oscillatory expression of the bHLH factor Hes1 regulated by a negative feedback loop. *Science* **298**, 840-843 (2002)

Holley S. A., The genetics and embryology of zebrafish metamerism. *Dev Dyn* **236**, 1422-1449 (2007)

Holley S. A., R. Geisler, C. Nusslein-Volhard, Control of her1 expression during zebrafish somitogenesis by a delta-dependent oscillator and an independent wave-front activity. *Genes Dev* **14**, 1678-1690 (2000)

Holley S. A., D. Julich, G. J. Rauch, R. Geisler, C. Nusslein-Volhard, her1 and the notch pathway function within the oscillator mechanism that regulates zebrafish somitogenesis. *Development* **129**, 1175-1183 (2002)

Horikawa K., K. Ishimatsu, E. Yoshimoto, S. Kondo, H. Takeda, Noise-resistant and synchronized oscillation of the segmentation clock. *Nature* **441**, 719-723 (2006)

Horikawa K., G. Radice, M. Takeichi, O. Chisaka, Adhesive subdivisions intrinsic to the epithelial somites. *Dev Biol* **215**, 182-189 (1999)

Hoyle N. P., D. Ish-Horowicz, Transcript processing and export kinetics are rate-limiting steps in expressing vertebrate segmentation clock genes. *Proc Natl Acad Sci U S A* **110**, E4316-4324 (2013)

Hukriede N. A., Y. Gu, R. J. Fleming, A dominant-negative form of Serrate acts as a general antagonist of Notch activation. *Development* **124**, 3427-3437 (1997)
Hwang W. Y., Y. Fu, D. Reyon, M. L. Maeder, P. Kaini, J. D. Sander, J. K. Joung, R. T. Peterson, J. R. Yeh, Heritable and precise zebrafish genome editing using a CRISPR-Cas system. *PLoS One* **8**, e68708 (2013)
Ishitani T., K. Matsumoto, A. B. Chitnis, M. Itoh, Nrarp functions to modulate neural-crest-cell differentiation by regulating LEF1 protein stability. *Nat Cell Biol* **7**, 1106-1112 (2005)
Jaeger J., Modeling the Drosophila embryo. *Mol Biosyst* **5**, 1549-1568 (2009)
Jiang Y. J., B. L. Aerne, L. Smithers, C. Haddon, D. Ish-Horowicz, J. Lewis, Notch signalling and the synchronization of the somite segmentation clock. *Nature* **408**, 475-479 (2000)
Johnston S. H., C. Rauskolb, R. Wilson, B. Prabhakaran, K. D. Irvine, T. F. Vogt, A family of mammalian Fringe genes implicated in boundary determination and the Notch pathway. *Development* **124**, 2245-2254 (1997)
Jouve C., I. Palmeirim, D. Henrique, J. Beckers, A. Gossler, D. Ish-Horowicz, O. Pourquié, Notch signalling is required for cyclic expression of the hairy-like gene HES1 in the presomitic mesoderm. *Development* **127**, 1421-1429 (2000)
Julich D., C. Hwee Lim, J. Round, C. Nicolaije, J. Schroeder, A. Davies, R. Geisler, J. Lewis, Y. J. Jiang, S. A. Holley, beamter/deltaC and the role of Notch ligands in the zebrafish somite segmentation, hindbrain neurogenesis and hypochord differentiation. *Dev Biol* **286**, 391-404 (2005)
Kadner D., A. Stollewerk, Neurogenesis in the chilopod Lithobius forficatus suggests more similarities to chelicerates than to insects. *Dev Genes Evol* **214**, 367-379 (2004)
Kawamura A., S. Koshida, H. Hijikata, T. Sakaguchi, H. Kondoh, S. Takada, Zebrafish hairy/enhancer of split protein links FGF signaling to cyclic gene expression in the periodic segmentation of somites. *Genes Dev* **19**, 1156-1161 (2005)
Keller P. J., A. D. Schmidt, J. Wittbrodt, E. H. Stelzer, Reconstruction of zebrafish early embryonic development by scanned light sheet microscopy. *Science* **322**, 1065-1069 (2008)
Kim W., T. Matsui, M. Yamao, M. Ishibashi, K. Tamada, T. Takumi, K. Kohno, S. Oba, S. Ishii, Y. Sakumura, Y. Bessho, The period of the somite segmentation clock is sensitive to Notch activity. *Mol Biol Cell* **22**, 3541-3549 (2011)
Kimmel C. B., W. W. Ballard, S. R. Kimmel, B. Ullmann, T. F. Schilling, Stages of embryonic development of the zebrafish. *Dev Dyn* **203**, 253-310 (1995)
Kobayashi A., K. Senzaki, S. Ozaki, M. Yoshikawa, T. Shiga, Runx1 promotes neuronal differentiation in dorsal root ganglion. *Mol Cell Neurosci* **49**, 23-31 (2012)
Krol A. J., D. Roellig, M. L. Dequeant, O. Tassy, E. Glynn, G. Hattem, A. Mushegian, A. C. Oates, O. Pourquié, Evolutionary plasticity of segmentation clock networks. *Development* **138**, 2783-2792 (2011)
Langeland J. A., S. F. Attai, K. Vorwerk, S. B. Carroll, Positioning adjacent pair-rule stripes in the posterior Drosophila embryo. *Development* **120**, 2945-2955 (1994)
Lauschke V. M., C. D. Tsiairis, P. Francois, A. Aulehla, Scaling of embryonic patterning based on phase-gradient encoding. *Nature* **493**, 101-105 (2013)
Lee J. E., I. Edery, Circadian regulation in the ability of Drosophila to combat pathogenic infections. *Curr Biol* **18**, 195-199 (2008)
Leimeister C., A. Externbrink, B. Klamt, M. Gessler, Hey genes: a novel subfamily of hairy- and Enhancer of split related genes specifically expressed during mouse embryogenesis. *Mech Dev* **85**, 173-177 (1999)

Leve C., M. Gajewski, K. B. Rohr, D. Tautz, Homologues of c-hairy1 (her9) and lunatic fringe in zebrafish are expressed in the developing central nervous system, but not in the presomitic mesoderm. *Dev Genes Evol* **211**, 493-500 (2001)
Lewis J., Autoinhibition with transcriptional delay: a simple mechanism for the zebrafish somitogenesis oscillator. *Curr Biol* **13**, 1398-1408 (2003)
Lewis J., A. Hanisch, M. Holder, Notch signaling, the segmentation clock, and the patterning of vertebrate somites. *J Biol* **8**, 44 (2009)
Li T., S. Huang, X. Zhao, D. A. Wright, S. Carpenter, M. H. Spalding, D. P. Weeks, B. Yang, Modularly assembled designer TAL effector nucleases for targeted gene knockout and gene replacement in eukaryotes. *Nucleic Acids Res* **39**, 6315-6325 (2011)
Libert S., M. S. Bonkowski, K. Pointer, S. D. Pletcher, L. Guarente, Deviation of innate circadian period from 24 h reduces longevity in mice. *Aging Cell* **11**, 794-800 (2012)
Linask K. K., C. Ludwig, M. D. Han, X. Liu, G. L. Radice, K. A. Knudsen, N-cadherin/catenin-mediated morphoregulation of somite formation. *Dev Biol* **202**, 85-102 (1998)
Liu P. Z., T. C. Kaufman, Short and long germ segmentation: unanswered questions in the evolution of a developmental mode. *Evol Dev* **7**, 629-646 (2005)
Lloyd D., M. Stupfel, The occurrence and functions of ultradian rhythms. *Biol Rev Camb Philos Soc* **3**, 275-299 (1991)
Mara A., J. Schroeder, C. Chalouni, S. A. Holley, Priming, initiation and synchronization of the segmentation clock by deltaD and deltaC. *Nat Cell Biol* **9**, 523-530 (2007)
Maroto M., J. K. Dale, M. L. Dequeant, A. C. Petit, O. Pourquié, Synchronised cycling gene oscillations in presomitic mesoderm cells require cell-cell contact. *Int J Dev Biol* **49**, 309-315 (2005)
Masamizu Y., T. Ohtsuka, Y. Takashima, H. Nagahara, Y. Takenaka, K. Yoshikawa, H. Okamura, R. Kageyama, Real-time imaging of the somite segmentation clock: revelation of unstable oscillators in the individual presomitic mesoderm cells. *Proc Natl Acad Sci U S A* **103**, 1313-1318 (2006)
McCammon J. M., S. L. Amacher, Using zinc finger nucleases for efficient and heritable gene disruption in zebrafish. *Methods Mol Biol* **649**, 281-298 (2010)
McGrew M. J., J. K. Dale, S. Fraboulet, O. Pourquié, The lunatic fringe gene is a target of the molecular clock linked to somite segmentation in avian embryos. *Curr Biol* **8**, 979-982 (1998)
Megason S. G., In toto imaging of embryogenesis with confocal time-lapse microscopy. *Methods Mol Biol* **546**, 317-332 (2009)
Meinhardt H., Models of Biological Pattern Formation. *Academic Press* (1982)
Meinhardt H., Models of Segmentation. R. Bellairs, D. Ede, J. Lash, Somites in Developing Embryos, *Plenum Press* 179-190 (1986)
Mito T., M. Ronco, T. Uda, T. Nakamura, H. Ohuchi, S. Noji, Divergent and conserved roles of extradenticle in body segmentation and appendage formation, respectively, in the cricket Gryllus bimaculatus. *Dev Biol* **313**, 67-79 (2008)
Morales A. V., Y. Yasuda, D. Ish-Horowicz, Periodic Lunatic fringe expression is controlled during segmentation by a cyclic transcriptional enhancer responsive to notch signaling. *Dev Cell* **3**, 63-74 (2002)
Morelli L. G., S. Ares, L. Herrgen, C. Schroter, F. Julicher, A. C. Oates, Delayed coupling theory of vertebrate segmentation. *Hfsp j* **3**, 55-66 (2009)
Moreno T. A., C. Kintner, Regulation of segmental patterning by retinoic acid signaling during Xenopus somitogenesis. *Dev Cell* **6**, 205-218 (2004)

Moreno-Risueno M. A., J. M. Van Norman, A. Moreno, J. Zhang, S. E. Ahnert, P. N. Benfey, Oscillating gene expression determines competence for periodic Arabidopsis root branching. *Science* **329**, 1306-1311 (2010)

Morimoto M., Y. Takahashi, M. Endo, Y. Saga, The Mesp2 transcription factor establishes segmental borders by suppressing Notch activity. *Nature* **435**, 354-359 (2005)

Morin-Kensicki E. M., E. Melancon, J. S. Eisen, Segmental relationship between somites and vertebral column in zebrafish. *Development* **16**, 3851-3860 (2002)

Muller M., E. v Weizsacker, J. A. Campos-Ortega, Expression domains of a zebrafish homologue of the Drosophila pair-rule gene hairy correspond to primordia of alternating somites. *Development* **122**, 2071-2078 (1996)

Nagai T., K. Ibata, E. S. Park, M. Kubota, K. Mikoshiba, A. Miyawaki, A variant of yellow fluorescent protein with fast and efficient maturation for cell-biological applications. *Nat Biotechnol* **20**, 87-90 (2002)

Ni Z., E. D. Kim, M. Ha, E. Lackey, J. Liu, Y. Zhang, Q. Sun, Z. J. Chen, Altered circadian rhythms regulate growth vigour in hybrids and allopolyploids. *Nature* **457**, 327-331 (2009)

Niederreither K., J. Vermot, B. Schuhbaur, P. Chambon, P. Dolle, Embryonic retinoic acid synthesis is required for forelimb growth and anteroposterior patterning in the mouse. *Development* **129**, 3563-3574 (2002)

Nikaido M., A. Kawakami, A. Sawada, M. Furutani-Seiki, H. Takeda, K. Araki, Tbx24, encoding a T-box protein, is mutated in the zebrafish somite-segmentation mutant fused somites. *Nat Genet* **31**, 195-199 (2002)

Niwa Y., Y. Masamizu, T. Liu, R. Nakayama, C. X. Deng, R. Kageyama, The initiation and propagation of Hes7 oscillation are cooperatively regulated by Fgf and notch signaling in the somite segmentation clock. *Dev Cell* **13**, 298-304 (2007)

Niwa Y., H. Shimojo, A. Isomura, A. Gonzalez, H. Miyachi, R. Kageyama, Different types of oscillations in Notch and Fgf signaling regulate the spatiotemporal periodicity of somitogenesis. *Genes Dev* **25**, 1115-1120 (2011)

Nozue K., M. F. Covington, P. D. Duek, S. Lorrain, C. Fankhauser, S. L. Harmer, J. N. Maloof, Rhythmic growth explained by coincidence between internal and external cues. *Nature* **448**, 358-361 (2007)

Nusslein-Volhard C., E. Wieschaus, Mutations affecting segment number and polarity in Drosophila. *Nature* **287**, 795-801 (1980)

Oates A. C., R. K. Ho, Hairy/E(spl)-related (Her) genes are central components of the segmentation oscillator and display redundancy with the Delta/Notch signaling pathway in the formation of anterior segmental boundaries in the zebrafish. *Development* **129**, 2929-2946 (2002)

Oates A. C., L. G. Morelli, S. Ares, Patterning embryos with oscillations: structure, function and dynamics of the vertebrate segmentation clock. *Development* **139**, 625-639 (2012)

Oginuma M., Y. Niwa, D. L. Chapman, Y. Saga, Mesp2 and Tbx6 cooperatively create periodic patterns coupled with the clock machinery during mouse somitogenesis. *Development* **135**, 2555-2562 (2008)

Oginuma M., Y. Takahashi, S. Kitajima, M. Kiso, J. Kanno, A. Kimura, Y. Saga, The oscillation of Notch activation, but not its boundary, is required for somite border formation and rostral-caudal patterning within a somite. *Development* **137**, 1515-1522 (2010)

Ozbudak E. M., J. Lewis, Notch signalling synchronizes the zebrafish segmentation clock but is not needed to create somite boundaries. *PLoS Genet* **4**, e15 (2008)

Ozbudak E. M., O. Pourquié, The vertebrate segmentation clock: the tip of the iceberg. *Curr Opin Genet Dev* **18**, 317-323 (2008)

Palmeirim I., D. Henrique, D. Ish-Horowicz, O. Pourquié, Avian hairy gene expression identifies a molecular clock linked to vertebrate segmentation and somitogenesis. *Cell* **91**, 639-648 (1997)

Patel N. H., The evolution of arthropod segmentation: insights from comparisons of gene expression patterns. *Dev Suppl*, 201-207 (1994).

Paul M. J., I. Zucker, W. J. Schwartz, Tracking the seasons: the internal calendars of vertebrates. *Philos Trans R Soc Lond B Biol Sci* **363**, 341-361 (2008)

Peel, A. D., The evolution of arthropod segmentation mechanisms. *Bioessays* **26**, 1108-1116 (2004)

Peel, A. D., A. D. Chipman, M. Akam, Arthropod segmentation: beyond the *Drosophlia* paradigm. *Nat Rev Genet* **6**, 905-916 (2005)

Pourquié O., Vertebrate somitogenesis. *Annu Rev Cell Dev Biol* **17**, 311-350 (2001)

Pourquié O., Vertebrate segmentation: from cyclic gene networks to scoliosis. *Cell* **145**, 650-663 (2011)

Pourquié O., P. P. Tam, in *Dev Cell*. (United States, 2001), vol. 1, pp. 619-620.

Prince V. E., S. A. Holley, L. Bally-Cuif, B. Prabhakaran, A. C. Oates, R. K. Ho, T. F. Vogt, Zebrafish lunatic fringe demarcates segmental boundaries. *Mech Dev* **105**, 175-180 (2001)

Pueyo J. I., R. Lanfear, J. P. Couso, Ancestral Notch-mediated segmentation revealed in the cockroach Periplaneta americana. *Proc Natl Acad Sci U S A* **105**, 16614-16619 (2008)

Qiu X., H. Xu, C. Haddon, J. Lewis, Y. J. Jiang, Sequence and embryonic expression of three zebrafish fringe genes: lunatic fringe, radical fringe, and manic fringe. *Dev Dyn* **231**, 621-630 (2004)

Rey G., A. B. Reddy, Connecting cellular metabolism to circadian clocks. *Trends Cell Biol* **23**, 234-241 (2013)

Riedel-Kruse I. H., C. Muller, A. C. Oates, Synchrony dynamics during initiation, failure, and rescue of the segmentation clock. *Science* **317**, 1911-1915 (2007)

Riek A., G. Kortner, F. Gieser, Thermobiology, enertetics, and activity patterns of the Eastern tube-nosed bat in the Australian tropics: teffect of temperature and lunar cycle. *J Exp Biol* **213**, 2557-2564 (2010)

Reinitz J., D. H. Sharp, Mechanism of *eve* stripe formation. *Mech Dev* **49**, 133-158 (1995)

Riley M. F., M. S. Bochter, K. Wahi, G. J. Nuovo, S. E. Cole, Mir-125a-5p-mediated regulation of Lfng is essential for the avian segmentation clock. *Dev Cell* **24**, 554-561 (2013)

Rohde L. A., C. P. Heisenberg, Zebrafish gastrulation: cell movements, signals, and mechanisms. *Int Rev Cytol* **261**, 159-192 (2007)

Ruiz I., A. Altaba, V. Nguyen, V. Palma, The emergent design of the neural tube: prepattern, *Shh* morphogen and GLI code. *Curr Opin Genet Dev* **5**, 513-521 (2003)

Saga Y., N. Hata, H. Koseki, M. M. Taketo, Mesp2: a novel mouse gene expressed in the presegmented mesoderm and essential for segmentation initiation. *Genes Dev* **11**, 1827-1839 (1997)

Sander J. D., L. Cade, C. Khayter, D. Reyon, R. T. Peterson, J. K. Joung, J. R. Yeh, in *Nat Biotechnol*. (United States, 2011), vol. 29, pp. 697-698.

Sarrazin A. F., A. D. Peel, M. Averof, A segmentation clock with two-segment periodicity in insects. *Science* **336**, 338-341 (2012)

Sasai Y., R. Kageyama, Y. Tagawa, R. Shigemoto, S. Nakanishi, Two mammalian helix-loop-helix factors structurally related to Drosophila hairy and Enhancer of split. *Genes Dev* **6**, 2620-

2634 (1992)
Sawada A., A. Fritz, Y. J. Jiang, A. Yamamoto, K. Yamasu, A. Kuroiwa, Y. Saga, H. Takeda, Zebrafish Mesp family genes, mesp-a and mesp-b are segmentally expressed in the presomitic mesoderm, and Mesp-b confers the anterior identity to the developing somites. *Development* **127**, 1691-1702 (2000)
Sbalzarini I. F., P. Koumoutsakos, Feature point tracking and trajectory analysis for video imaging in cell biology. *J Struct Biol* **151**, 182-195 (2005)
Schoenwolf G. C., V. Garcia-Martinez, M. S. Dias, Mesoderm movement and fate during avian gastrulation and neurulation. *Dev Dyn* **193**, 235-248 (1992)
Schroder R., D. G. Jay, D. Tautz, Elimination of EVE protein by CALI in the short germ band insect Tribolium suggests a conserved pair-rule function for even skipped. *Mech Dev* **90**, 329 (2000)
Schroter C., S. Ares, L. G. Morelli, A. Isakova, K. Hens, D. Soroldoni, M. Gajewski, F. Julicher, S. J. Maerkl, B. Deplancke, A. C. Oates, Topology and dynamics of the zebrafish segmentation clock core circuit. *PLoS Biol* **10**, e1001364 (2012)
Schroter C., L. Herrgen, A. Cardona, G. J. Brouhard, B. Feldman, A. C. Oates, Dynamics of zebrafish somitogenesis. *Dev Dyn* **237**, 545-553 (2008)
Schroter C., A. C. Oates, Segment number and axial identity in a segmentation clock period mutant. *Curr Biol* **20**, 1254-1258 (2010)
Scott M. P., S. B. Carroll, The Segmentation and homeotic gene network in early *Drosophila* development. *Cell* **51,** 689-698 (1987)
Serth K., K. Schuster-Gossler, R. Cordes, A. Gossler, Transcriptional oscillation of lunatic fringe is essential for somitogenesis. *Genes Dev* **17**, 912-925 (2003)
Sieger D., B. Ackermann, C. Winkler, D. Tautz, M. Gajewski, her1 and her13.2 are jointly required for somitic border specification along the entire axis of the fish embryo. *Dev Biol* **293**, 242-251 (2006)
Small S., R. Kraut, T. Hoey, R. Warrior, M. Levine, Transcriptional regulation of a pair-rule stripe in Drosophila. *Genes Dev* **5**, 827-839 (1991); published online EpubMay (
Smith J. M., Continuous, quantized and modal variation. *Proc R Soc Lond B Biol Sci* **152**, 397-409 (1960)
Sommer R. J., D. Tautz, Involvement of an orthologue of the Drosophila pair-rule gene hairy in segment formation of the short germ-band embryo of Tribolium (Coleoptera). *Nature* **361**, 448-450 (1993)
Soroldoni D., A. C. Oates, Live transgenic reporters of the vertebrate embryo's Segmentation Clock. *Curr Opin Genet Dev* **21**, 600-605 (2011)
Spemann, H. Entwickelungsphysiologische Studien am Tritonei III. *Arch. f. Entw.mech.* **16**, 551-631 (1903)
Stern C. D., D. Vasiliauskas, Clocked gene expression in somite formation. *Bioessays* **20**, 528-531 (1998)
Stickney H. L., M. J. Barresi, S. H. Devoto, Somite development in zebrafish. *Dev Dyn* **219**, 287-303 (2000)
Stollewerk A., M. Schoppmeier, W. G. Damen, Involvement of Notch and Delta genes in spider segmentation. *Nature* **423**, 863-865 (2003)
Takahashi Y., K. Koizumi, A. Takagi, S. Kitajima, T. Inoue, H. Koseki, Y. Saga, Mesp2 initiates somite segmentation through the Notch signalling pathway. *Nat Genet* **25**, 390-396 (2000)
Takashima Y., T. Ohtsuka, A. Gonzalez, H. Miyachi, R. Kageyama, Intronic delay is essential

for oscillatory expression in the segmentation clock. *Proc Natl Acad Sci U S A* **108**, 3300-3305 (2011)

Takke C., J. A. Campos-Ortega, her1, a zebrafish pair-rule like gene, acts downstream of notch signalling to control somite development. *Development* **126**, 3005-3014 (1999)

Thom R., Structural Stability and Morphogenesis, *Westfield Press*, 1972

Trofka A., J. Schwendinger-Schreck, T. Brend, W. Pontius, T. Emonet, S. A. Holley, The Her7 node modulates the network topology of the zebrafish segmentation clock via sequestration of the Hes6 hub. *Development* **139**, 940-947 (2012)

Turing, A. M. The chemical basis of morphogenesis. *Philos. Trans. R. Soc. Lond., B* **237** 37-72 (1952)

Uriu K., Y. Morishita, Y. Iwasa, Synchronized oscillation of the segmentation clock gene in vertebrate development. *J Math Biol* **61**, 207-229 (2010)

van Eeden F. J., M. Granato, U. Schach, M. Brand, M. Furutani-Seiki, P. Haffter, M. Hammerschmidt, C. P. Heisenberg, Y. J. Jiang, D. A. Kane, R. N. Kelsh, M. C. Mullins, J. Odenthal, R. M. Warga, M. L. Allende, E. S. Weinberg, C. Nusslein-Volhard, Mutations affecting somite formation and patterning in the zebrafish, Danio rerio. *Development* **123**, 153-164 (1996)

van Eeden F. J., S. A. Holley, P. Haffter, C. Nusslein-Volhard, Zebrafish segmentation and pair-rule patterning. *Dev Genet* **23**, 65-76 (1998)

Vermot J., O. Pourquié, Retinoic acid coordinates somitogenesis and left-right patterning in vertebrate embryos. *Nature* **435**, 215-220 (2005)

Wahl M. B., C. Deng, M. Lewandoski, O. Pourquié, FGF signaling acts upstream of the NOTCH and WNT signaling pathways to control segmentation clock oscillations in mouse somitogenesis. *Development* **134**, 4033-4041 (2007)

Wainwright S. M., D. Ish-Horowicz, Point mutations in the Drosophila hairy gene demonstrate in vivo requirements for basic, helix-loop-helix, and WRPW domains. *Mol Cell Biol* **12**, 2475-2483 (1992)

Wang W., J. Y. Barnaby, Y. Tada, H. Li, M. Tor, D. Caldelari, D. U. Lee, X. D. Fu, X. Dong, Timing of plant immune responses by a central circadian regulator. *Nature* **470**, 110-114 (2011)

Wartlick O., P. Mumcu, F. Julicher, M. Gonzalez-Gaitan, Understanding morphogenetic growth control – lessons from flies. *Nat Rev Mol Cell Biol* **12**, 594-604 (2011)

Weidinger G., C. J. Thorpe, K. Wuennenberg-Stapleton, J. Ngai, R. T. Moon, The Sp1-related transcription factors sp5 and sp5-like act downstream of Wnt/beta-catenin signaling in mesoderm and neuroectoderm patterning. *Curr Biol* **15**, 489-500 (2005)

Wollnik F., Physiology and regulation of biological rhythms in laboratory animals: an overview. *Lab Anim* **23**, 107-125 (1989)

Wright D., Z. Ferjentsik, S. W. Chong, X. Qiu, Y. J. Jiang, P. Malapert, O. Pourquié, N. Van Hateren, S. A. Wilson, C. Franco, H. Gerhardt, J. K. Dale, M. Maroto, Cyclic Nrarp mRNA expression is regulated by the somitic oscillator but Nrarp protein levels do not oscillate. *Dev Dyn* **238**, 3043-3055 (2009)

Zhang L., C. Kendrick, D. Julich, S. A. Holley, Cell cycle progression is required for zebrafish somite morphogenesis but not segmentation clock function. *Development* **135**, 2065-2070 (2008)

Appendix A: Documentation of MATLAB Programs for Image Segmentation, Cell Tracking, and Data Analysis

The following documentation will act as a primer for the scripts used in my thesis. While I do my best to define relevant terminology, readers are expected to have some baseline understanding of the MATLAB (matrix laboratory) programming language. MATLAB is a numerical computing environment, useful for storing and analysis large data sets. It is licensed software, requiring an annual subscription. This programming language is well-documented and supported on the website: www.mathworks.com. There is also a large community online that shares scripts on the Mathworks forums. The language itself is relatively easy to learn, allows for rapid coding, and has many graphical functions that are optimized and intuitive. Because MATLAB is a consumer product, a lot of work is built-in to guide and protect users in an otherwise unforgiving coding environment. This appendix is based on MATLAB version R2012b. Scripts run in earlier versions (with the earliest being R2011a) ran without any difficulty. All scripts described here are either written by or collaboratively generated with Dr. Paul Francois of McGill University.

This Appendix is by no means comprehensive, and much of the code is already commented. This is merely a primer for those who have no MATLAB experience or want to quickly become oriented to the strategies and thought process of the code.

- *Key functions*: will be denoted by this arrow and italicized

Learning MATLAB

For useful texts to supplement this appendix, please reference the following:

Attaway, Stormy. *MATLAB: A Practical Introduction to Programming and Problem Solving*. Oxford: Butterworth-Heinemann, 2009. Print
This book is useful for those who have never programmed before. It explains concepts of programming along with the actual programming language. Written in a more conversational, candid style, his descriptions and logic are easy to follow. The problem sets are also quite useful.

Hanselman, Duane and Bruce Littlefield. *Mastering MATLAB 7*. Upper Saddle River: Pearson Education, 2005. Print
A more technical text (and older) that helps one learn the nuances of the language and how to utilize it in problem-solving. It also explores some available toolboxes and deeper challenges in writing more complicated code.

Installation

Upon installing the base MATLAB software, several optional toolboxes should also be installed to ensure proper availability of scripts used in my work. Full descriptions of these toolboxes and their content are available on the Mathworks website.

Image Processing Toolbox: important for processing images for automated cell detection and the cell tracking graphical user interface (GUI)

Parallel Computing Toolbox: significantly decreases processing time for computationally-intensive scripts by computing them in parallel. Requires a computer with multiple processors

Statistics Toolbox: useful for running a gauntlet of statistical tests based on data extracted from our timelapses

MATLAB 3d_tools Files

The bulk of files were initially developed for the Deluane 2012 publication. All files developed for that paper can be found in the folder: "3Dtools_unstable 8-4-11", denoting its function in detecting cells in 3D space, the dynamic state of its development (though not many changes were made at this point), and the last date of major revisions. This version was developed specifically for images generated on the Olympus FV1000 and associated image processing software. This software created outputs for each individual channel, with the fluorescence recorded in grayscale and pseudo-colored. MATLAB processes these images as a two-dimensional matrix, meaning that there are not separate channels for red, green, and blue.

Unfortunately, the Olympus confocal was removed from the UC Berkeley Imaging Facility, and a replacement had to be found. A suitable replacement was found in the Zeiss LSM780. The image processing software, ZEN, can be downloaded for free on the Zeiss website. One key difference in how this program exports .tiff files is that MATLAB reads these files in three dimensions: one for each of the red, green, and blue channel. This is the case despite the fact that exported files can be separated into individual channels. What occurs then is that MATLAB interprets a red, green, and blue channel despite two of the channels being blank. So if the green fluorescence of Venus is recorded in the green channel (the 2nd channel, since colors are stored in RGB) in a 600x200 pixel image (denoted as [600 200]), the 1st and 3rd channels are also present, but filled with 0's. While the outputs from the Olympus were [600 200 1] in size, the third dimension in the Zeiss images had to be accounted for: [600 200 3].

Edits were made to the "Segmentation" folder to adjust for this difference in input so that the program would only read the relevant channel out of the three. Along with some changes to the GUI (graphical user interface), these modifications were created in a new version of the 3D tools, called "3Dtools_unstable 3-7-12", denoting the new date the changes were made. Analysis tools are most up-to-date in this version.

To ensure that you can access these scripts even when browsing different folders, use the "Set Path" button, click "Add with Subfolder", and click on the 3Dtools_unstable of your choice. Be sure the correct 3D tools are used with the correct set of images; otherwise you will receive an error message.

Raw File Inputs

All image processing and analyses are based on the assumption that images are tagged image file format (.tiff). Image files must be separated into one color channel per image, with channel 1, 2, and 3 designated for red, blue, and green, respectively.

Each file is named with this format: "stub_t020_z05_c02" (actual file name without parentheses)

- "stub" indicates the movie name, such as e2-tl1, short for embryo 2, timelapse 1. The actual filename would be: e2-tl1_t01_z05_c02

- t20 indicates the timepoint. In this case, this image is the 20th timepoint in this timelapse. Note that movies are often two to four sequential timelapses stitched together, each with timelapse having a timepoint that starts at t01. Note that numbers 1 through 9 are actually designated 01 through 09, with numbers from 10-99 having the normal two digit designation.
- z05 indicates this is the fifth z-stack in the image set. Again, numbering of stacks 1 through 9 are preceded by a 0 (01 to 09).
- c02 indicates the channel, blue. 01, 02, and 03 designate red, blue, and green

The folders are also specifically named:

- title folder: stub-tiffs
    - subfolder 1: stub-tl1-tiffs
    - subfolder 2: stub-tl2-tiffs
    - subfolder n: stub-tln-tiffs

This naming scheme is important for the proper recognition in retrieving files throughout image processing and analyses.

Nomenclature is hard-coded into our scripts for the sake of simplicity. Deviations from this naming scheme will result in an error message indicating the proper files cannot be found. Future users can either change the script to properly direct the search, or use a script to change the names of each of the .tiff files. One script has been created to perform the latter task.

- ➢ *rename_files*: stored in the Utilities folder in the 2012 3D_tools_unstable. A tool developed to rename the .tiff files generated from the Zeiss image processing software, ZEN 2011. In this script, you can input the new stub name of your choice. You must also input the number of timepoints and zstacks in your timelapse.
    - WARNING: this script hard codes a lot of aspects, with the assumption that files are organized by time, zstacks, and then channels. This script does not take into account the file name of any of the .tiff files, processing each file in the order they appear in the directory. This code permanently changes file names, so please test with a copied version of files, rather than the original.

A couple notes on lingo: when I refer to a “timelapse,” I am referring to the subfolder with the raw images inside. When I refer to a “movie,” this is the sum of the several timelapses that constitutes the whole movie. Each timelapse is usually 20-40 timepoints, and each movie has 2-4 timelapses.

Automated Cell Detection

All files discussed in this section are found under the subfolder “Segmentation”.

The initial step in analyzing our timelapses was to allow the MATLAB script to automatically detect as many cells as possible. Broadly, these scripts use the membrane and nuclear fluorescence to predict the outlines of cells. Fluorescent images of both of these cellular structures are translated into a MATLAB compatible format (using the “imread” function in the Image Processing Toolbox). This converted matrix is then processed by low-pass filters to remove noise from these two channels. The separate optical slices were then merged into a single matrix and each continuous three-dimensional cluster of fluorescent pixels was indexed. To isolate individual cells out of these clusters, we adapted a script (Keller, 2008) that searched for

two peaks of intensity in each cluster of fluorescence and separated them into unique cells. Every cluster was segmented repeatedly until only single peaks of fluorescence were detected.
These individual cells were then connected across time using a tracking program outlined in Sbalzarini and Kounoutsakos (2005). The potential problems in tracking due to mitosis were circumvented by tracking the cells in reverse, starting from the last time point.
For each cell, the optical section with the highest average was recorded as the cell's fluorescence for each given time point. The cell's reporter fluorescence, position in the embryo, Cartesian coordinates, catalog number, and mitotic activity were recorded in a data matrix for future analyses.

The detection script does only works for images in each subfolder of the timelapse. If there are three timelapses in an imaging session (where imaging was briefly stopped every hour or two to readjust the embryo), this script will have to be run three times. To connect across different timelapses, the GUI will have to be used (more on this later). In order for the script to work, the "Current Folder" in the MATLAB interface has to be set to the subfolder of interest. This allows MATLAB to access the files based on their names. MATLAB will not by default search outside of the "Current Folder."

To run the detection script, only one command is needed:

- ➢ *analyze_movie_2_inverse*: For this script to work, the current folder function requires three inputs: number of timepoints in the timelapse, file name (stub), and the number of z-stacks in the timelapse. The "2" is the version of this script, and the "inverse" signifies the tracking begins at the last timepoint and works backwards. **Note**: These variables apply to the subfolder and not the total number of timepoints.

Example: If the folder/subfolder is named e2-tiffs/e2-tl2-tiffs, the last file will be e2-tl2_t20_z25_c03.tif. To run the script, type:

```
>>analyze_movie_2_inverse(20,”e2-tl2”,25).
```

This function will create several files in the same subfolder:

- detect_cells_2d: The outlines of cell nuclei at each timepoint after low-pass filter processing. One matrix for each timepoint.
- membrane: The outlines of cell membranes at each timepoint after low-pass filter processing. One matrix for each timepoint.
- labeled: the outlines of cells detected at each timepoint. These files can be amended using the GUI to manually highlight cells
- peaks_3d: all relevant information of each labeled cell. Relevant information of each cell is stored in a structure[5], including data about coordinates, area, and any tags to label the cell (mitotic, dorsal, ventral, adaxial, somite compartment, etc). One file for each timepoint

---

[5] If unfamiliar with data storage methods in MATLAB, look up differences between a matrix, cell, and structure.

- peaks: the most important file, as it contains the same information as the peaks_3d files, but with every single timepoint in the timelapse. Most analysis is done using this file. Any changes made by the GUI are immediately altered here. This file is periodically backed up via the GUI. These backups are labeled with the date and time of the backup (peaks_8_8_12_h_57 for example, with the date and then time).

Cell Validation and Oscillation Smoothing

After cells are automatically detected and connected, additional steps are required to completely link them and validate them across the movie. This was done using a custom GUI, which is discussed below. Before going into the nuances of how to validate cells, it is important to understand how these validated tracks will be stored for further analysis. Each cell that is validated will cause two events: an individual file will be generated for this validated cell (in a .mat file named "traject_cellxxx", where xxx is the cell number) and the file "all_validated_tracks" will be appended with the data of the additional cell. The information in both these files is the same, except that "all_validated_tracks" is a cell array containing every single validated cell (as the name implies). These files can be found in the title folder of any movie. Each cell is identified by its index number in the last timepoint in the movie. Each cell within the array represents the possible index numbers of cells outlined in the last timepoint, but cells only contain information if validated via the GUI. Once they are validated, a t by 16 matrix (t being the number of timepoints in the movie) is created in the corresponding cell.

- Column 1: the index number of the cell. This is how the cell is identified
- Column 2-4: the Cartesian coordinates (x,y,z) of the cell's center. If the cell is spread across several z-stacks
- Column 5: Raw fluorescence of green channel (Venus signal) within the outline of the cell, as defined by the automated script/the user. If the cell is traced across several z-stacks, the section with the brightest fluorescence is chosen as the representative fluoresence
- Column 7: Inferred phase of the oscillation based on our smoothing heuristic. See below for the equation and functions used.
- Column 9: Mitotic tag. At the timepoint where current cell is mitotic, that cell is marked with a "1". All other timepoints will be marked with "0" or "-1"
- Column 8, 10-16: Various other tags. Again, tagged cells will be marked with a "1", untagged cells will be marked with "0" or "-1"

A smoothed version of the fluorescence pattern was generated by assuming values of amplitude, angular velocity and DC bias remain mostly unchanged across periods of time. Our smoothing heuristic (equation below) removed the average fluorescence in a given time, estimated the new amplitude and rescaled the sine wave to that amplitude. The raw fluorescence was treated twice by this method to isolate a smoothed expression pattern of each cell. Assuming this readout behaved like a harmonic oscillator, the periodicity was then obtained by estimating the angular velocity of each period. One obstacle with this calculation is that the period calculation assumes a period exists. This challenge, coupled with the necessity to validate the automated trackings, led to the development of a graphical user interface (GUI) to efficiently make necessary edits to our data matrices.

$$F(t) = A(t)\sin\omega(t)t + B(t) \implies \sin\omega(t)t \simeq \frac{(F(t) - < F(t) >_T)}{\sqrt{2 < (F(t) - < F(t) >_T)^2 >_T}}$$

To convert the raw fluorescence into an inferred sine wave, three functions are of interest (though oscillations are already converted in the “all_validated_tracks” file in the 7th column):

- *smooth*: this is the smoothing heuristic as seen in the equation above. It requires two inputs, the vector of oscillation readouts, and the smoothing window. The larger the smoothing window, the more the signal will be averaged.

- *compute_sin*: estimates the sin wave based on the smoothed oscillation readout. Only requires the vector of oscillation data as input

- *compute_phase_traject*: This combines the smoothing heuristic and estimated sine wave to generate the phase for each timepoint. Again, the function only requires the vector of oscillation data as input. Compare column 5 and 7 in any traject_cell file.

Graphical User Interface

We developed a GUI that displayed a given time frame and z-slice as well as the previous time frame at the same z-slice (Figure A.1A). The interface allowed for rapid navigation across space and time, simple tagging and manual correction of individual cells, and filters to display different fluorescence channels, labels, and contours. This configuration allowed us to properly link cells across time frames that were previously unconnected. An option was included in this GUI to crop out ranges of calculated periods in cells that were not visibly oscillating to remove any noise generated by the automated tracking.

The GUI can be called up in the command window by simply typing:

- *stack_GUI*: This brings up the user interface, which allows users to track, tag, and validate cells

To edit the buttons on the GUI, use the GUI Development Environment:

- *guide*: this allows you to access “Open Existing GUI” to add, remove, or move buttons in the GUI to maximize your efficiency.

I will not go into GUI development, as it was not necessary for me to do so while using it. There are quite a few key points in understanding and using this GUI, and I will outline them here (as numbered in Figure A.1A)

1: Set names. This brings up a window that requires three inputs. Click “Set Directory” and open the title folder of the movie you want to track. In the box labeled “Index1”, delete the text and type in 1. In the box labeled “Last Index”, delete the text and type in the number of subfolders the movie has. For example, if the title folder is named “e3” and there are three subfolders, “e3-tl1.tiffs,” “e3-tl2.tiffs,” and “e3-tl3.tiffs”, you would type in “3” in the “Last Index” box. Once finished, click okay. Remember, nomenclature is important before you select any file to be analyzed. Folders/files not named based on the specific nomenclature mentioned above will result in an error.

2. Load settings! Once you have set the name of the files you want to read, simply click this button to instruct the GUI to start loading all the images, cell traces, and tags.

3. The tracking windows. The top window corresponds to your current timepoint and z-stack, and the bottom window corresponds to the previous timepoint, same z-stack. The green contours are how the scripts detect cell boundaries. There are three numbers that index each cell. For example, one cell could be labeled: "382-> 279; 86." The 1st number is the current cell index at the given timepoint. The 2nd number is the index number of the cell it is connected to in the previous timepoint. If it is not connected to anything, this number will be "1" and the text will be yellow. The 3rd number is the index number of the earliest connected timepoint. So continuing the example, if a cell is connected across 15 timepoints, all 15 of these cells will have "86" as the 3rd number in the label. Useful for making sure you still have the same cell.

Clicking on a cell in the upper window will cause the number in both "Current Cell" windows to update. This will also transfer the previous number in "Current Cell" to the box labeled "Older index." Clicking on a cell in the lower window will cause the number in "New Cell Index" to update. Selecting cells will be essential to the cell tracking process.

4. Time and Z-section. As the labels imply, these two boxes display the current z-stack and timepoint that is displayed. The timepoint is based on the sum of all timepoints in the various subfolders. To quickly navigate to the time and z-stack of choice, delete the current value, type in the value desired, and hit Enter.

5. Go to Time. This allows you to follow a specific cell across time. So if the cell shifts in the frame of the movie or changes z-stacks, the program can jump to that timepoint with the cell centered in the screen. This can also be navigated using the D and F keys.

6 and 7. Various display options and tags. You can turn on or off each channel of fluorescence, as well as the indexing numbers and cell outline traces. Tags for the cell's position or behavior are also available.

8. Merge Cells function. Sometimes two cell traces actually represent one cell, often across several z-stacks. To merge these two cells together, click the cells consecutively in the top box, using the key bindings to navigate to each cell of choice. Then click the button "Merge Cells." To ensure this works, make sure you check that the correct index numbers are in the boxes, and that you do not click anything else during this process. A second option is to directly type in the cell index numbers as listed in the top box, hitting Enter after typing in each one. Then click "Merge Cells." This function was rarely used, since it was often faster to just create a new cell and/or delete the old cell.

9. Delete Current cell. This button deletes all data associated with the cell listed in "Current Cell." This deletes every slice of the cell contour as well. Only applies to cells clicked in the upper window.

10. Delete Current Slice. This function only removes the single contour in the current z-stack. The cell is divided into two cells (when deleting from the middle of the stack of contours). The cell with the lower z-stack will be connected to the original trace (before and after, when applicable), while the higher cell will be an orphan and connected to nothing.

11. New Cell. (Figure A.1B) Your best friend for cell tracking. More often than not, the scripts cannot detect the cell outline. This button opens up a new window for you to manually outline the cell. To save time, only press the button when you are in a stack near the middle of the cell body and relatively zoomed for accurate outlining. This new window that pops up will display the red channel showing nuclear fluorescence. To highlight the new cell, simply click an outline around the cell. When the polygon is complete, double click on the last point to create the cell. The window should automatically close.

12. Cell traces across time. The top graph represents the z-position of the cell. This is a useful method to compare the tracks of cells in a similar area, despite the embryo itself moving. The middle plot shows the raw oscillations of the cell you are currently tracking. Useful for quality control (no random peaks or valleys in the middle of tracks). The last window is the inferred phase based on the smoothing heuristic discussed above. During initial cell tracking, this window is blank. Buttons 15 and 16 must be used to generate the inferred phase.

13. Reconnect tls GUIS. (Figure A1.C) This button allows you to connect your multiple timelapses. Often when timelapses are stopped and started, the microscope's z-axis is shifted to center the embryo again. This will often cause images in the end of one timelapse and the beginning of the other to not line up. Clicking this button will bring up a window that looks like a simplified version of the stack_GUI. The additional function of this tool is the Zshift, which allows you to change which z-stack is displayed in the bottom window (and previous timepoint). For example, if the top screen is at [time 10 z-stack 15], a Z-shift value of -5 will display [time 9 z-stack 10] in the bottom window. The connect cells, simply click the cell desired in the top window and bottom window, then click the "Correct tracking" button. Close window manually when finished.

14. Correct Tracking. As stated earlier, the "Current Cell" lists the most recent clicked cell in the upper window, and the "New Cell Index" listed the most recent cell clicked in the bottom window. By clicking the "Correct Tracking" button, the GUI would link these two timepoints, along with any timepoints already connected to either of them.

15. Compute Phase Current Cell. This infers the phase of the raw oscillations, plotting the oscillations in the bottom window of (12).

16. Correct phase current cell. This button brings up a correction GUI that allows the user to crop the oscillations based on what is reasonable. For example, if a cell clearly stops oscillating after timepoint 30 out of a total of 60, enter the "t1" value as "31" and the "t2" value as 60. This will

erase those timepoints to prevent them from being used in analysis. If you are satisfied with your crop, click “Update.” If you felt that you made a mistake, simply close the window and try again. Sometimes more than one crop has to be done to properly clean up the oscillation signal. How to crop the signal is at the discretion of the cell tracker.

18. Finalize Current Cell. Takes the record of the cell listed in “Current Cell” from the “peaks” file and makes a record in a “traject_cell” and the “all_validated_tracks” file. Validating a cell once will make a broken box around the validated index number in the image window, and validating twice will make a complete box. This system is useful when two people are validating the cells, so they know which ones have been double checked. Finalizing a cell at least once is required for the tracked cell to be considered in further analyses. Only validate cells that can be tracked from start to finish.

17. Devalidate Current Cell. If a cell is accidentally or incorrectly validated, you can devalidate it with this button. This will remove the record of the validated cell and allow you to retrack and revalidate at a future time.

Key bindings: Along with using the mouse to navigate the GUI, they keyboard is required to manipulate which image is displayed in the GUI window. Here are the keys used and what they do. Video game experience may be helpful for rapid navigation.

A: move to previous timepoint
S: move to next timepoint
W: move to next z-stack (+1)
Z: move to previous z-stack (-1)
D: move to previous timepoint while following the same cell. Will follow the most recent cell you clicked. This key also centers the cell to the middle of your display
F: move to next timepoint while following same cell
J: move left in space
K: move right in space
I: move up in space
M: move down in space
1: zoom in
2: zoom out

User considerations and known bugs:

- When navigating images using the GUI, be mindful of the computer’s processing power. Rapid clicking and keystrokes are known to cause outstrip the computer’s processing and cause unwanted glitches or freezing
- The most important bug to note can occur when the movie first loads. The bug causes the system to lock and prevents the user from properly navigating through the movie. To fix this, when the movie loads, immediately click on a highlighted cell contour. Press the “D” and “F” keys a couple of times each, just so the GUI registers and can follow this cell a couple of times. After this, the glitch does not seem to occur.
- To follow a cell using “D” and “F”, you have to click on the cell of interest and not click on any other cell. Clicking on empty space is okay, if you need to readjust the display.

- To input a number into the GUI, do NOT click on any other space than the boxes you want. Just hit enter and click the next one. Otherwise you'll get 0 as the cell number.

Analysis

Several different methods of analyses were used to quantify the oscillations of PSM cells. While the "Analysis" folder carries quite a number of scripts, only the main ones that produced meaningful analysis will be included here. These scripts will often have functions within them that handle modular tasks. These secondary functions will not all be described here. Most of these scripts also contain comments, so please see those for additional information.

- *study_correl*: Calculates the inferred phase of every single cell in a tracked movie and compares the phase of each cell with the phase of neighboring cells at every given timepoint both cells are still oscillating. Responsible for Figure 3J-M in Delaune *et al.* 2012. Requires the all_validated_tracks file of the movie of interest, and one of 5 tags (outlined in the code's comments). This script could compare all cells, or exclude/include mitotic cells. The code can also take into account the cropping done by users to correct abhorrent oscillations.

- *plot_ensemble_cells*: This code is actually not used anymore, but this was a quick way to plot the fluorescence of a cluster of cells and highlight which cells these were in the movie. This code contains useful information if new users are interested how to call up the necessary matrices and variables to plot the oscillations of single cells and display where these cells are. Oscillations can also be plotted by simply using the command:
  ```
  >> plot(all_validated_tracks{i}(:,5))
  ```
  Where all_validated_tracks is for the movie of interest and "i" represents the cell index number of the cell you want to plot

- *make_global_movie_phase*: This script generated Figure 3F-I in Delaune *et al*. 2012. The script takes the inferred phase of the oscillations and assigns a color to each phase value. Then at each timepoint, validated cells display that phase color within the outline of the cell, against a darkened background. A key parameter is "deep", which determines how many z-sections will be displayed on the single image.

- *make_movie_single_cell*: A simple script that generates consecutive images, containing the membrane and reporter fluorescence channels. Requires a cell_index to center the movie, and you can pick any cell of you want (just the number will suffice). Again, the "deep" parameter will determine how many z-stacks will be combined in the image. Responsible for the supplemental movies from Delaune *et al.* 2012.

- *stat_meta_mitotic*: This script calculates the phase difference between two recently divided sister cells, as well as each of the sister cells compared to their neighbors. These will be displayed as 2D histograms using the function *plot_2d_hist_phases*, a user-shared function from the MATLAB forums. The actual calculations of phase difference are done using the function *compare_phase_shift_meta*, which simply makes a list of all mitotic cells and calculates its oscillations after mitosis. This function is responsible for generating Figure 4D, 5B, 5D, 5F in Delaune *et al.* 2012.

- *amplitude_calc*: Takes the timepoints where each cell peaks and finds the amplitude at each of those timepoints. Also calculates the change in amplitude between two adjacent timepoints as a fluorescence value and a percentage. The timepoints for each cell peak was actually curated manually (with help from the GUI). See Appendix B for how this data is organized. This generated figure 1E in Shih *et al.* 2013.

- *correl_borders*: A similar script to study_correl, except that it requires the user to input two lists of cells. The script will then compare the phase of each cell from one list with the phase of each in the other list. This allows the user to decide which set of cells to compare to another, including cells from one somite boundary with cells in another somite boundary. Generated Figure 2F-I in Shih *et al.* 2013.

- *compute_phase_profiles*: This script analyzes the tissue fluorescence across the entirety of each movie. It requires the user to be in the title folder of the movie they want to analyze. The user must input the total time in the movie (in timepoints) and a "traject" file of a validated cell they want as a reference point. This is important because depending on the z-stack, the fluorescence considered will be slightly different (sometimes signal is clearer in a more lateral z-stack). A couple of other components have to be changed at the code level rather than as an input to the function. The user must specify the root directory and how many subfolders there are. This script generates a .mat file called "Recapitulation". In it, there are two main matrices of value: phase_profile and position_profile. The phase_profile is the measure of fluorescence within each stripe at each timepoint (each row) and each spatial stripe (each column). The position_profile is organized in a similar fashion, except it records the distance from the reference cell to the slice. This script uses 3 main functions:
    - *load_movie1*: this uses a similar code as the GUI to retrieve the necessary images. User has to manually change the "nstack" value to reflect how many z-stacks are present in target movie
    - *detect_psm_2*: an automated embryo and axis detection script that uses low-pass filters to determine the shape of the embryo. After doing so, the script will designate a central axis for the next step of the analysis.
    - *spatial_fluorescence*: divides the detected embryo into slices of equal size. User must change the "bin" value to reflect how large each slice is. At bin=40, there are three slices per somite (approximately). The larger the bin size, the larger the digital slices. The script then measures the fluorescence of reporter expression within each slice.

A

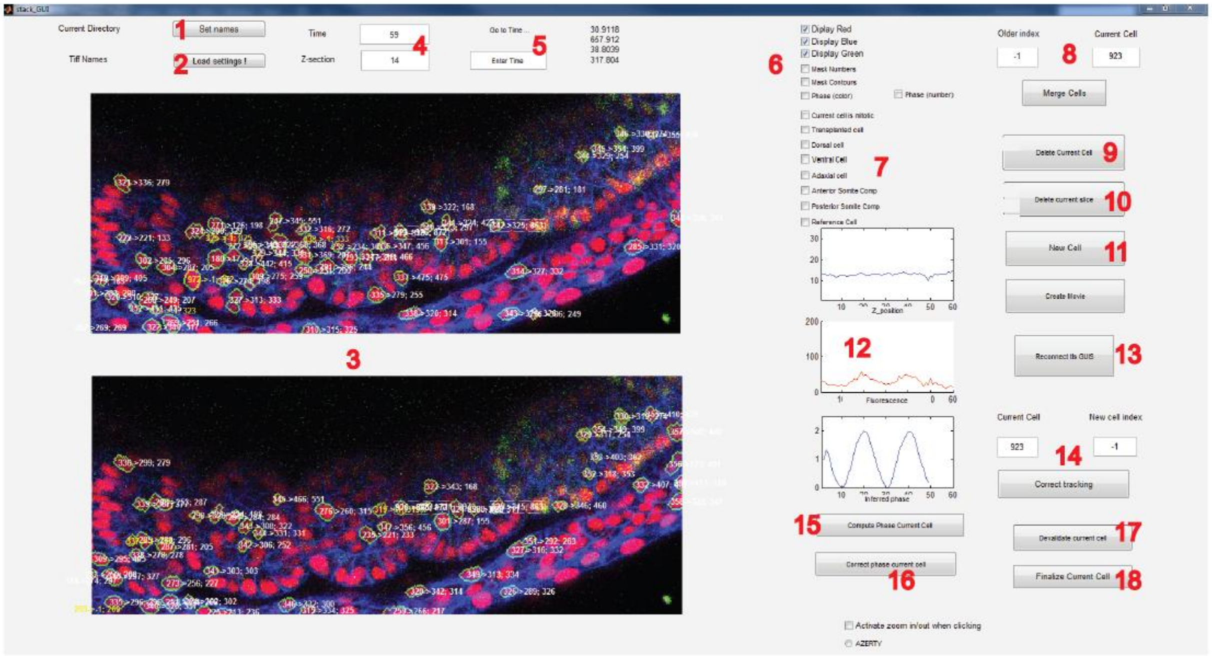
stack_GUI
Current Directory
Tiff Names
1
Set names
2
Load settings !
Time
Z-section
4
Go to Time ...
5
Enter Time
3
6
7
8
9
10
11
12
13
14
15
16
17
18
☑ Diplay Red
☑ Display Blue
☑ Display Green
☐ Mask Numbers
☐ Mask Contours
☐ Phase (color)
☐ Phase (number)
☐ Current cell is mitotic
☐ Transplanted cell
☐ Dorsal cell
☐ Ventral Cell
☐ Adaxial cell
☐ Anterior Somite Comp
☐ Posterior Somite Comp
☐ Reference Cell
Z_position
Fluorescence
Inferred phase
Older index
Current Cell
Merge Cells
Delete Current Cell
Delete current slice
New Cell
Create Movie
Reconnect the GUIS
Current Cell
New cell index
Correct tracking
Compute Phase Current Cell
Correct phase current cell
Devalidate current cell
Finalize Current Cell
☐ Activate zoom in/out when clicking
○ AZERTY

Time 59

Z-section 14

30.9118
657.912
38.8039
317.804

Older index -1

Current Cell 923

Current Cell 923

New cell index -1

B

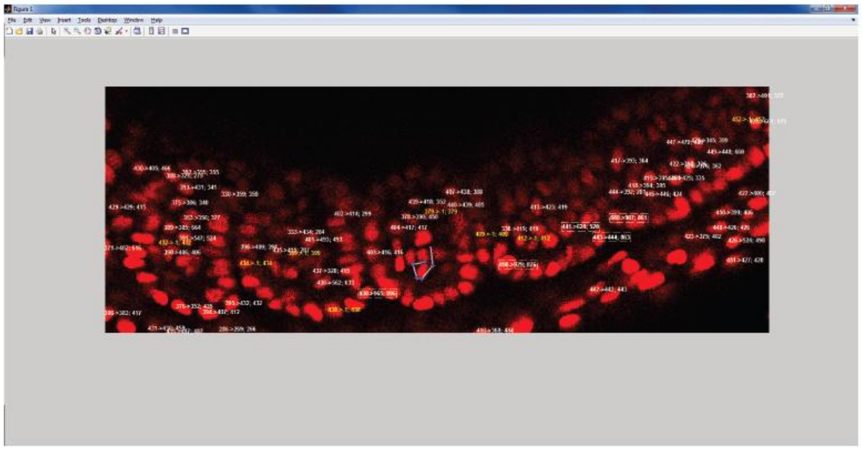
Figure 1
File Edit View Insert Tools Desktop Window Help

C

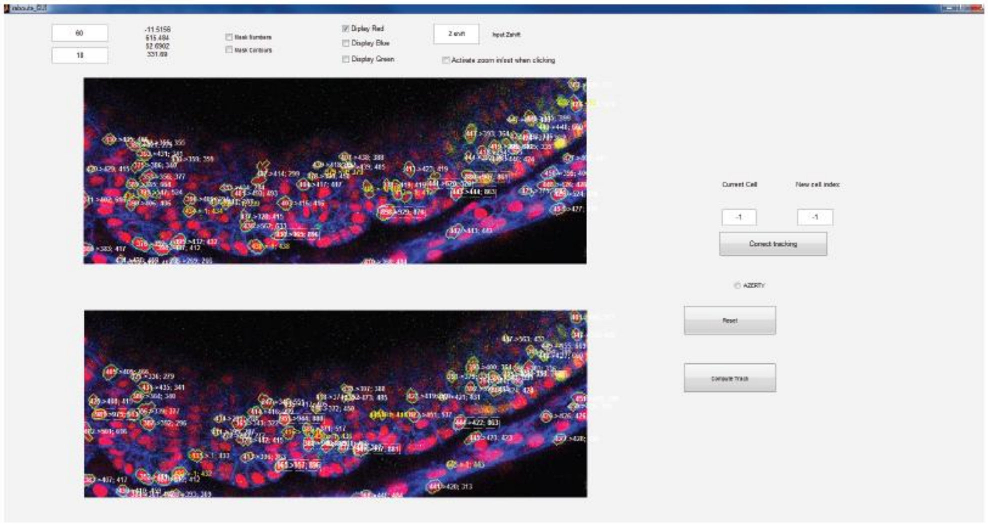
zebcuts_GUI
☐ Mask Numbers
☐ Mask Contours
☑ Diplay Red
☐ Display Blue
☐ Display Green
Input Zshift
☐ Activate zoom in/out when clicking
Current Cell
New cell index
Correct tracking
○ AZERTY
Reset
Compute Track

60

18

-11.5156
615.484
52.6902
331.08

Z shift

Current Cell -1

New cell index -1

Figure A.1 Screenshots of GUI interface
(A) The main *stack_GUI* interface. See main text for description of components. (B) The “Create New Cell” trace interface. (C) “Connect timelapses” interface. Allows for off-setting z-stacks when comparing two timepoints

Appendix B

Materials and Methods

Fish Stocks

Adult fish strains (AB WT, bea^{b663} [Henry et al., 2005], des^{b638} [Gray et al., 2001], and aei^{tr233} [van Eeden et al., 1996], *Tg(her1:her1-Venus)*^{bk15} [Delaune and Francois *et al.*,2012]) were kept at 28.5°C on a 14-hr light/10-hr-dark cycle. Embryos were obtained by natural crosses or *in vitro* fertilization and staged as previously described (Kimmel et al., 1995).

Plasmid Construction and Transgenesis

The *her1:her1-venus* plasmid was assembled as follows: The 8.6 kb PstI-NcoI *her1* upstream region was isolated from Construct I (Gajewski et al., 2003). The *her1* coding sequence was amplified from pCS2+her1 plasmid (Takke and Campos-Ortega, 1999) using 5'-ACCTGCCAGCCATGGTTACTCCAAAAATG-3' forward and 5'-GCTAGCAGTCGACCCTCCACTACCTCCCCAGGGTCTCCACAAAGG-3' reverse primers. The Venus coding sequence was amplified from Venus/pCS2 plasmid (Nagai et al., 2002) using 5'-GCTAGCGGTGGAATGGTGAGCAAGGGCGAGGA-3' forward and 5'-CTTAAGACGCGTTACTTGTACAGCTCGTCCATGCCG-3' reverse primers. A fragment containing 1.1 kb of *her1* 30 noncoding sequence was amplified from AB genomic DNA using 5'-ACCCTCTTAAGCAAAACTGAAGACACTTAGCATGAGAATAACCAGCG-3' forward and 5'-AAACAGCGGCCGCCGTCATTATTTACTCTTAAACCTGTTTGAACACC-3' reverse primers. Fragments containing the 8.6 kb PstI-NcoI *her1* upstream region, *her1* coding sequence (digested with BfuAI [to create an NcoI-compatible end] and NheI), Venus coding sequence (NheI/AflII digested), and 1.1kb *her1* 3' noncoding sequence (AflII/NotI-digested) were inserted in that order into the pBSKI2 plasmid (Thermes et al., 2002) between the PstI and NotI sites. Transgenic lines were generated as previously described using I-SceI-based transgenesis (Thermes et al., 2002). Reporter transcripts from both founders analyzed gave striped expression by in situ hybridization. The *Tg(her1:her1-Venus)*^{bk15} stable line, which was generated from founder m7, displays reproducibly strong oscillating expression and transmits as a single Mendelian locus.

Whole-Mount *In Situ* Hybridization and Immunohistochemistry

Digoxygenin-labeled antisense RNA probes were synthesized from the templates *deltaC* (Jiang et al., 2000), *her7* (Gajewski et al., 2003), *mespa* (Sawada et al., 2000), and *Venus* (Nagai et al., 2002). In situ hybridization was performed as previously described (Thisse and Thisse, 2008). For Venus immunohistochemistry, standard protocols were followed, using 4% paraformaldehyde fixation, 2% Triton X-100/PBS permeabilization, 2% BSA/2% goat serum/1% DMSO/0.1% Tween 20/PBS blocking, anti-GFP rabbit antibody (diluted 1:1,000; Molecular Probes), peroxidase-conjugated anti-rabbit goat secondary antibody (diluted 1:200; Molecular Probes), and diaminobenzidine staining. For double Venus transcript and protein staining, immunohistochemistry was performed before in situ hybridization. The head and yolk were removed in 70% ethanol and embryos were flat-mounted in 80% glycerol. Images were captured using a Zeiss AxioPlan upright microscope and Axio-Cam camera.

Live Imaging

Zebrafish embryos were injected at the one-cell stage with ~40 pg *H2B-cerulean* and 20 pg *membrane-mCherry mRNA* (Megason, 2009), raised at 28°C to 30 °C until 11 hpf, and then held at 23°C for several hours prior to imaging. At the 8- to 12-somite stage, the embryos were mounted laterally, with no coverslip, in embryo arrays (Megason, 2009) in Embryo Medium plus 0.01% Tricaine. Confocal sections were performed every 1.34 mm, with stacks taken every 4 min, using an upright Olympus FV1000 confocal microscope, a XLUMPXFL 203 water objective (NA 0.95), and temperature-controlling ring set to 23°C. Image resolution was 2.092 pixels/mm. Images were converted to 8-bit before processing.

Timelapse images in Chapter 3 and 4 were generated using methods modified from Delaune *et al.* 2012. Embryos were imaged on a LSM 780 with 32-channel GaAsP detector on the AxioExaminer microscope (Carl Zeiss) with the W Plan-Apochromat 20x/1.0 NA objective (Carl Zeiss), using Zeiss Zen 2010 software. Due to low level fluorescence, we have found that the numerical aperture of the objective is a critical component. Confocal sections were taken every 2µm, with a stack of 30-35 slices taken approximately every four minutes. Images were converted to 8-bit tagged image file format before processing.

3D Cell Contour Detection and Tracking

We developed a MATLAB script for the sole purpose of automatically and accurately detecting PSM cells in our experiments. Our cell-tracking and data-analysis tools have not been optimized or validated for any other purpose. After initially converting the membrane and nuclear channels fluorescence images into compatible MATLAB files, we removed noise in both the membrane and nuclear channels using a low-pass filter, treating for noise and nonuniform illumination. The separate optical slices were then merged into a single matrix and each continuous 3D cluster of fluorescent pixels was indexed. Cell contours were predicted and connected across time and space based on previous work (Keller et al., 2008; Sbalzarini and Koumoutsakos, 2005). We circumvented potential problems in tracking due to mitosis by tracking the cells in reverse, starting from the last time point. For each cell, the optical section with the highest average brightness was recorded as the cell fluorescence for each given time point. The cell's reporter fluorescence, position in the embryo, Cartesian coordinates, catalog number, and mitotic activity were recorded in a data matrix for future analyses.

To validate the automated tracking and efficiently make necessary edits to our data matrices, we developed a graphical user interface (GUI) that displayed images for a given time point and z-slice as well as for the previous time point at the same z-slice (Figure S3). The interface allowed for rapid navigation across space and time, simple tagging and manual correction of the 3D contour of individual cells, and filters to display different fluorescence channels, labels, and contours. This configuration allowed us to properly link cells across time frames that were previously left unconnected by the automatic analysis. We also used the GUI to tag cells manually for complex qualitative properties that cannot be easily computed automatically, such as mitotic activity, relative position within somites, and cell type.

Fluorescence Smoothing and Phase Calculation

Because fluorescence is highly variable over time (due in part to noise and to increasing oscillation period and amplitude along the PSM), we had to make simplifying assumptions about the form of the signal to smoothen the fluorescence signal and define a phase for the oscillators. We assumed that fluorescence F(t) behaves as a harmonic oscillator where values of amplitude

A(t), basal fluorescence B(t) and angular velocity u(t) slowly change with time (left-hand side of Equation 1). Our smoothing heuristic (Equation 1) removed the average fluorescence in a given time window T comparable to the period, estimated the new amplitude over the same time window, and rescaled the sine wave to that amplitude. We treated the raw fluorescence twice by this method to isolate a pseudo sine wave for each cell. Assuming that this readout behaves like a harmonic oscillator, one can simply compute the angular velocity and consequently the phase (4(t) = u(t)t, taken modulo 2π. This heuristic is extremely simple to implement, and we checked many examples to confirm that it gives robust and realistic results. The phase shift between two oscillations is the absolute value of the difference of the two computed phases, taken between 0 and π. MATLAB scripts were developed to automatize all these calculations. One obstacle with this calculation is that the period calculation assumes that a period exists. An option was included in the GUI to crop out ranges of calculated periods in cells that were not visibly oscillating.

$$F(t) = A(t)\sin\omega(t)t + B(t) \Rightarrow \sin\omega(t)t \simeq \frac{\left(F(t) - \langle F(t)\rangle_T\right)}{\sqrt{2\left\langle \left(F(t) - \langle F(t)\rangle_T\right)^2 \right\rangle_T}} \quad \text{(Equation 1)}$$

where $\langle F(t)\rangle_T = 1/T \int_{t-T/2}^{t+T/2} F(u)\ du$, and T is a fixed time window of the order of the period.

Statistical Analysis

We generated two-dimensional histograms by plotting the calculated periods of cells after mitosis as a function of their sibling or their neighbor at each time point. We made statistical comparisons of synchrony levels between these two groups by comparing the overall phase differences using a two-sample t-test. Other details are provided in the figure legends.

Tissue-wide Partitioning and Fluorescence Binning

The developing embryo was detected based on the stack of nuclear and membrane fluorescence images at each timepoint. Image stacks were treated with low-pass filters. A binary image was constructed to detect embryo contour and to compute a skeleton corresponding to center axis. We then defined a curved coordinate along this axis, and computed position of each cell along this coordinate. This center axis was then binned into equal portions, with the extended segment boundaries corresponding to bins. Fluorescence within each slice was measured as an average compared to slice size, and stored based on tissue position and timepoint. Embryo movement was accounted for by anchoring tissue position to a known reference cell as a landmark.

Hes6-morpholino injection

Embryos were injected using a previously described morpholino, with the sequence: TGCAGTTCAGGACGCTTGAATGGG (Kawamura *et al.* 2005, Schroter and Oates 2010). The morpholino was diluted to a .5mM final concentration, with 1-3nL injected into the single cell immediately after fertilization.

Calcein staining

A 0.2% calcein solution was used by mixing the calcein powder with fish water. 21dpf fish larvae were netted and inverted into a petri dish of the calcein solution. Fish were soaked for 15-

20 minutes in this calcein solution. To wash out the calcein, the fish were pouredback into the net, and the net was inverted into a clean dish of MU water. This process was repeated 3 times to remove excess calcein. Fish were allowed to swim in clean water for 10-15 water, to rinse excess calcein. Fish were then netted and dipped into a beaker of ice water to euthanize. Larvae were removed and imaged for calcein fluorescence.